

THERMAL/HYDRAULIC ANALYSIS METHODS FOR PWR'S

by

PABLO MORENO *PALACTOS*

Ingeniero Industrial  
Escuela Tecnica Superior de Ingenieros Industriales  
Madrid (Spain)

(1974)

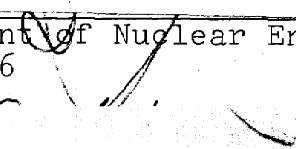
Submitted in Partial Fulfillment of  
the Requirements for the  
Degree of Nuclear Engineer

at the


MASSACHUSETTS INSTITUTE OF TECHNOLOGY

(May, 1976)

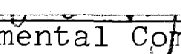
Signature of Author

  
Department of Nuclear Engineering,  
May, 1976

Certified by

  
Thesis Supervisor

Accepted by

  
Chairman, Departmental Committee on Graduate  
Students

ARCHIVES



THERMAL/HYDRAULIC ANALYSIS METHODS FOR PWR'S

by

Pablo Moreno PALACIOS

Submitted to the Department of Nuclear Engineering,  
May 1976, in partial fulfillment of the requirements  
for the Degree of Nuclear Engineer.

ABSTRACT

In order to perform a hot subchannel analysis in a PWR and include the effects of crossflows, the "standard" procedure being used is the so called cascade or chain method. It requires excessive effort as well as computation time.

An alternative procedure called the simplified method, has been examined here. It combines a fine mesh of actual subchannels around the hot subchannel with a courser one as we move further away from the hot region.

Our simplified method has been checked against the cascade method. From the study of the characteristics of each method, it is concluded that our simplified method yields better results than the cascade method. Additionally it requires considerably less effort and it costs less than the cascade method.

Analysis was initiated on the effect on the simplified method of reduction in the number of channels in which the core is divided. It is concluded that when the hot subchannel is surrounded by a fine mesh of actual subchannels, the effect of this reduction upon the properties of the hot subchannel and neighbors is small. But if the mesh of actual subchannels around the hot one becomes small, the properties in the hot region change noticeably.

To further improve our simplified method to such an extent that it will yield identical results to those of an actual subchannel analysis, proper transport coefficients have to be used. The effect of an approximation to one of these transport coefficients (i.e.  $N_H$ ) is investigated. It is concluded that their effect is important enough to recommend their development and use in our simplified method. For this reason, the terms that affect the properties of the channels have been isolated and indications are given about where such transport coefficients must be introduced.

Additionally the analytical deduction of one of these transport coefficients ( $N_H$ ) for a two-dimensional problem and the modifications introduced in COBRA IIIC in order to be able to execute our simplified method are given.

Thesis Supervisor: Neil E. Todreas

Title: Professor of Nuclear Engineering

#### ACKNOWLEDGEMENTS

The author wishes to express his sincere gratitude to all who assisted him during the preparation of this thesis. In particular, to the following:

Professor Neil E. Todreas, who, as my thesis advisor, has so generously given his time and advice. His valuable guidance and careful thought have contributed much to this work and are sincerely appreciated.

Dr. Ehsan U. Khan for his valuable assistance and advice on the problems that occurred during the preparation of this thesis.

To Chong Chiu for his helpful suggestions and comments during the course of this work.

To Mrs. Lynda DuVall and Ms. Irene Battalen who patiently typed this thesis.

This work was initiated under the sponsorship of the Electric Power Research Institute. It was completed as part of the Nuclear Reactor Safety Research Program under the Electric Power Program sponsored by New England Electric System and Northeast Utilities Service Company.

TABLE OF CONTENTS

	<u>Page</u>
Chapter 1. Description of the Problem	17
1.0 Introduction	17
Chapter 2. Cascade Method Versus the Simplified Method	20
2.0 Introduction	21
2.1 Cascade Method	21
2.1.0 Introduction	21
2.1.1 Assembly to Assembly Analysis	22
2.1.2 Hot Assembly Analysis	22
2.1.2.0 Introduction	22
2.1.2.1 Inlet Condition for Each Slice	28
2.1.2.1.1 Total Inlet Mass Flow Rate of a Slice	29
2.1.2.1.2 Inlet Massflow Rate for Each Particular Channel of the Slice	34
2.1.2.2 Results	35
2.2 Simplified Method	37
2.2.0 Introduction	37
2.2.1 Case Analyzed	37
2.2.2 Results	37

TABLE OF CONTENTS  
(Continued)

	<u>Page</u>
2.3 Comparison Between Results	37
2.3.1 Differences Observed Between Both Methods	37
2.3.2 Analysis of These Differences	41
2.4 Conclusions	46
Chapter 3. Simplified Method	48
3.0 Introduction	49
3.1 Simplified Method with No Coupling Parameters ( $N_H = 1$ )	51
3.1.1 101 Channel Case	51
3.1.2 61 Channel Case	52
3.1.3 30 Channel Case	52
3.1.4 10 Channel Case	52
3.2 Simplified Method Using Transport Parameter $N_H$	52
3.2.0 Introduction	52
3.2.1 101 Channel Case	69
3.2.2 61 Channel Case	69
3.2.3 30 Channel Case	69
3.2.4 10 Channel Case	78

TABLE OF CONTENTS  
(Continued)

	<u>Page</u>
3.3 Analysis of the Results	78
3.3.1 Analysis of the $N_H = N$ Case	83
3.3.1.1 Analysis of the MDNBR Results	83
3.3.1.2 Analysis of the Enthalpy Results	83
3.4 Simplified Analysis Using Exact Transport Coefficients	98
 Chapter 4. Modifications to the First Version of COBRA IIIC/MIT	 100
 Chapter 5. Transport Coefficients	 102
5.0 Introduction	103
5.1 Two Dimensional Transport Coefficients for the Energy Conservation Equation	103
5.1.0 Introduction	103
5.1.1 Problem Statement	104
5.1.2 Solution Procedure	107
5.1.3 Solution of the Problem	112
5.1.3.1 Equation to be Solved	112
5.1.3.2 Boundary Conditions	112
5.1.3.3 Changes of Variables	113
5.1.3.4 Final Expression	120

TABLE OF CONTENTS

(Continued)

	<u>Page</u>
5.1.4 Calculation of the Transport Parameters ( $N_H$ and $N_H'$ )	127
5.1.5 Comparison of $N_H(z)$ Obtained as Previously Indicated with the Values Obtained by Using COBRA - IIIC/MIT	128
5.1.5.0 Introduction	128
5.1.5.1 Enthalpy Upset Case (No Heat Generation)	129
5.1.5.2 Heat Generation Upset with Constant Inlet Enthalpy	135
Chapter 6. Conclusions and Recommendations for Future Work	141
6.1 Conclusions	141
6.2 Recommendations	142



LIST OF FIGURES

	<u>Page</u>
Figure 2.1 Assembly to Assembly Analysis: Numbering scheme and radial peaking factors	23
Figure 2.2 Assembly to Assembly Analysis: Exit enthalpy of each assembly	24
Figure 2.3 Hot assembly	25
Figure 2.4 Numbering scheme and radial peaking factors of the hot assembly	27
Figure 2.5 Variation of the mass flow of the hot assembly with z	33
Figure 2.6 Analysis of the hot assembly: Exit enthalpy of each channel	36
Figure 2.7 Simplified method: Numbering Scheme	38
Figure 2.8 Simplified method: Exit enthalpy for each assembly	39
Figure 2.9 Simplified method: Exit enthalpy for each channel of the hot assembly	40
Figure 2.10 Normalized differences in exit enthalpy between the cascade and simplified methods (assemblies)	42
Figure 2.11 Normalized differences in exit enthalpy between the cascade and simplified methods (hot assembly)	43
Figure 3.1 101 channel case: Numbering scheme	53
Figure 3.2 101 channel case: Numbering scheme of the hot bundle	54
Figure 3.3 101 channel case: Exit enthalpies	55
Figure 3.4 101 channel case: Exit enthalpies for the channels of the hot assembly	56
Figure 3.5 61 channel case: Numbering scheme	57
Figure 3.6 61 channel case: Numbering scheme inside the hot bundle	58

LIST OF FIGURES - continued

		<u>Page</u>
Figure 3.7	61 channel case: Exit enthalpies outside the hot assembly	59
Figure 3.8	61 channel case: Exit enthalpies inside the hot bundle	60
Figure 3.9	30 channel case: Numbering scheme	61
Figure 3.10	30 channel case: Numbering scheme of the hot assembly	62
Figure 3.11	30 channel case: Exit enthalpies outside the hot assembly	63
Figure 3.12	30 channel case: Exit enthalpies inside the hot assembly	64
Figure 3.13	10 channel case: Numbering scheme	65
Figure 3.14	10 channel case: Numbering scheme of the hot assembly	66
Figure 3.15	10 channel case: Exit enthalpies outside the hot assembly	67
Figure 3.16	10 channel case: Exit enthalpies inside the hot assembly	68
Figure 3.17	$N_H = N$ and 101 channel case: Exit enthalpies outside the hot assembly	70
Figure 3.18	$N_H = N$ and 101 channel case: Exit enthalpies inside the hot assembly	71
Figure 3.19	$N_H = N$ and 60 channel case: Exit enthalpies outside the hot assembly	72
Figure 3.20	$N_H = N$ and 60 channel case: Exit enthalpies inside the hot assembly	73
Figure 3.21	$N_H = N$ and 60 channel case: Difference in enthalpy with respect to the $N_H = N$ and 101 channel case	74
Figure 3.22	$N_H = N$ and 30 channel case: Exit enthalpies inside the hot assembly	75

LIST OF FIGURES - continued

	<u>Page</u>
Figure 3.23 $N_H = N$ and 30 channel case: Exit enthalpies inside the hot assembly	76
Figure 3.24 $N_H = N$ and 30 channel case: Difference in enthalpy with respect to the $N_H = N$ and 101 channel case	77
Figure 3.25 $N_H = N$ and 10 channel case: Exit enthalpies outside the hot assembly	80
Figure 3.26 $N_H = N$ and 10 channel case: Exit enthalpies inside the hot assembly	81
Figure 3.27 $N_H = N$ and 10 channel case: Difference in enthalpy with respect to the $N_H = N$ and 101 channel case	82
Figure 3.28 $N_H = N$ case: Comparison between flows crossing the upper boundary of the hot subchannel in the four cases	87
Figure 3.29 $N_H = N$ case: Comparison between flows crossing the left boundary of the hot subchannel in the four cases	88
Figure 3.30 $N_H = N$ case: Comparison between flows crossing the right boundary of the hot subchannel in the four cases	89
Figure 3.31 $N_H = N$ case: Comparison between flows crossing the lower boundary of the hot subchannel in the four cases	90
Figure 3.32 Comparison between the total crossflow leaving the hot subchannel in the four cases	93
Figure 5.1 Two channel case and multichannel case	106
Figure 5.2 Geometrical description of the analytical problem	111
Figure 5.3 Comparison of the analytical results. Enthalpy upset; $\beta = 0.005$	132

LIST OF FIGURES - continued

	<u>Page</u>
Figure 5.4 Comparison of the analytical results. Enthalpy upset; $\beta = 0.02$	132
Figure 5.5 Comparison of the analytical results. Enthalpy upset; $\beta = 0.06$	134
Figure 5.6 Comparison of the analytical results. Power upset; $\beta = 0.006$	137
Figure 5.7 Comparison of the analytical results. Power upset; $\beta = 0.02$	138
Figure 5.8 Comparison of the analytical results. Power upset; $\beta = 0.06$	139
Figure A.1.1 Radial peaking factors inside the hot assembly	150
Figure A.3.1 Example case	155
Figure A.9.1 Sample problem	178
Figure A.9.2 Redivision of the sample problem	180

LIST OF TABLES

		<u>Page</u>
Table 2.1	Costs of the Cascade and Simplified Methods	47
Table 3.1	Cases that should be analyzed	50
Table 3.2	MDNBR for the Different Cases Analyzed	79
Table 3.3	DNB Results	84
Table 3.4	Energy Errors of the Whole Core	95
Table 3.5	Errors Due to Truncation and Marching Technique Used	96
Table 3.6	Comparison of Energy Added to the Hot Subchannel	97
Table A.5.1	Testing of Equation (A.5.13)	166
Table A.9.1	Boundaries For the Example Problem	183

LIST OF APPENDICES

	<u>Page</u>
Appendix 1. Description of the Data Used in the Analysis	143
A.1.0 Introduction	144
A.1.1 Operating Conditions	144
A.1.2 Dimensions of the Assemblies	144
A.1.3 Dimensions of the Subchannels	145
A.1.4 Dimensions of the Rods	145
A.1.5 Axial Heat Flux Distribution	145
A.1.6 Radial Power Factors	146
A.1.6.1 Assemblies	146
A.1.6.2 Hot Assembly	146
A.1.7 Spacer Data	147
A.1.8 Thermal-Hydraulic Model	147
A.1.8.1 Mixing	147
A.1.8.2 Single-Phase Friction	148
A.1.8.3 Two-Phase Friction	148
A.1.8.4 Void Fraction	148
A.1.8.5 Flow Division at Inlet	148
A.1.8.6 Constants	148
A.1.8.7 Iteration	149
A.1.8.8 Coupling Parameters	149

LIST OF APPENDICES

(Continued)

	<u>Page</u>
Appendix 2. Actual Calculation of the Average Enthalpy of the Hot Assembly in the Hot Assembly Analysis	151
Appendix 3. Mass Flow Rates of Each Channel at the Inlet of a Slice as a Function of the Values at the Outlet of the Previous Slice	153
Appendix 4. Subroutine TABLES	156
Appendix 5. Development of an Expression to Calculate the Truncation and Marching Technique Errors Associated with COBRA IIIC/MIT	160
Appendix 6. Improvements Suggested in Order to Eliminate Truncation Errors and Errors Associated with the Marching Technique Used in COBRA IIIC/MIT	167
Appendix 7. Computer Program to Calculate $N_H$ for the Enthalpy Upset Case.	170
Appendix 8. Computer Program to Calculate $N_H$ for the Power Upset Case	172
Appendix 9. Description of the Modifications Introduced in COBRA IIIC/MIT	174
A.9.1 Modifications to Allow for More than Four Channels Surrounding any Single One.	174
A.9.2 Modifications to Allow for No Square Channels	182

LIST OF APPENDICES

(Continued)

	<u>Page</u>
A.9.3 Modifications to Allow for Having Actual Subchannels Together with Lumped Channels	186
A.9.4 Modifications Required to Obtain the MDNBR	189
A.9.5 Modifications Required in Order to Obtain the Fuel Temperatures when the Original COBRA IIIC Input Data Presentation is Used	190
A.9.6 Modifications Required when Wire Wraps are Used	190
A.9.7 Modifications Required in Order to Analyze More than One Case in the Same Run	192
A.9.8 Modifications Required to Print Out More than 14 Channels, Rods or Nodes	192
A.9.9 Modifications Required to Use a Transport Parameter in the Turbulent Interchange Term of the Energy Equation.	193



## Chapter 1

### DESCRIPTION OF THE PROBLEM

#### 1.0 Introduction

The goal of this thesis is to develop a method for steady state analysis of the core of a Pressurized Water Reactor using publically available computer codes. The Connecticut Yankee PWR core was selected and its physical characteristics are presented in Appendix 1. The computer code chosen is COBRA IIIC<sup>(1)</sup> in its MIT version, COBRA IIIC/MIT<sup>(2)</sup>.

It is clear that the best way to analyze a reactor core is by taking each radial node in the analysis at least as an actual subchannel. This implies that for the Connecticut Yankee PWR core 35,325 radial nodes should be considered (because of symmetry reasons this number may be reduced to 4,416). These numbers are so large that there is no available computer which could handle this problem, and even if such a computer were available the cost would be prohibitive. Therefore this possibility has historically been ruled out and other approaches have been developed based on the following characteristic of the parameters which limit PWR core operation.

The most limiting parameter of a PWR in steady state is the Minimum Departure from Nucleate Boiling Ratio (MDNBR). A second potential limit is void fraction. However in almost all practical cases the MDNBR is the governing limit not channel void fraction. For a typical PWR the MDNBR is dependent on enthalpy and on heat generation rate. The enthalpy of the channel is dependent upon the heat generation rate and the characteristics of its neighbor channels which effect interchannel energy exchange. The dominant parameter is the heat generation rate, which implies that the most restrictive conditions will take place in the subchannel where the heat generation rate is large and not necessarily in the subchannel with largest enthalpy. This will allow identification, by inspection of the core radial power distribution, of that area of the core where the most restrictive conditions are going to occur. Then a fine mesh of subchannels will be required in this zone while outside of this zone a coarse mesh will suffice.

This simplification leads to two general approaches. One is the so-called cascade or chain method, and the other will be named as the simplified method.

The cascade method consists basically of a two stage analysis of the core. In the first stage the whole core

is analyzed on assembly to assembly basis (each radial node represents an actual assembly). From this analysis the hot assembly, i.e. the one with the largest enthalpy, and its boundary conditions can be identified. In the second stage the hot assembly is analyzed on a subchannel basis, (each radial node is an actual subchannel or is created by lumping of a few subchannels) taking advantage of the boundary conditions found in the previous stage.

The simplified method is simpler than the cascade method. Here the core is analyzed in only one stage using a fine mesh in a zone consisting of those subchannels with the larger radial peaking factors and a coarse one outside this zone.

The methods will be compared in Chapter 2 and one of these (the simplified method) will be selected as the one that yields better results.

Then in Chapter 3, the selected method will be analyzed in full detail, the terms that need to be improved will be isolated and recommendations will be made to achieve these improvements.

To be able to execute the simplified method some modifications were made in the first version of COBRA IIIC/MIT. These are given in Chapter 4.

In Chapter 5 an analytical derivation of one of the transport parameters required to improve the simplified method is given.

## Chapter 2

### CASCADE METHOD VERSUS THE SIMPLIFIED METHOD

- 2.0 Introduction
- 2.1 Cascade Method
  - 2.1.0 Introduction
  - 2.1.1 Assembly to Assembly Analysis
  - 2.1.2 Hot Assembly Analysis
- 2.2 Simplified Method
- 2.3 Comparison Between Results
- 2.4 Conclusion

## 2.0 Introduction

The initial goal of this thesis was to develop a simplified method to analyze the thermo-hydraulic core performance of a PWR. Because no experimental information was available on the behavior of the core and because the analysis of the core on a subchannel basis (i.e., each radial node being an actual subchannel) is absolutely prohibitive, the results obtained with our simplified analysis were to be compared against those obtained by using a standard method. The standard method selected was the so-called cascade (or chain) method.

In this chapter more specific details will be given about the cascade and simplified methods. The results obtained with both methods for the core of the CONN. YANKEE Reactor will be presented. And finally, the conclusions drawn from these results will be indicated.

## 2.1 Cascade Method

### 2.1.0 Introduction

The second stage of the cascade method normally requires a computer analysis code which allows input of the transverse flows on the hot assembly boundary. Neither COBRA IIIC/MIT or any other publically available code includes this capability. Therefore our approach was to perform the hot

assembly analysis on a series of axial slices of the assembly. The slices are analyzed consecutively starting from the bottom of the reactor until the top is reached. The conditions at the inlet of a slice are those at the outlet of the previous slice but corrected in a manner to take into account the transverse boundary condition applicable to that slice.

#### 2.1.1 First Stage: Assembly to Assembly Analysis

The assembly to assembly analysis of the CONN. YANKEE PWR core was carried out with the pattern of assemblies given in Figure 2.1. The results are those of Figure 2.2. From these results, as expected, assembly 21 is the hot assembly and it will be analyzed in full detail.

#### 2.1.2 Second Stage: Hot Assembly Analysis

##### 2.1.2.0 Introduction

For this analysis the hot assembly was divided into 11 axial slices as indicated in Figure 2.3. All the slices are 12.066 inches high except the last one which is only 6.033 inches high.

To analyze each of these slices we need to fix both a pattern of channels applicable to all and the initial condi-

						1 0.32	2 0.31
				3 0.74	4 0.89	5 0.68	6 0.37
			7 0.75	8 1.45	9 1.37	10 0.65	11 0.64
		12 0.75	13 0.85	14 1.71	15 1.72	16 1.14	17 0.66
	18 0.74	19 1.45	20 1.71	21 1.86	22 1.53	23 1.23	24 1.01
	25 0.89	26 1.37	27 1.72	28 1.53	29 0.82	30 0.96	31 0.63
32 0.32	33 0.68	34 0.65	35 1.14	36 1.23	37 0.96	38 0.89	39 0.79
40 0.31	41 0.37	42 0.64	43 0.66	44 1.01	45 0.63	46 0.79	47 0.53

Numbering scheme and radial power factors

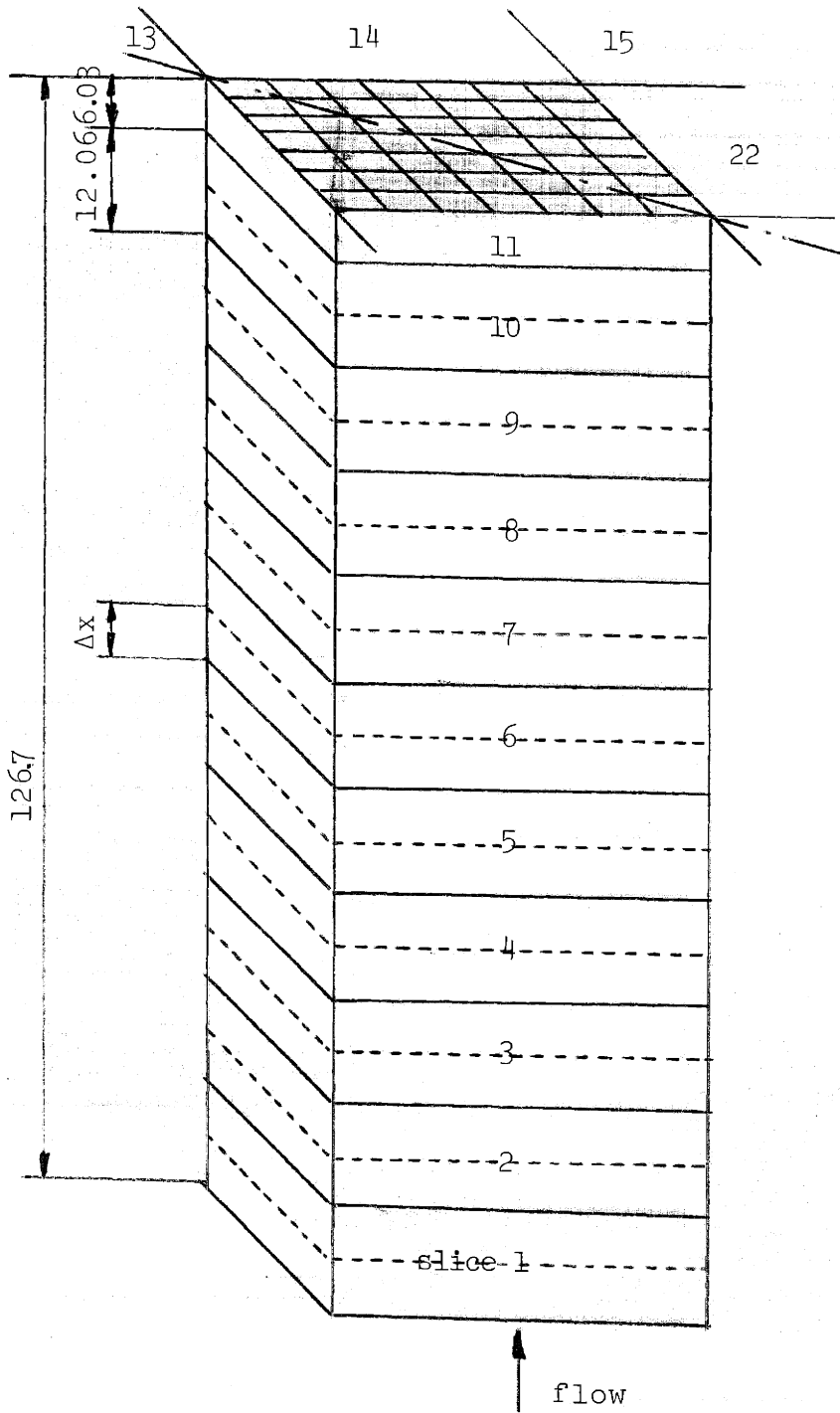
Figure 2.1



Enthalpy at the exit of each assembly

Figure 2.2





Hot assembly

Figure 2.3

tions at the inlet of each particular slice. The initial conditions required are the massflow rate and the enthalpy for each individual channel.

The pattern of channels used is that of Figure 2.4.

The enthalpy at the inlet of every slice for each channel is given by the enthalpy at the outlet of the previous slice for the same channel.

The mass flow rate has to be reduced to account for the diversion crossflow leaving the assembly. Ideally the diversion crossflow should be represented as a boundary condition of transverse flow leaving the assembly. However, because COBRA IIIC/MIT does not allow such boundary conditions, the only way to account for that flow leaving the assembly is by decreasing the inlet mass flow rate of each slice with respect to the outlet of the previous slice.

Finally, notice that each of these slices represents two axial steps (except the last which is only one) of the hot assembly in the assembly to assembly calculations. This system was selected in order to have small axial steps in the Assembly to Assembly analysis which leads to small truncation errors, and at the same time to avoid analysis of too many slices thereby keeping the length and cost of the analysis bounded.

1.917 1	1.973 2	1.799 3	1.974 4	1.799 5	1.973 6	1.917 7
	1.556 8	1.859 9	2.011 10	1.859 11	1.556 12	1.973 13
		1.553 14	2.039 15	1.553 16	1.859 17	1.799 18
			1.512 19	2.039 20	2.011 21	1.974 22
				1.553 23	1.859 24	1.799 25
					1.556 25	1.973 27
						1.917 28

Numbering scheme of the hot assembly

Figure 2.4

### 2.1.2.1 Inlet Conditions for Each Slice

#### 2.1.2.1.1 Total Inlet Mass Flow Rate of A Slice

As noted above, to account for the diversion cross flow that leaves the assembly along each slice, we have to reduce the inlet mass flow rate of such a slice with respect to the outlet mass flow rate of the previous slice. Let us take slice number 1 (Figure 2.3) and compare how the enthalpy at the outlet of the slice is calculated. The procedure which is developed makes the average enthalpy of the hot assembly at the exit of each slice equal to the enthalpy of the same assembly as calculated by the first stage of the cascade calculation at the same axial position.

The energy conservation equation used in COBRA IIIC/MIT when applied to the first axial step of assembly 21 in the assembly to assembly calculations is:

$$h_2(21) = h_1(21) + \left[ \frac{q'_{1+\frac{1}{2}}(21)}{m_1(21)} - \frac{w_1(21,22) (h_1^*(21,22) - h_1(21))}{m_1(21)} - \frac{w_1(21,14) (h_1^*(21,14) - h_1(21))}{m_1(21)} \right] \Delta X \quad (2.1)$$

where

$h_2(21)$  = enthalpy of assembly 21 at axial station 2

$h_1(21)$  = enthalpy of assembly 21 at axial station 1

$q'_{1+\frac{1}{2}}$  = average linear heat generation rate of assembly 21 in the interval corresponding with the first axial step.

$m_1(21)$  = mass flow rate of assembly 21 at axial station 1

$w_1(21,22)$  or  $w_1(21,14)$  = diversive crossflow leaving assembly 21 toward assembly 22 or 14 at axial station 1

$h_1^*(21,22)$  or  $h_1^*(21,14)$  = enthalpy of the donor assembly for flow between assembly 21 and assembly 22 or 14

$\Delta X$  = length of the axial step.

Recall that no turbulent interchange term is introduced. i.e.  $\beta$  is taken equal to zero. This is necessitated in the application of COBRA IIIC/MIT to the hot assembly stage of the chain method since the boundary conditions allowed by this code at the assembly boundary are zero energy and mass exchange.

For the first axial step:

$$w_1(21,22) = w_1(21,14) = 0 \quad (2.2)$$

Because in this case, and in most of the others, the hot assembly experiences transverse outflow all along the length of the core, we can in general take:

$$h_1^*(21,22) = h_1(21) \quad (2.3)$$

$$h_1^*(21,14) = h_1(21) \quad (2.4)$$

And then equation (2.1) becomes:

$$h_2(21) = h_1(21) + \frac{q_{1+\frac{1}{2}}'(21)}{m_1(21)} \Delta X \quad (2.5)$$

Analogously for the second axial step:

$$h_3(21) = h_2(21) + \frac{q_{2+\frac{1}{2}}'(21)}{m_2(21)} \Delta X \quad (2.6)$$

Combining these two last equations we obtain:

$$h_3(21) = h_1(21) + \left[ \frac{q_{1+\frac{1}{2}}'(21)}{m_1(21)} + \frac{q_{2+\frac{1}{2}}'(21)}{m_2(21)} \right] \Delta X \quad (2.7)$$

which gives us the average enthalpy of assembly 21 at the outlet of the second axial step.

Now for the hot assembly analysis the total mass flow rate of the assembly axially within the slice has to be kept constant because no flow can leave through the periphery of the assembly. Then the average enthalpy at the exit of the slice (which corresponds with axial station 3) has to be calculated as follows: (See Appendix 2).

$$h_3'(21) \cong h_1'(21) + \left[ \frac{\bar{q}'(21)}{m_1'(21)} \right] \Delta X' \quad (2.8)$$

where the primes are introduced to identify parameters of the hot assembly analysis and where  $h_1'(21) = h_1(21)$  (2.9)

$$\bar{q}'(21) \Delta X' = \left[ q_{1+\frac{1}{2}}'(21) + q_{2+\frac{1}{2}}'(21) \right] \Delta X \quad (2.10)$$

$$\Delta X' = 2\Delta X$$

Then in order to have:

$$h_3(21) = h_3'(21) \quad (2.11)$$

we need:

$$\left[ \frac{q_{1+\frac{1}{2}}'(21)}{m_1(21)} + \frac{q_{2+\frac{1}{2}}'(21)}{m_2(21)} \right] = 2 \left[ \frac{\bar{q}'(21)}{m_1'(21)} \right] \quad (2.12)$$

and from this equation we could find  $m_1'(21)$  since all other parameters are known.

It was decided to take  $m_1'(21)$  as equal to  $m_2(21)$  even though we know that this simplification is going to produce slightly different values of the enthalpy. But because the differences between the mass flow rates are not too large (figure 2.5), the errors introduced are negligible.

Then at the inlet of each slice the total mass is:

$$m_J'(21) = m_{2J+1}(21) \quad (2.13)$$

where:

$m_J'(21)$  = total inlet mass flow rate of slice J in the hot assembly analysis.

$m_{2J+1}(21)$  = total inlet mass flow rate at axial station (2J+1) in the assembly to assembly analysis.

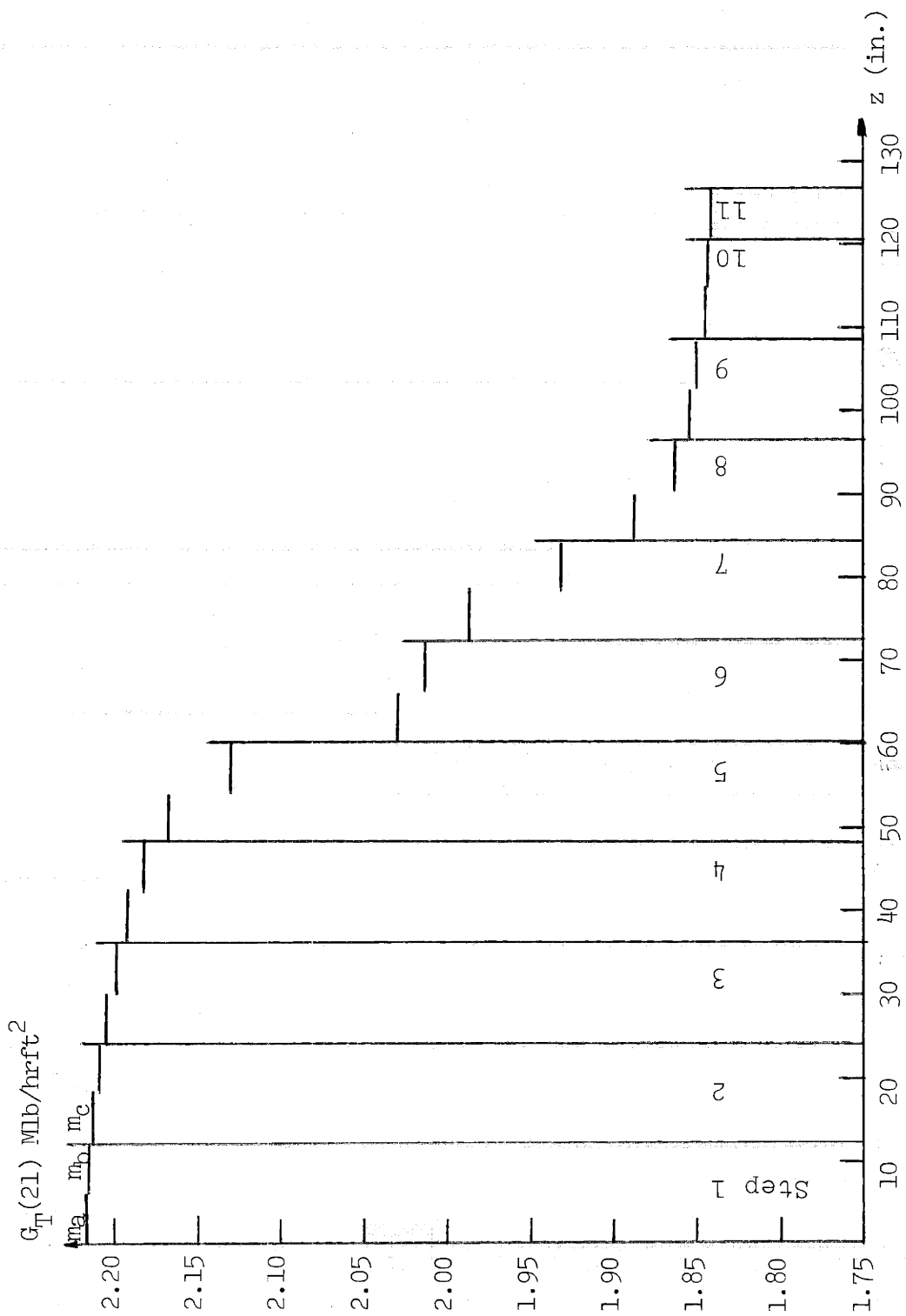
Then to relate  $m_J'(21)$  with  $m_{J-1}'(21)$  we have to use the following expressions:

$$m_{J-1}'(21) = m_{2(J-1)+1}(21) = m_{2J-1}(21) \quad (2.14)$$

Subtracting equations (2.13) and (2.14):

$$m_J'(21) - m_{J-1}'(21) = m_{2J+1}(21) - m_{2J-1}(21) \quad (2.15)$$





Mass flow rates along the hot assembly

Figure 2.5

But because the right hand side is equal to the summation of all the crossflows leaving the hot assembly in axial stations (2J) and (2J-1) we can express finally:

$$m'_J(21) - m'_{J-1}(21) = \sum_{i=1}^I w_{2J-1}(21,i) + \sum_{i=1}^I w_{2J}(21,i) \quad (2.16)$$

where I represents the assemblies adjacent to assembly 21 in the assembly to assembly calculations.

It can be noticed that the manipulations of equations 2.13 through 2.16 would be avoided by taking each slice of the hot assembly analysis as an axial step of the assembly to assembly analysis since this would permit selecting exactly the same mass flow rate in both cases. The problem is then that the number of slices doubles making application of the method very expensive and time consuming.

#### 2.1.2.1.2 Inlet Massflow Rate for each Particular Channel of the Slice.

So far we have indicated how to obtain the total inlet massflow rate to any slice and why we chose that value. The question remains as to how that total massflow should be redistributed among the channels. For this purpose it was assumed that the diversion crossflow leaves the assembly homogeneously only from the outer row of channels of the corresponding boundary.

This implies that after one slice is analyzed and the mass flow rates at the outlet of the slice are known, in order to find the massflow rates at the inlet of the next slice, we need to modify the mass flow rates of the outer row of channels while the channels in the interior of the assembly remain unchanged. The procedures by which these calculations are carried out is given in Appendix 3.

#### 2.1.2.1.3 Inlet Enthalpy of Each of the Channels that Make-up a Slice

The inlet enthalpies to any slice are taken equal to those at the outlet of the previous slice. Notice that no correction in the enthalpies is made to take into account the effect of the energy carried by the crossflow when it is entering the hot assembly.

#### 2.1.2.2 Results

In Figure 2.6 the enthalpies to the outlet of the last slice (which is the top of the core) are given. One very important conclusion that can be derived from these results is that the hot channel (i.e. channel with the largest radial peaking factor) is not that of the largest enthalpy. This shifting is due to the effect of the diversion crossflow. This conclusion will be very important for the selection of a fine mesh around the hot sub-channel in the simplified method.

731.87	732.25	717.02	737.24	718.33	731.57	733.32
	696.62	718.89	740.62	721.17	698.33	730.10
		696.06	737.47	698.99	717.14	718.05
			696.82	733.95	740.25	738.72
				701.08	718.90	719.83
					700.42	729.52
						734.55

Analysis of the hot assembly: Exit enthalpy of each channel

Figure 2.6

## 2.2 Simplified Method

### 2.2.0 Introduction

It is clear that the best lumped method of analysis, should be one that assigns a radial node to each actual sub-channel. Then the closer this goal is approached in our simplified method the better the results should be. For that reason, it was decided to use a case with as many channels as possible limited only by the cost of the analysis.

### 2.2.1 Case Analyzed

In order to compare the simplified method with the cascade method, the 89 channel case of Fig. 2.7 was analyzed. It can be observed that the pattern of channels of the hot assembly is that of the cascade analysis while outside of the hot assembly a finer mesh of channels was selected.

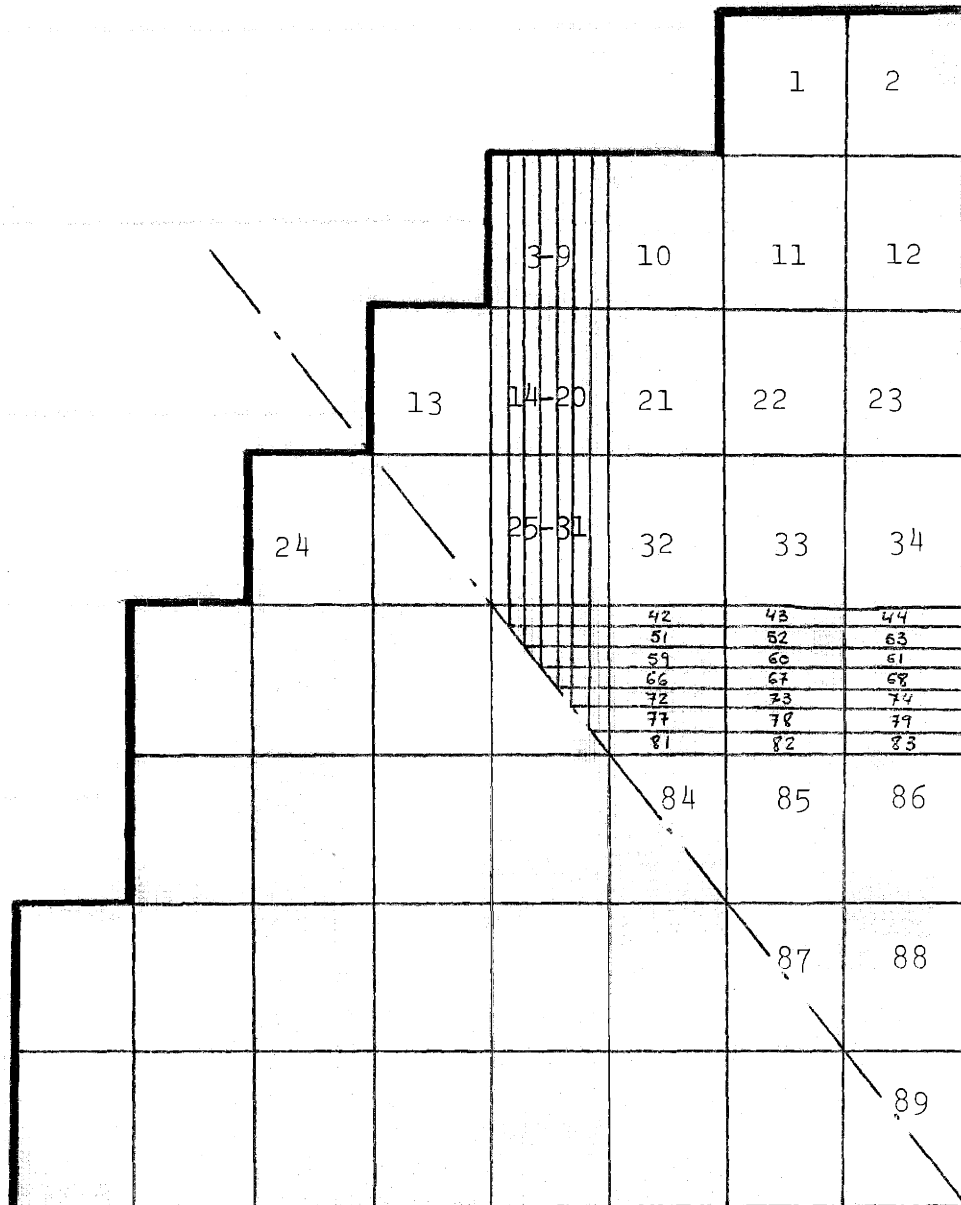
### 2.2.2 Results

In both Figure 2.8 and Figure 2.9 the exit enthalpies obtained with the simplified method are given.

## 2.3 Comparison of Results

### 2.3.1 Differences Observed Between Both Methods.

The exit enthalpies obtained with the cascade and the simplified method were compared and the differences are given



Simplified method: Numbering Scheme

Figure 2.7

						576.58	575.23		
						1	2		
					814.50	626.08	607.24	581.41	
					3-9	10	11	12	
					613.85	674.22	668.79	607.25	608.52
					13	14-20	21	22	23
					624.27	703.66	704.60	649.43	607.25
					24	25-31	32	33	34
						721.29	684.36	656.03	635.97
							621.56	631.40	603.55
							84	85	86
							625.25	616.26	
							87	88	
								594.31	
								89	

Simplified method: Exit enthalpy for each assembly

Figure 2.8

h = 728.63	730.06	717.20	732.80	718.62	728.80	728.09
	699.25	718.86	738.85	723.24	701.43	724.26
		699.16	734.70	702.65	715.88	715.80
			701.95	728.85	736.98	733.20
				705.20	719.83	718.55
					704.64	723.32
						723.76

Simplified method: Exit enthalpy for each channel of the hot assembly

Figure 2.9



in Figures 2.10 and 2.11. These differences are calculated for each channel using the following expression:

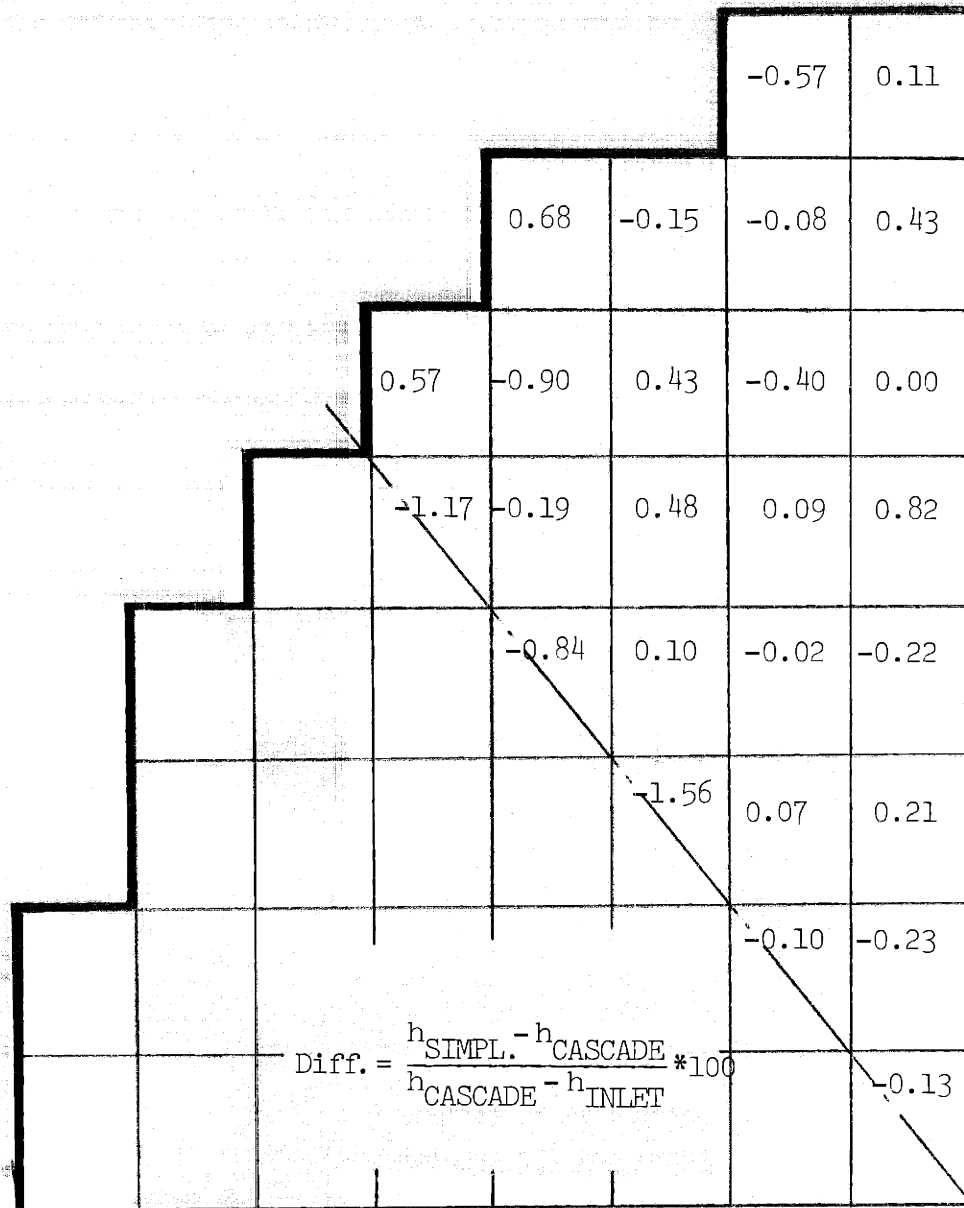
$$\text{Difference} = \frac{h_{\text{simplified}}(\text{exit}) - h_{\text{cascade}}(\text{exit})}{h_{\text{cascade}}(\text{exit}) - h(\text{inlet})} \times 100 \quad (2.17)$$

### 2.3.2 Analysis of These Differences

From Figure 2.10 we can observe that the assembly differences are quite small, nearly all are below 1%, and then we can conclude that both methods are comparable with respect to assembly results.

From Figure 2.11, it can be observed that all the hot channel differences are inside a 6% range, which is not a large value but significant enough to require further analysis in order to determine the causes of such differences.

As was said before, it is clear that the analysis of the whole core should be done on a subchannel basis in order to obtain the best results. When a lumped channel analysis is made, as in the simplified method, specific attention must be given to developing transport parameters between the lumped channels to obtain the same enthalpy results, for the lumped regions, that a subchannel analysis would yield. Then our simplified method will require use of such transport parameters to generate better results.



Normalized differences in exit enthalpy between the cascade and simplified methods (Assemblies)

Figure 2.10

1.76	-1.19	0.09	-2.35	-1.17	-1.51	-2.83
	1.77	0.00	-0.92	1.20	2.07	-3.22
		21.0	-1.46	2.43	-0.74	-1.33
			3.46	-2.75	-1.70	-2.90
				2.70	0.54	-0.75
					2.78	-3.48
						-5.80

Diff. =  $\frac{h_{\text{SIMPL.}} - h_{\text{CASCADE}}}{h_{\text{CASCADE}} - h_{\text{INLET}}}$

Normalized differences in exit enthalpy between the cascade and the simplified methods (hot assembly)

Figure 2.11

On the other hand, the cascade method would also require such transport parameters to deal with the lumped regions. In addition to that, the hot assembly analysis stage of the chain method has some very important problems due to the lack of good boundary conditions. Specifically these problems are:

a) Flow distribution inside the hot assembly.

The only information that is obtained from the first stage of the cascade method is the total crossflow that is leaving or entering each boundary of the assembly. No information is obtained regarding the distribution of axial and transverse flow between subchannels of the hot assembly. Some assumption must be made for the flow distribution but the present lack of a means to verify the assumption leads to questionable results. These problems will be more noticeable at the outer rows (where the boundary conditions established for the whole assembly will have a larger effect) of subchannels while in the interior of the assembly this effect will be smaller. Notice that because in the present analysis the channels are not actual subchannels but lumped channels, the effect described above is not too noticeable.

Additionally this treatment of diversion crossflow will introduce a further approximation due to averaging in the estimation of lateral energy and momentum transport. Specifically, for example, the energy transport will need to be based on the average assembly enthalpy and this average crossflow whereas in fact the actual number of subchannels on a face through which crossflow and energy exchange is occurring may be localized. Further the enthalpy of the coolant undergoing crossflow may be significantly different than the bundle average. In those steps where diversion crossflow is entering the hot assembly the problem becomes important.

One final uncertainty relates to the adequacy of the crossflow boundary condition applied to the hot assembly analysis. It is clear that local conditions inside the hot assembly affect the crossflow distribution. These local conditions are not taken into account in the assembly to assembly analysis where the boundary conditions for the hot assembly analysis are established.

- b) Mixing between the hot assembly and its adjacent channels in the hot assembly analysis.

Recall that for this case no turbulent interchange is taken into account ( $\beta = 0.0$ ) because in the analysis

of the hot assembly no interconnection exists with the actual adjacent assemblies. This can lead to significant overestimation of the enthalpy in the outer row of hot assembly subchannels. We can visualize some method to take into account this effect but the fact is that a new set of assumptions have to be made and there is not a data base to support those assumptions.

All these problems do not exist in the simplified method.

#### 2.4 Conclusions

Based on the factors discussed in Section 2.3.2 it is clear that the simplified method is better than the cascade, even without transport parameters for the lumped regions. Additionally as shown in Table 2.1 the cost of the cascade method as performed here is much more expensive than the simplified method. These factors led us to drop the cascade method as a standard and to develop adequate transport parameters to be used in the simplified method in order to obtain results as close as possible to those that would be given in a subchannel analysis.

Cost		Reading(\$)	Calculations(\$)	Printing(\$)
CASCADE ANALYSIS	Ass. to Ass. Analysis	0.11	14.17	4.13
	First slice	.12	.74	1.20
	Second	.12	.70	1.23
	Third	.12	.72	1.23
	Fourth	.12	.77	1.23
	Fifth	.12	1.29	1.23
	Sixth	.12	1.23	1.23
	Seventh	.12	1.03	1.23
	Eighth	.12	.95	1.23
	Ninth	.12	.69	1.23
	Tenth	.12	.78	1.23
	Eleventh	.12	.69	1.23
	TOTAL	1.43	23.76	17.63
SIMPLIFIED METHOD		.18	18.65	5.99

Costs of the cascade and the simplified methods

TABLE 2.1

## Chapter 3

### SIMPLIFIED METHOD

- 3.0 Introduction
  
- 3.1 Simplified Method with No Coupling Parameters
  - 3.1.1 - 101 channel case
  - 3.1.2 - 61 channel case
  - 3.1.2 - 30 channel case
  - 3.1.4 - 10 channel case
  
- 3.2 Simplified Method Using Transport Parameter  $N_H$ ,  
( $N_H = N$  case)
  - 3.2.0 - Introduction
  - 3.2.1 - 101 channel case
  - 3.2.2 - 61 channel case
  - 3.2.3 - 30 channel case
  - 3.2.4 - 10 channel case
  
- 3.3 Analysis of the Results
  - 3.3.1 Analysis of the  $N_H = N$  case
    - 3.3.1.1 Analysis of the MDNBR Results
    - 3.3.1.2 Analysis of the Enthalpy Results
  
- 3.4 Simplified Analysis Using Exact Transport Parameters.



### 3.0 Introduction

In this chapter the simplified method will be studied in some detail.

Two parameters selected to carry out that job are the number of channels used to describe the problem and the transport coefficients (see Chong Chiu's S.M. Thesis, 1976)<sup>5</sup>. Then for a selected transport coefficient, the core will be analyzed using different patterns of channels to describe it. From the results, we will observe the effect of nodal representation upon the MDNBR. In order to isolate the effect of the transport coefficients, cases with the same pattern of channels but different coefficients also need to be analyzed.

It was concluded then, that the different cases of Table 3.1 should be analyzed. The first column corresponds to the case in which no transport parameters are used, as in COBRA IIIC. The second column represents the case in which the only transport parameter used is  $N_H$  and it is assumed that  $N_H$  is independent of  $z$  and equal to the number of subchannels existing between the center lines of the channel that make-up the boundary considered. This assumption is equivalent to an assumption of a linear enthalpy variation along the channels.<sup>(5)</sup> This parameter is that suggested in reference (4) as reported in reference (3).

Transport Parameter

Pattern of Channels	$N_H = 1$	$N_H = N$	$N_H$ $N_H$ $\vdots$
	101 Channels		
	61		
	30		
	10		

Cases that should be analyzed

TABLE 3.1

The third column has not yet been analyzed because of lack of time to carry out the work. In this column it is intended to introduce not only  $N_H'$  (required in the diversion crossflow term of the energy conservation equation), and also some other parameters ( $N_H$ ,  $N_{TP}$ , ...) that are required in the axial and transverse momentum equations. These coefficients have been developed in Chong Chiu's S.M. thesis<sup>(5)</sup> for two dimensional problems. However, for all the cases considered in the present thesis, the problems are three dimensional. Two options are available at this point. One is to show that the two-dimensional coefficients outlined above also yield good results for three dimensional problems. The other is to develop some new transport coefficients for three dimensional problems. Exploration of these options is required in the future.

In this chapter, the results obtained for the first and second columns of Table 3.1 will be given. Also the conclusions derived from these results are presented.

### 3.1 Simplified Method with No Coupling Parameters ( $N_H=1$ )

#### 3.1.1 101 channel case

The radial power factor of the lumped regions are obtained by averaging the values given in Appendix 1 over the region.

The core was analyzed using the pattern of channels given in Figures 3.1 and 3.2. The results are summarized in Figures 3.3 and 3.4.

### 3.1.2 61 channel case

The core was divided as indicated in Figures 3.5 and 3.6. The results are given in Tables 3.7 and 3.8.

### 3.1.3 30 channel case

The division of the core is given in Figures 3.9 and 3.10, while the results are those of Figures 3.11 and 3.12.

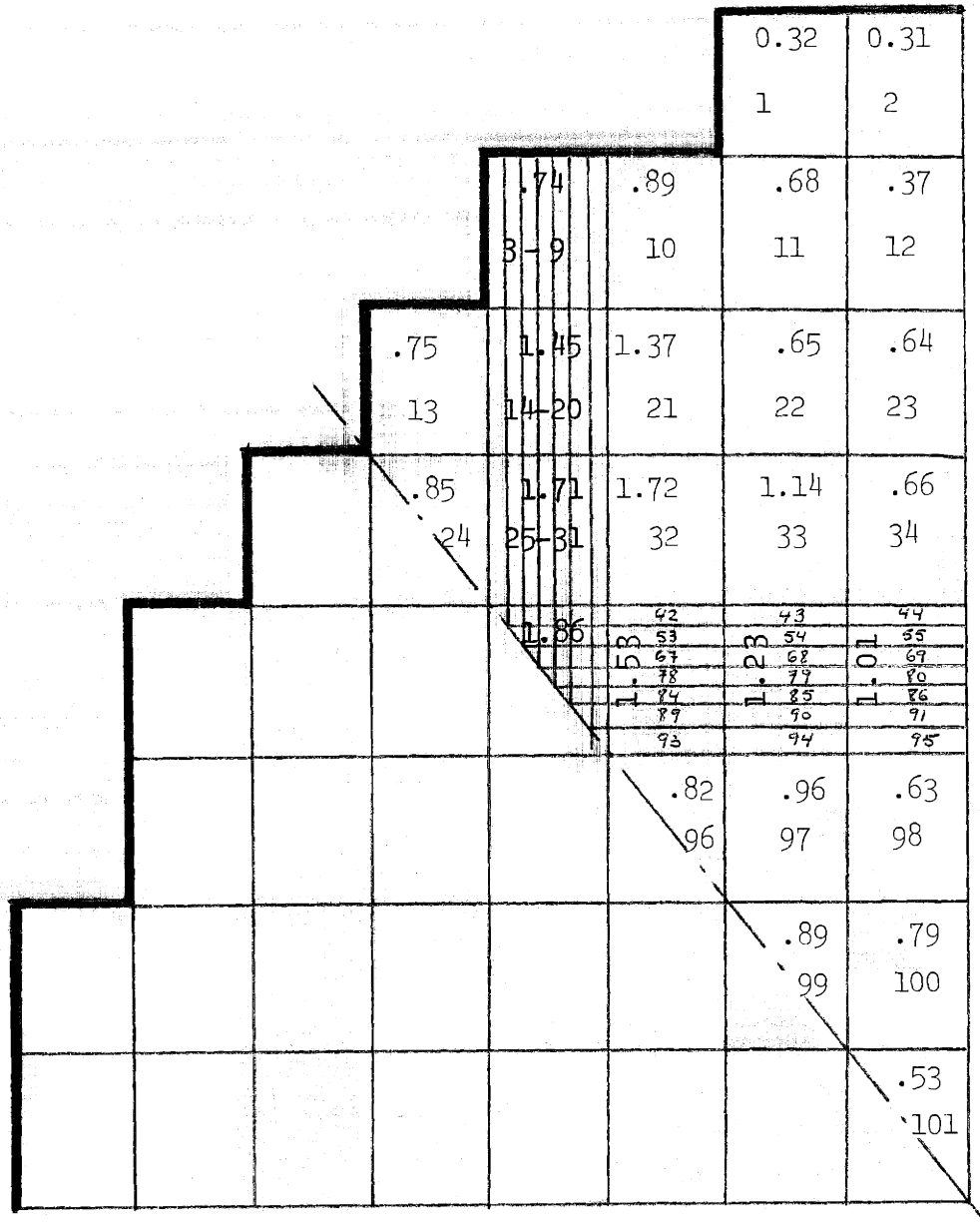
### 3.1.4 10 channel case

The core was divided as in Figures 3.13 and 3.14. The results for this case are presented in Figures 3.15 and 3.16.

## 3.2 Simplified Method Using Transport Parameter $N_H$

### 3.2.0 introduction

In this section, the four cases described in the previous section will be analyzed, but here a transport coefficient is introduced in the energy equation. This equation becomes:



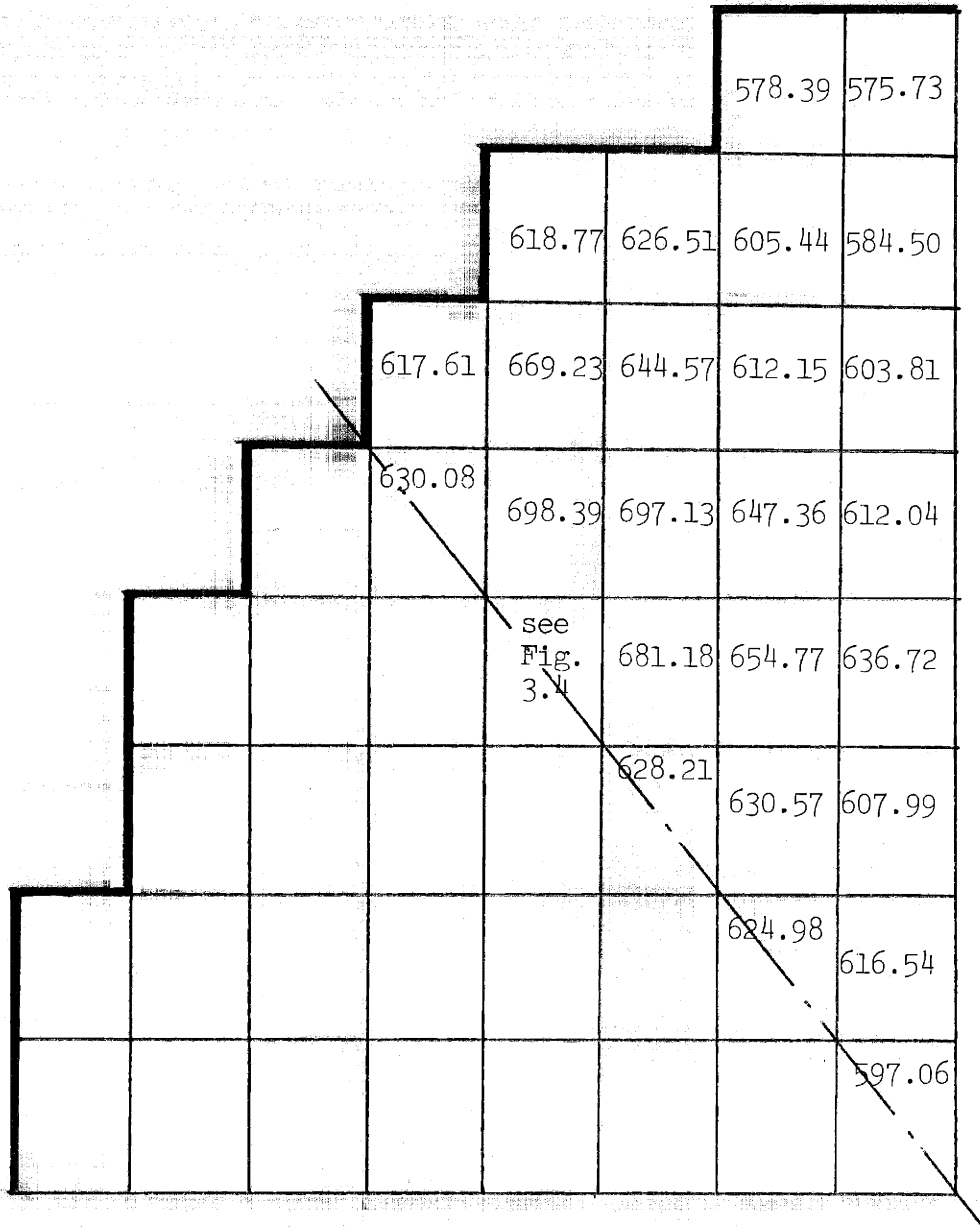
101 Channel case: Numbering scheme

Figure 3.1

35 1.917	36 1.973	37 1.799	38 1.974	39 1.799	40 1.973	41 1.917		
	45 1.556	46 1.859	47 2.011	48 1.539 56 2.060	49 1.571 57 2.266	50 1.561 58 1.582	51 1.519 59 1.561	52 1.973
		60 1.553	61 2.039	62 1.547 70 1.547	63 1.570 71 1.547	64 2.266 72 2.063	65 1.573 73 1.541	66 1.799
			74 1.510	75 2.039	76 2.011	77 1.974		
				81 1.553	82 1.859	83 1.799		
					87 1.556	88 1.973		
							92 1.917	

101 Channel case: Numbering scheme of the hot bundle

Figure 3.2



101 Channel case: Exit enthalpies

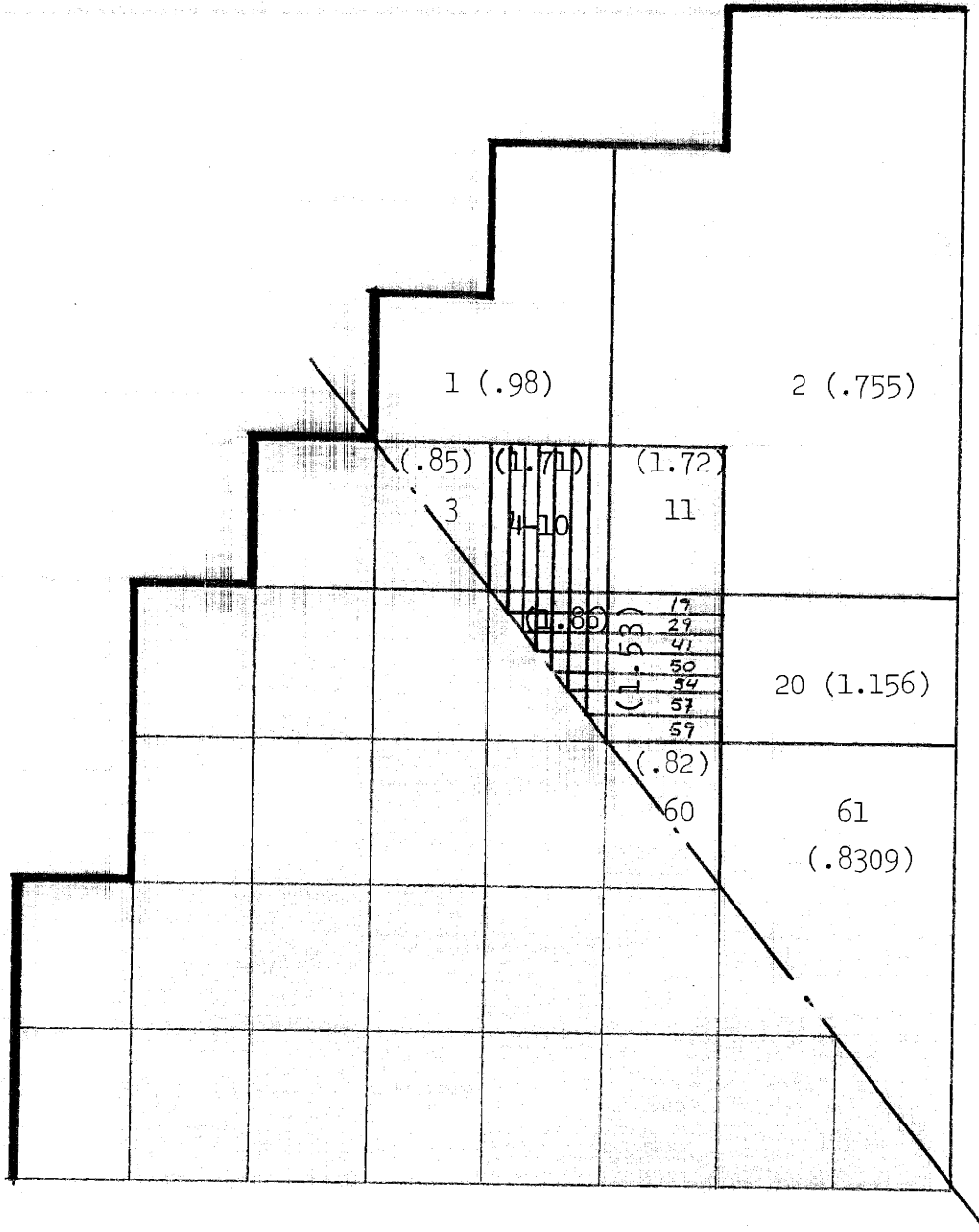
Figure 3.3

708.89	715.47	717.11	719.70	715.87	714.66	708.31		
	715.40	718.65	723.10	718.51	715.63	713.57	711.74	706.83
				719.81	717.37	714.79	711.59	
		717.43	720.25	718.50	717.78	717.14	712.67	706.94
				719.18	719.16	719.70	716.05	
			717.93	720.03	720.36			710.26
				710.16	715.33			707.47
						711.03		702.61
								688.19

101 Channel case: Exist enthalpies for the channels of the hot assembly

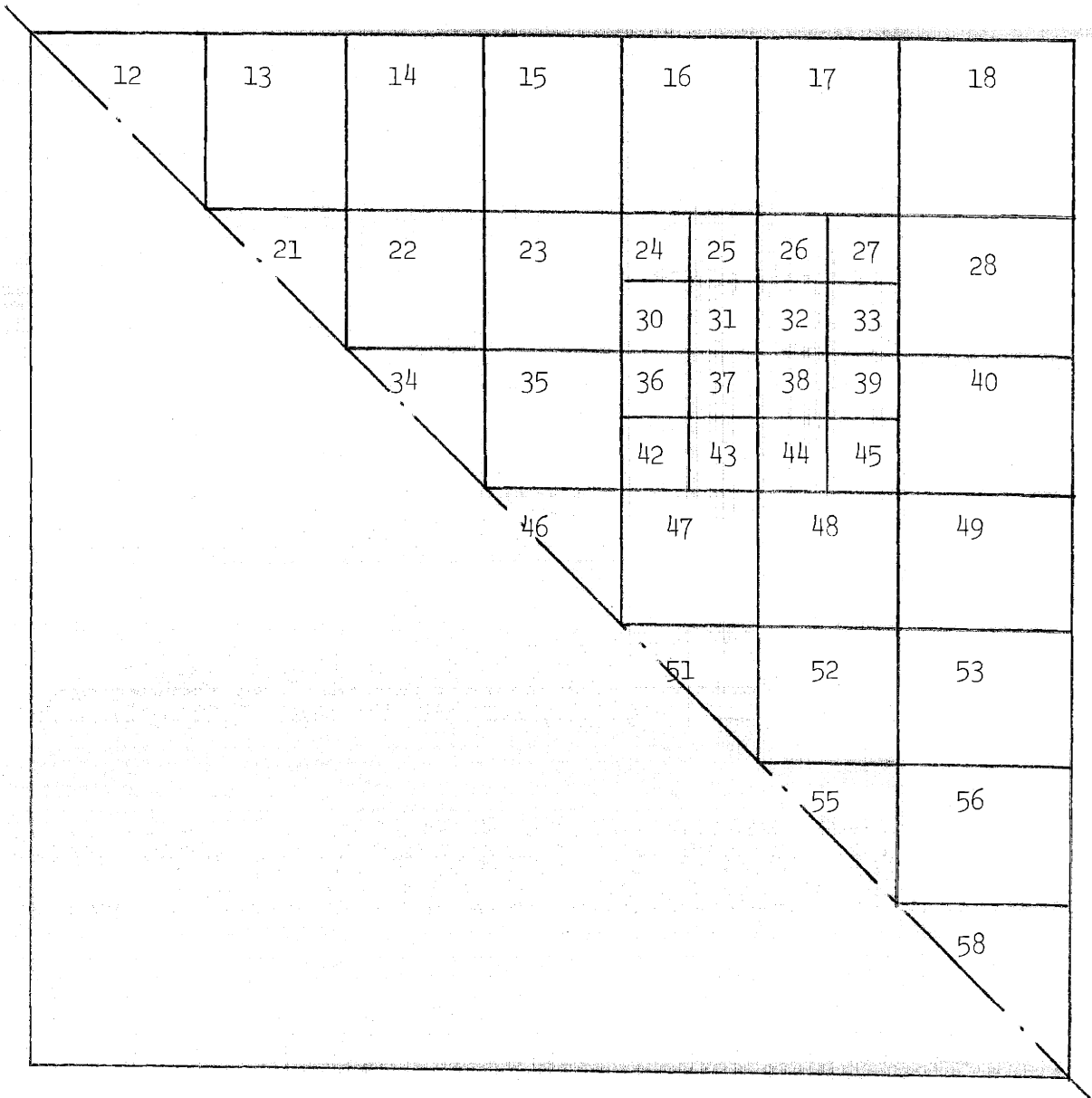
Figure 3.4





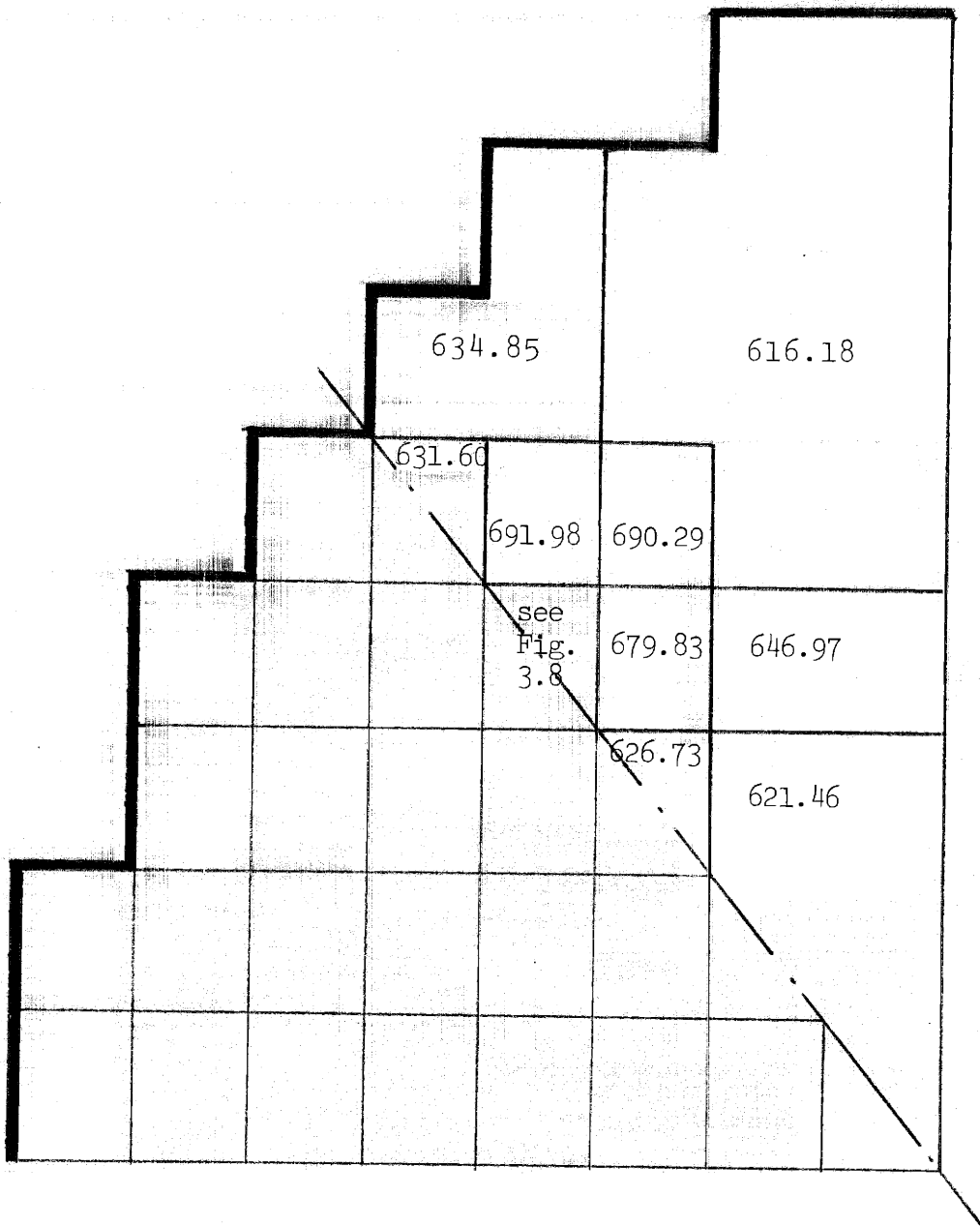
61 Channel case: Numbering scheme

Figure 3.5



61 Channel case: Numbering scheme inside the hot bundle

Figure 3.6



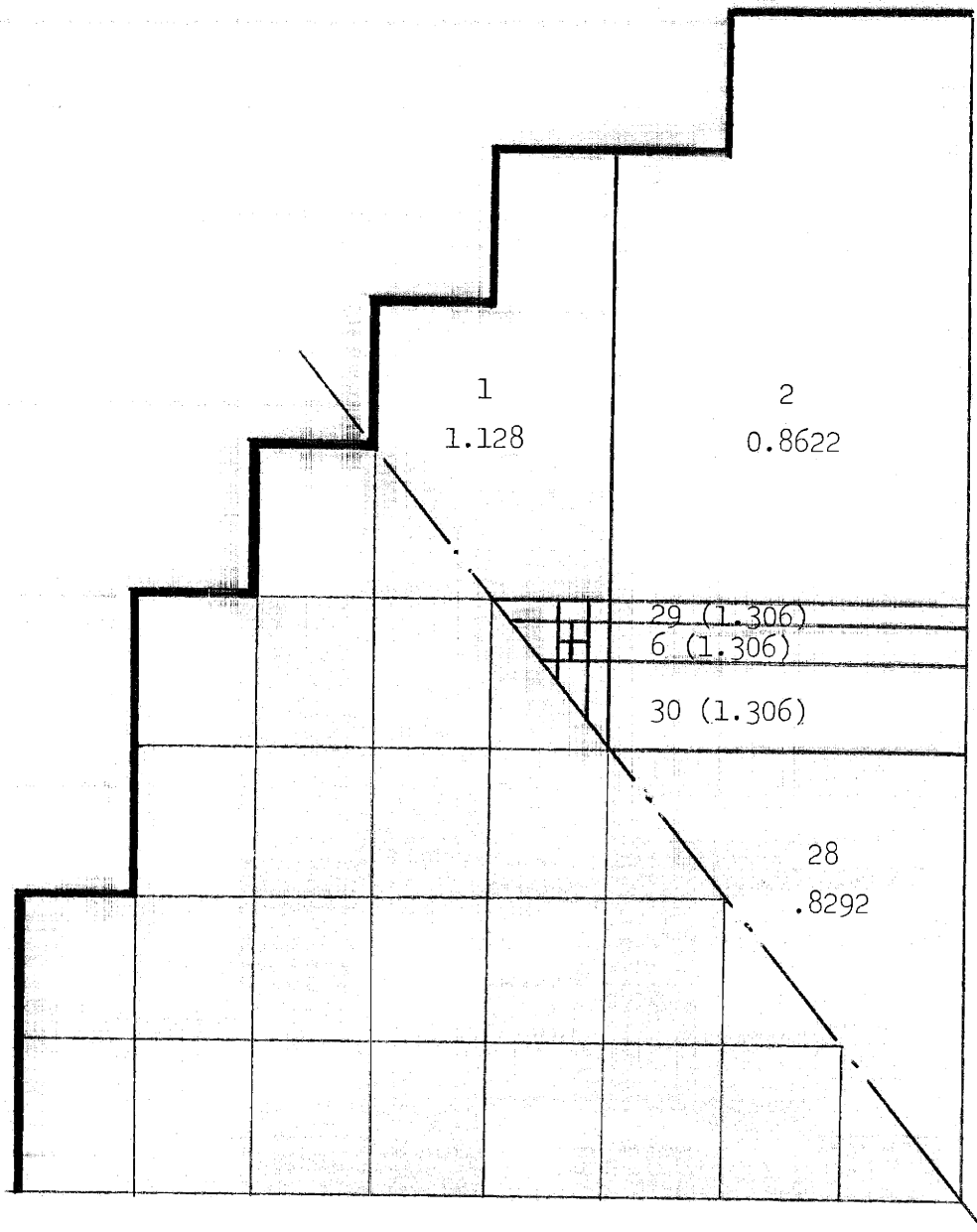
61 Channel case: Exit enthalpies outside the hot assembly

Figure 3.7

706.01	714.61	715.60	718.70	714.57	714.22	710.21	
714.22	718.03	724.73	719.22	715.77	713.35	711.67	708.61
			721.38	718.61	715.35	711.77	
	715.99	721.26	718.39	717.44	717.98	713.11	707.65
			718.34	718.09	720.60	716.80	
		717.12	720.51	722.60			711.93
			715.62	716.40			709.52
					711.95		707.19
							694.46

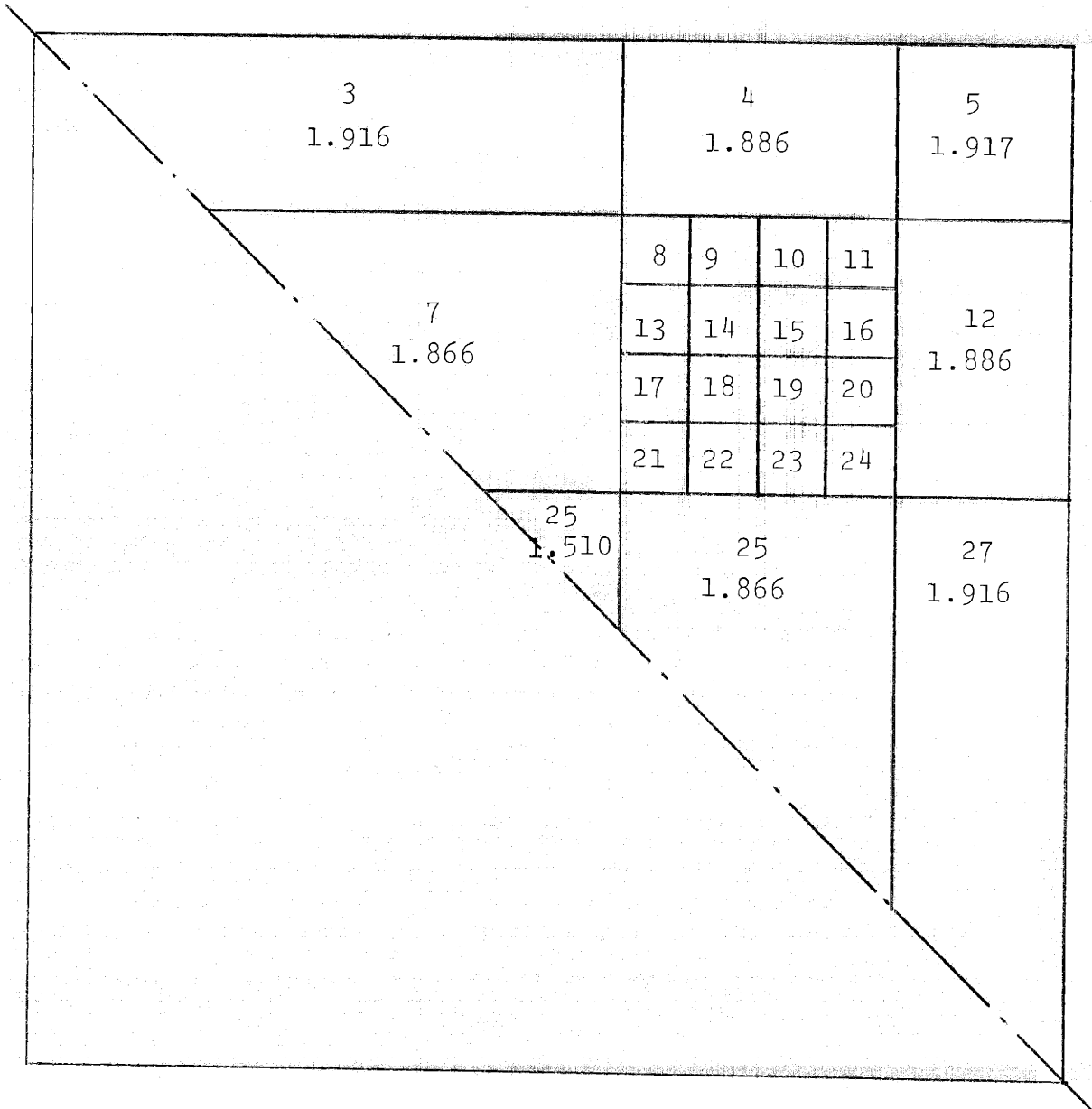
61 Channel case: Exit enthalpies inside the hot assembly

Figure 3.8



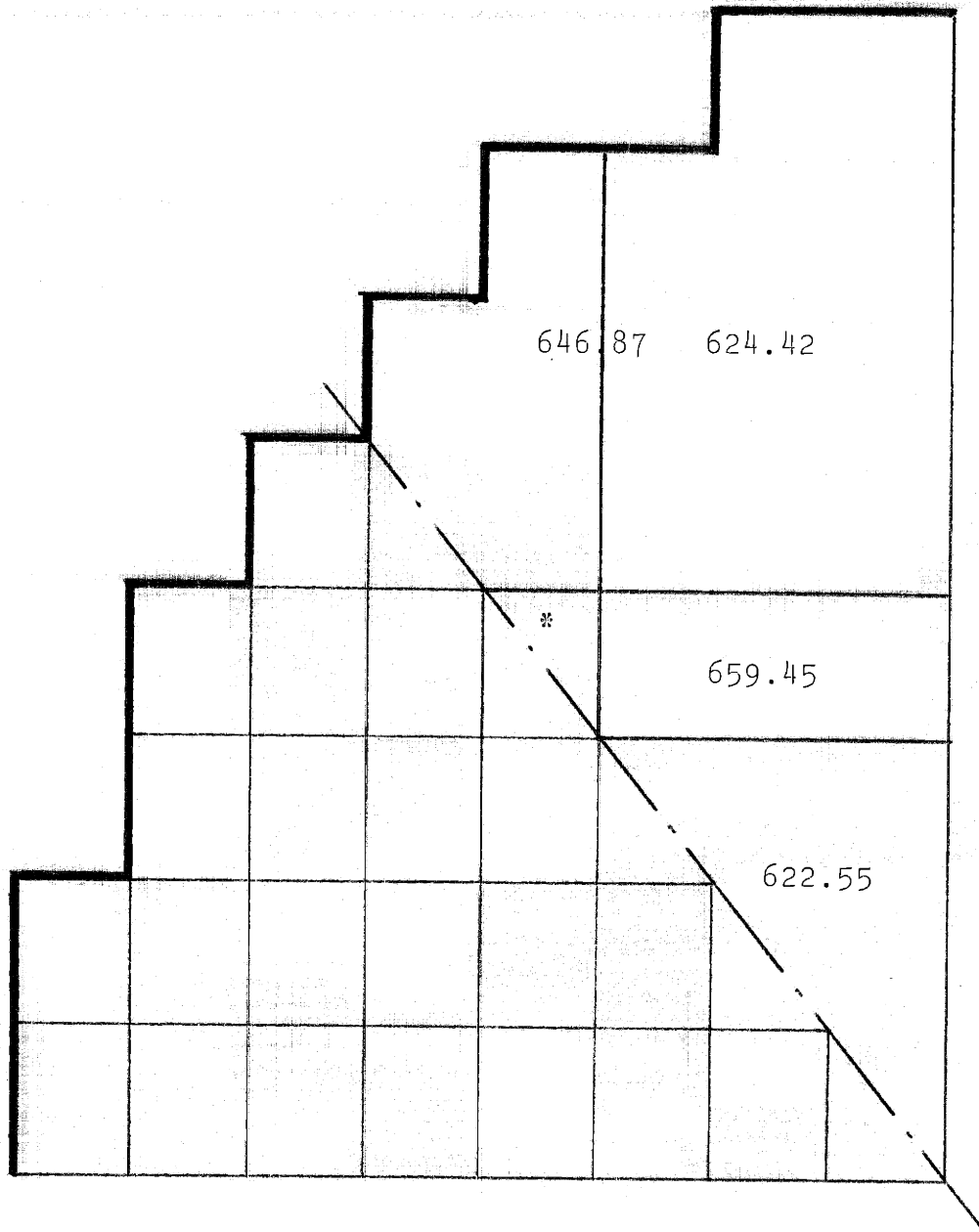
30 Channel case: Numbering scheme

Figure 3.9



30 Channel case: Numbering scheme of the hot assembly

Figure 3.10

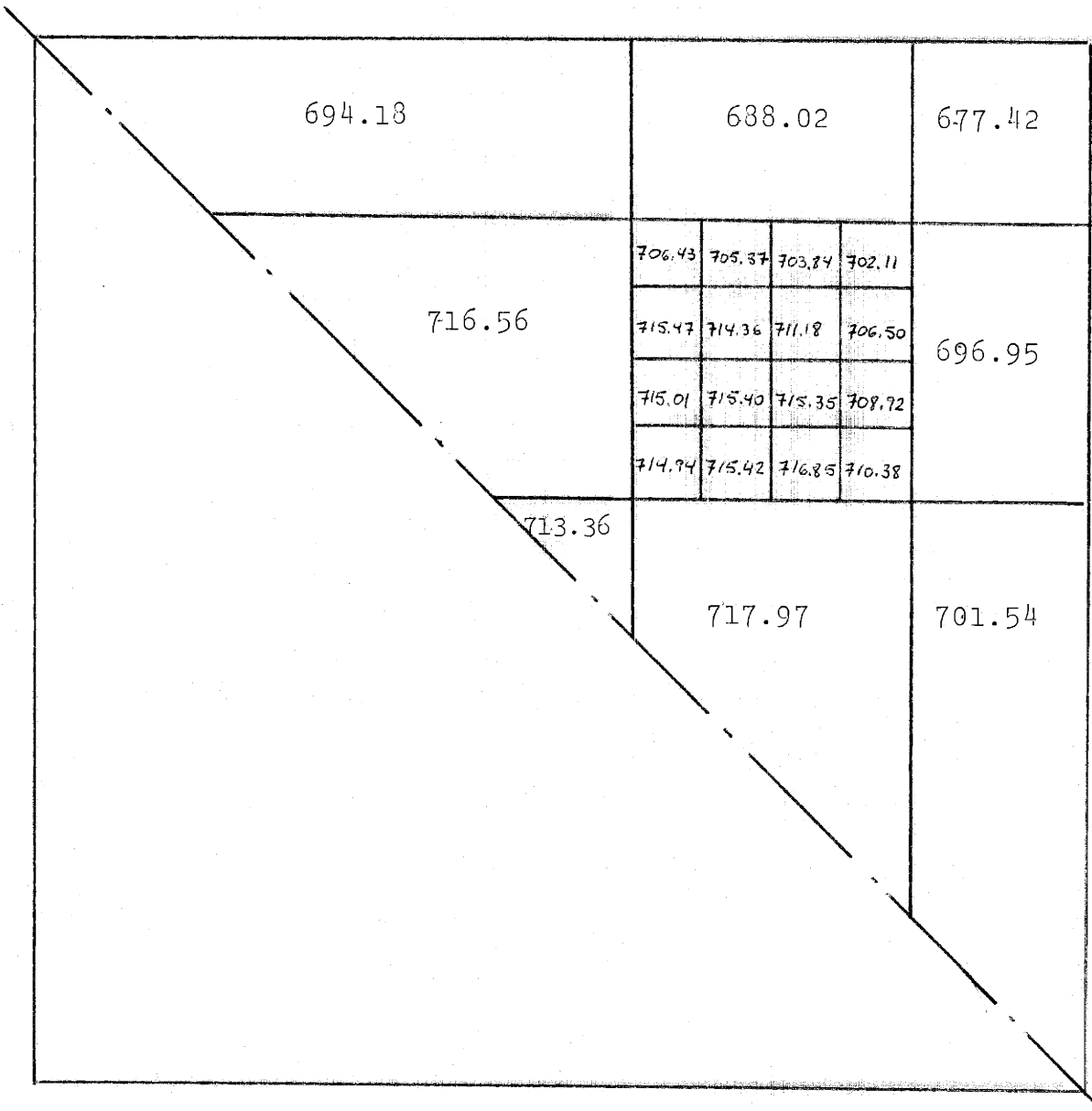


30 Channel Case

Exit Enthalpies Outside the Hot Assembly

Figure 3.11

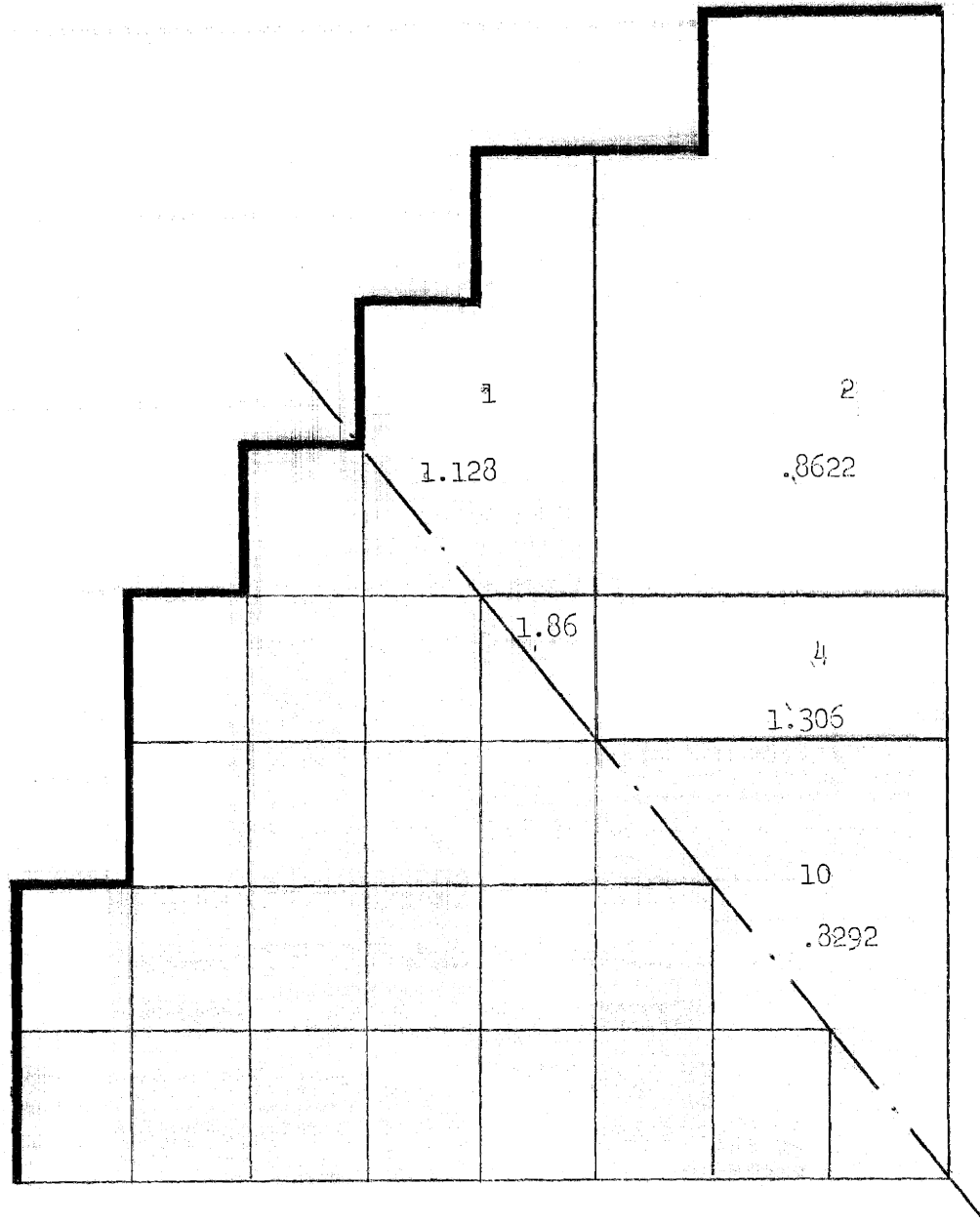
\*see figure 3.12



30 channel case  
exit enthalpies inside the hot assembly

Figure 3.12

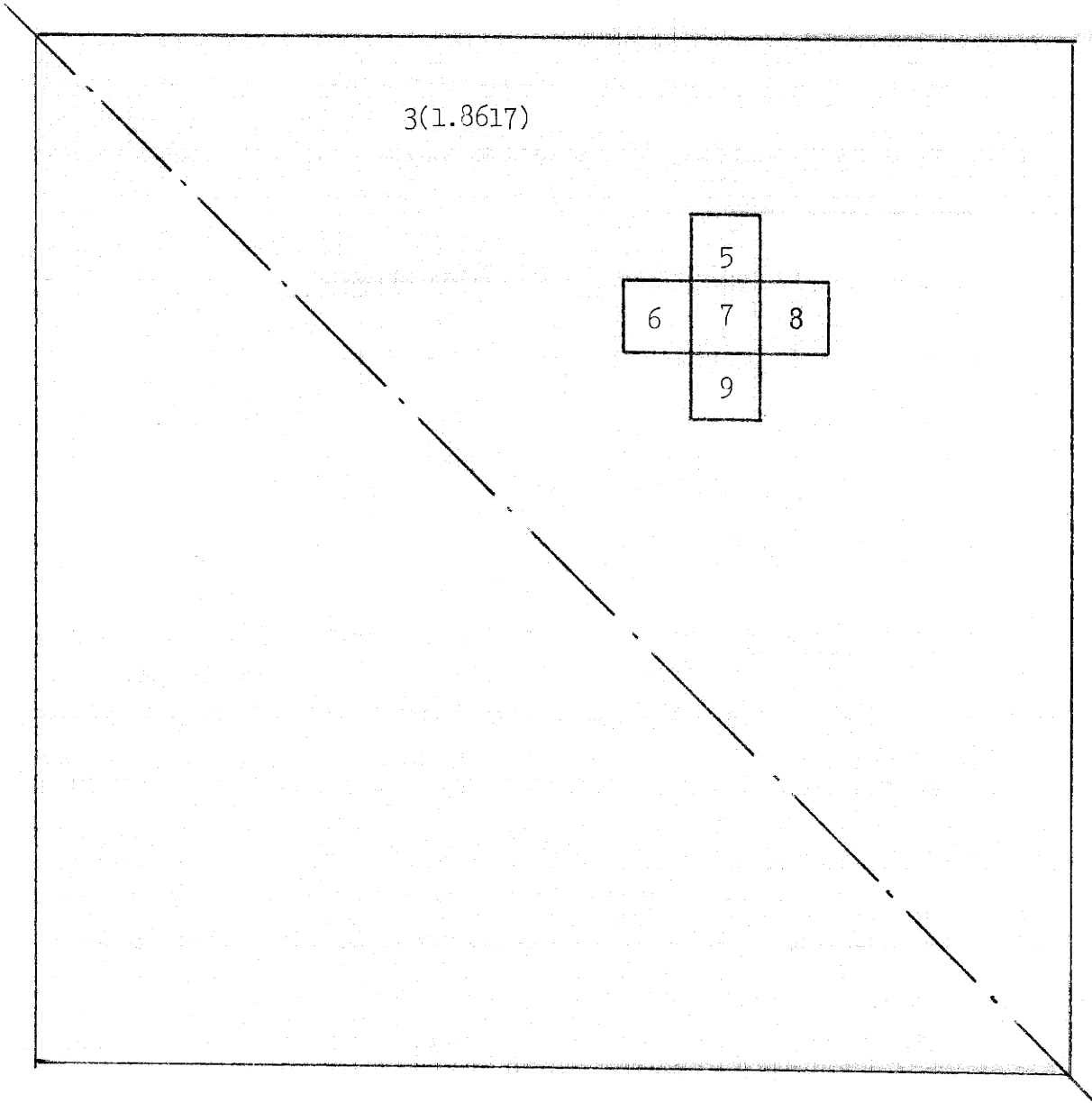




10 Channel Case

Numbering Scheme Radial Peaking Factors

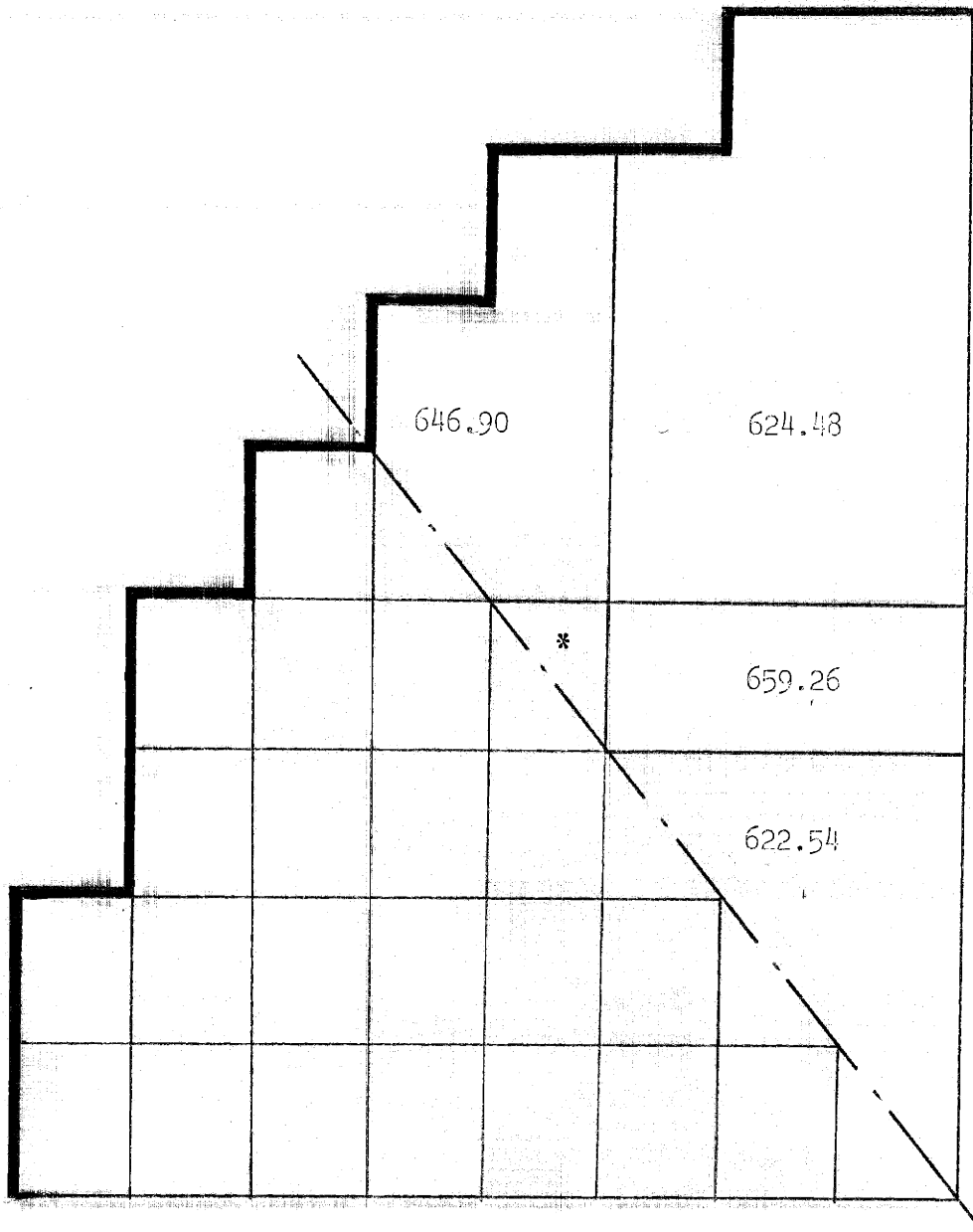
Figure 3.13



10 Channel Case

Numbering Scheme of the Hot Assembly  
Radial Peaking Factors

Figure 3.14

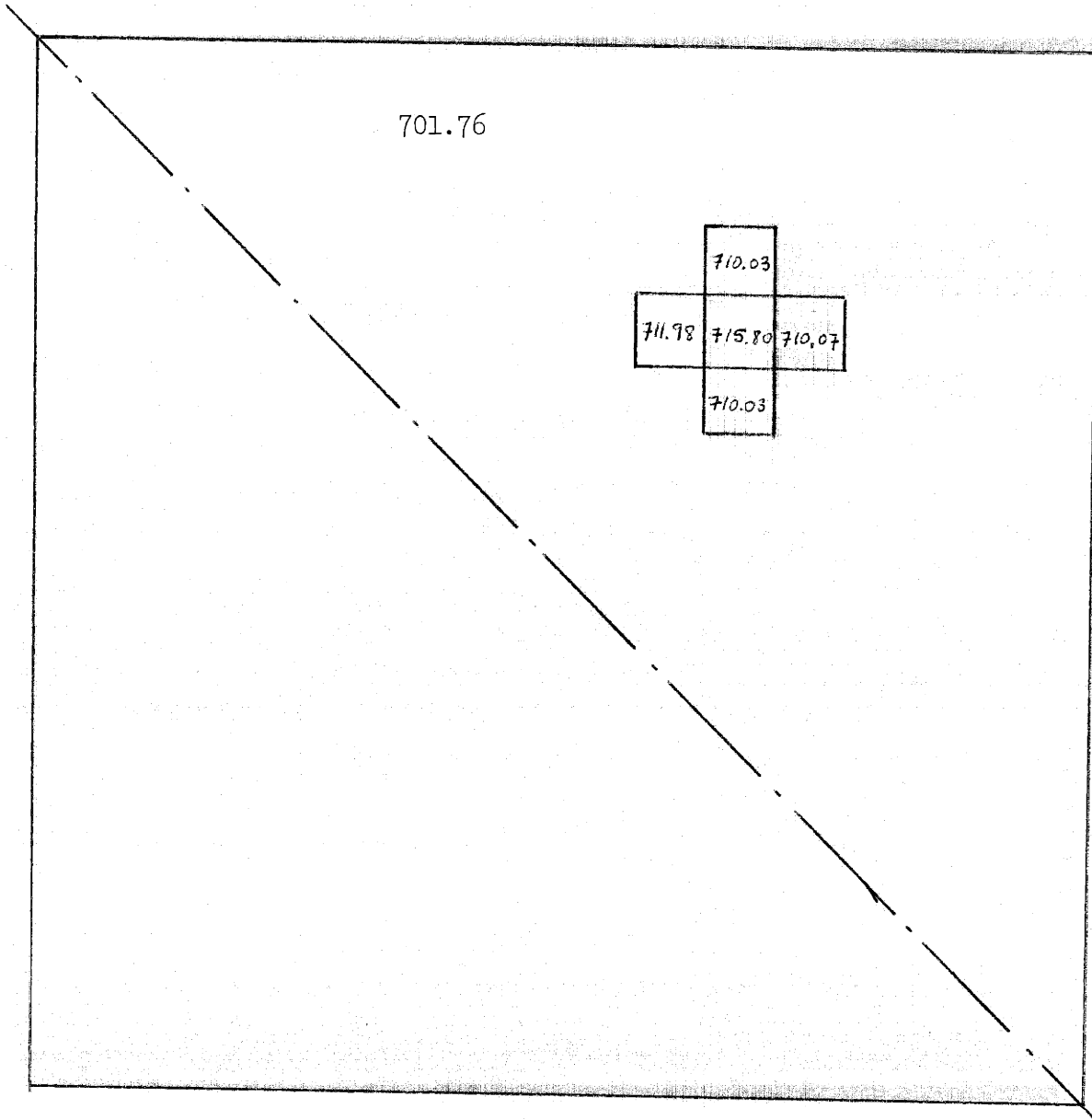


10 Channel Case

Exit Enthalpies Outside the Hot Assembly

Figure 3.15

\* see figure 3.16



10 Channel Case

Exit Enthalpies Inside the Hot Assembly

Figure 3.16

$$\begin{aligned}
 h_{J+1}(a) = h_J(A) + \frac{q'_{J+\frac{1}{2}}(A)}{M_J(A)} \Delta x - \sum_B \frac{W_J(A,B) (h_J^* - h_J(A))}{M_H(A)} - \\
 - \sum_B \frac{W'_J(A,B)}{M_J(A)} \frac{(h_J(A) - h_J(B))}{N_H(A,B)} \quad (3.1)
 \end{aligned}$$

where comparing it with equation (5.1) we can notice the introduction of the  $N_H(A,B)$  parameter.

The parameter  $N_H(A,B)$  is assumed to be only a function of the number of subchannels that separate the center lines of channels A and B and it is taken as being exactly that value.

### 3.2.1 101 Channel Case

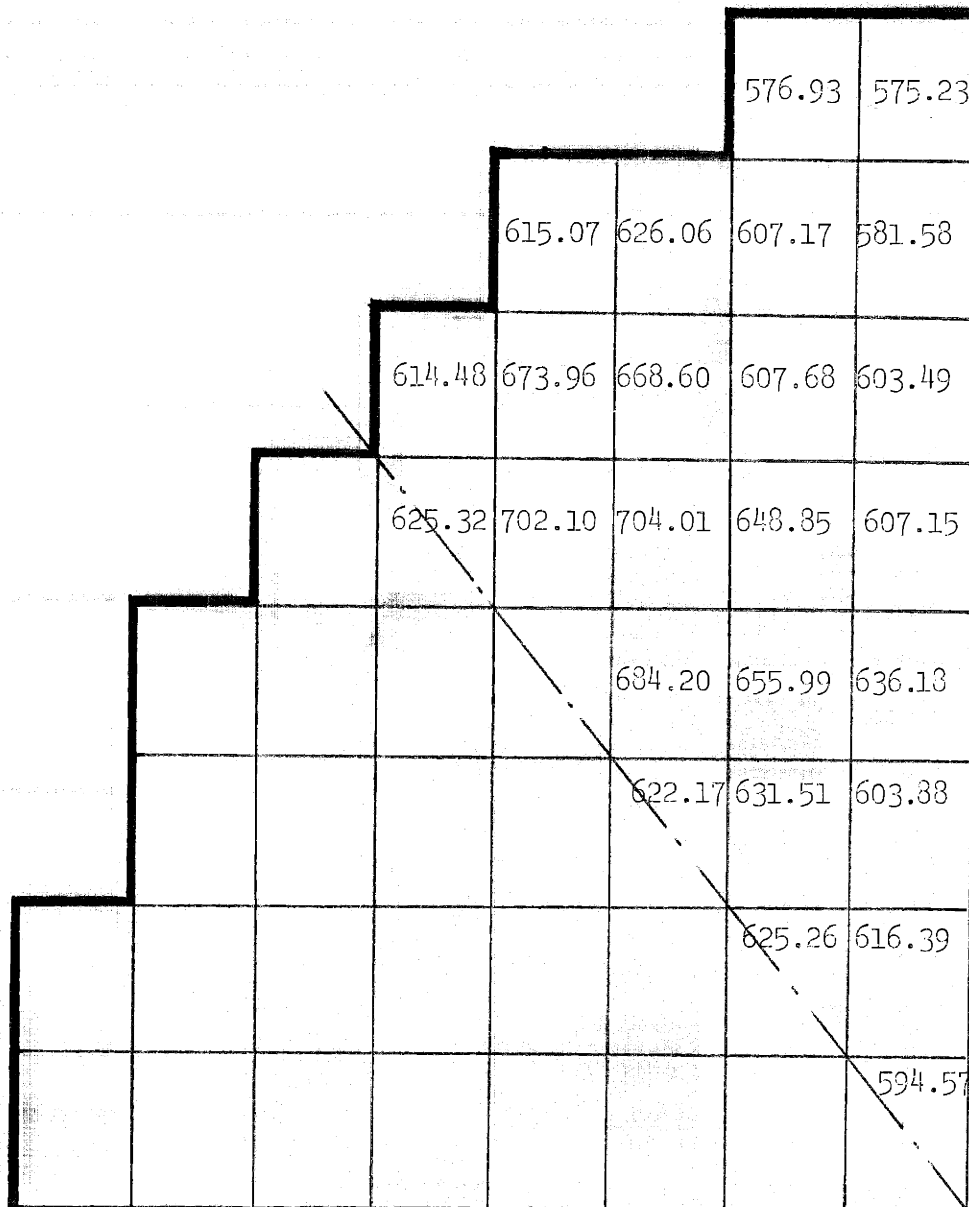
The exit enthalpies for each assembly and for each channel of the hot assembly are given in Figures 3.17 and 3.18.

### 3.2.2 61 Channel Case

The results are those of Figures 3.19, 3.20 and 3.21. Also in these figures the differences in enthalpy with respect to the 101 channel case are given.

### 3.2.3 30 Channel Case

The results are presented in Figures 3.22, 3.23 and 3.24.



$N_H = N$  and 101 Channel Case.

Exit Enthalpies Outside the HOT Assembly

Figure 3.17

718.05	722.20	720.77	726.74	720.17	722.25	723.54		
	714.36	717.61	728.01	721.47	716.66	713.99	713.44	720.29
				722.76	718.72	715.51	713.53	
		712.55	722.39	719.05	717.10	717.77	715.53	717.56
				718.73	717.32	720.87	717.81	
			712.23	722.03	727.62			725.99
				712.23	717.39			719.74
						712.44		719.67
								713.51

$N_H = N$  and 101 Channel Case.

Exit Enthalpies Inside the Hot Assembly

Figure 3.18



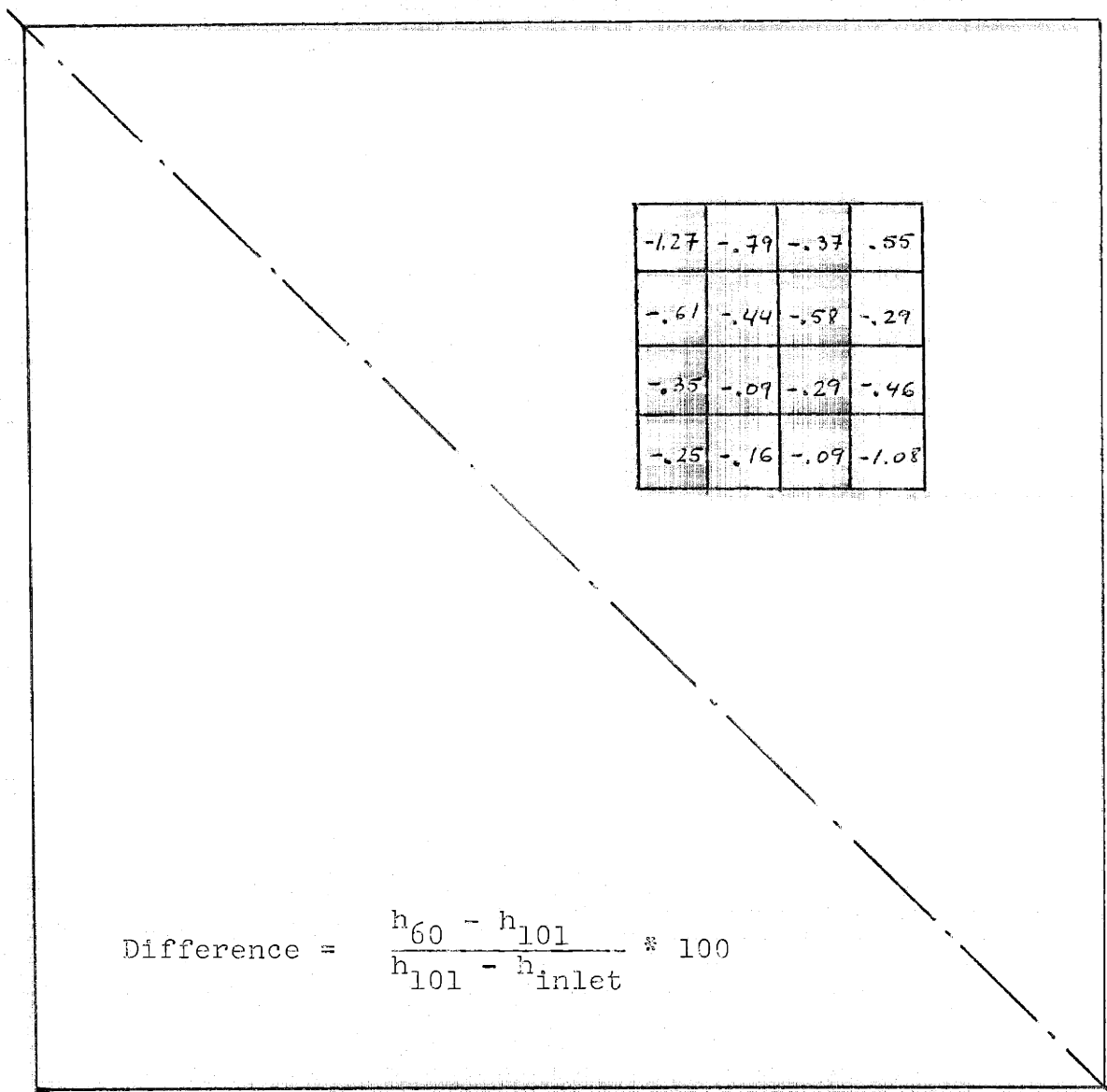


727.69 (5.69%)	725.21 (1.73%)	720.53 (-0.14%)	728.41 (.94%)	718.31 (-.79%)	723.04 (.45%)	723.59 (.03%)
	709.80 (-2.75%)	718.25 (.38%)	730.66 (1.48%)	719.27 715.32 713.38 714.35		719.36 (-.54%)
		710.55 (-1.22%)	724.42 (.88%)	721.70 717.76 714.53 713.05		715.64 (-1.13%)
			712.60 (-.37%)	718.45 716.95 717.28 714.75		725.50 (-.27%)
				718.30 717.55 720.70 717.75		
				712.68 (.27%)	718.48 (.35%)	719.28 (-.27%)
					711.58 (-.52%)	721.49 (1.06%)
						721.27 (4.71%)

$N_H = N$  and 60 Channel Case.

Exit Enthalpies and Differences Inside the Hot Assembly

Figure 3.20

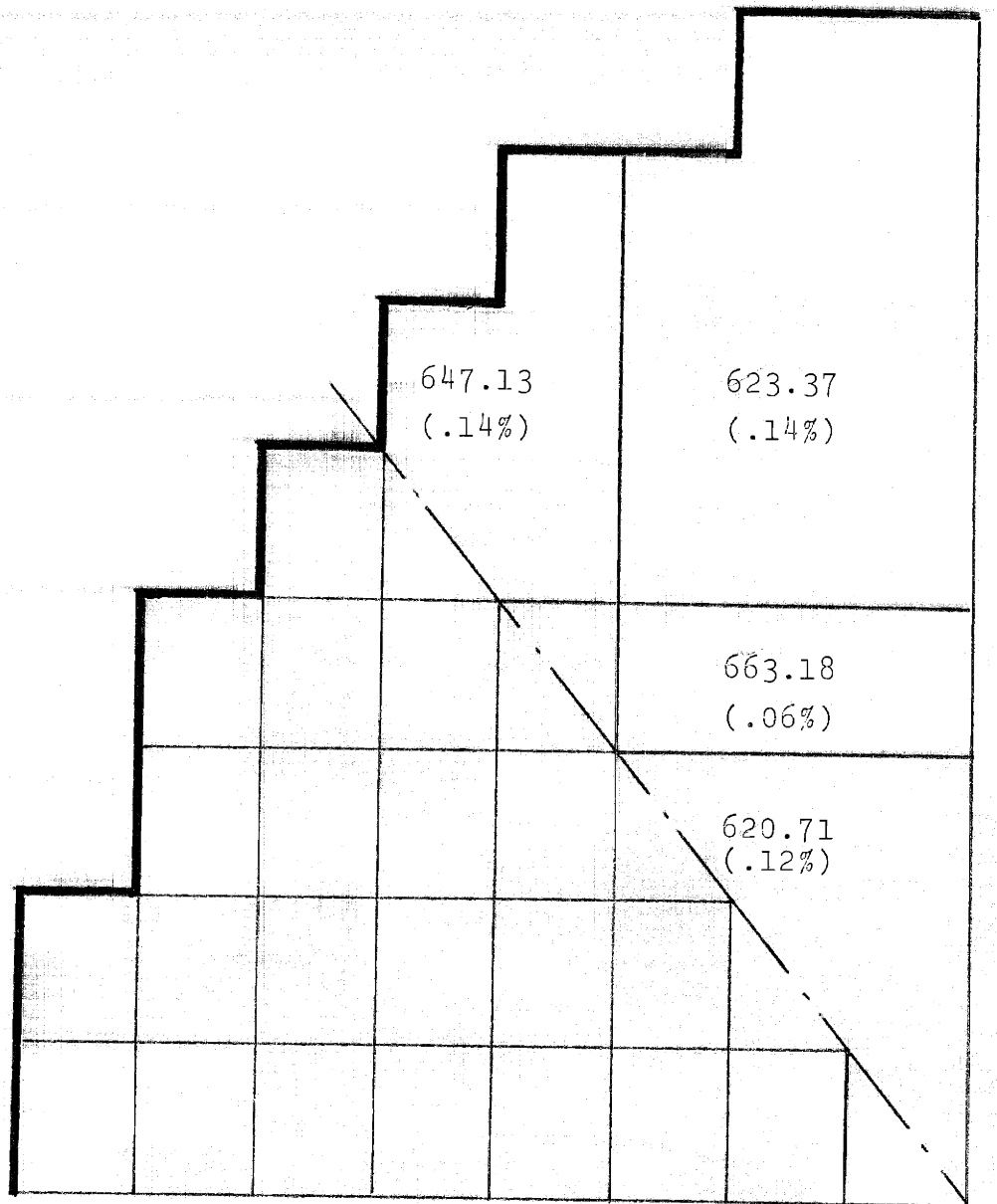


$$\text{Difference} = \frac{h_{60} - h_{101}}{h_{101} - h_{\text{inlet}}} * 100$$

$N_H = N$  and 60 Channel Case.

Differences in Enthalpy with Respect  
to the  $N_H = N$  and 101 Channel Case

Figure 3.21

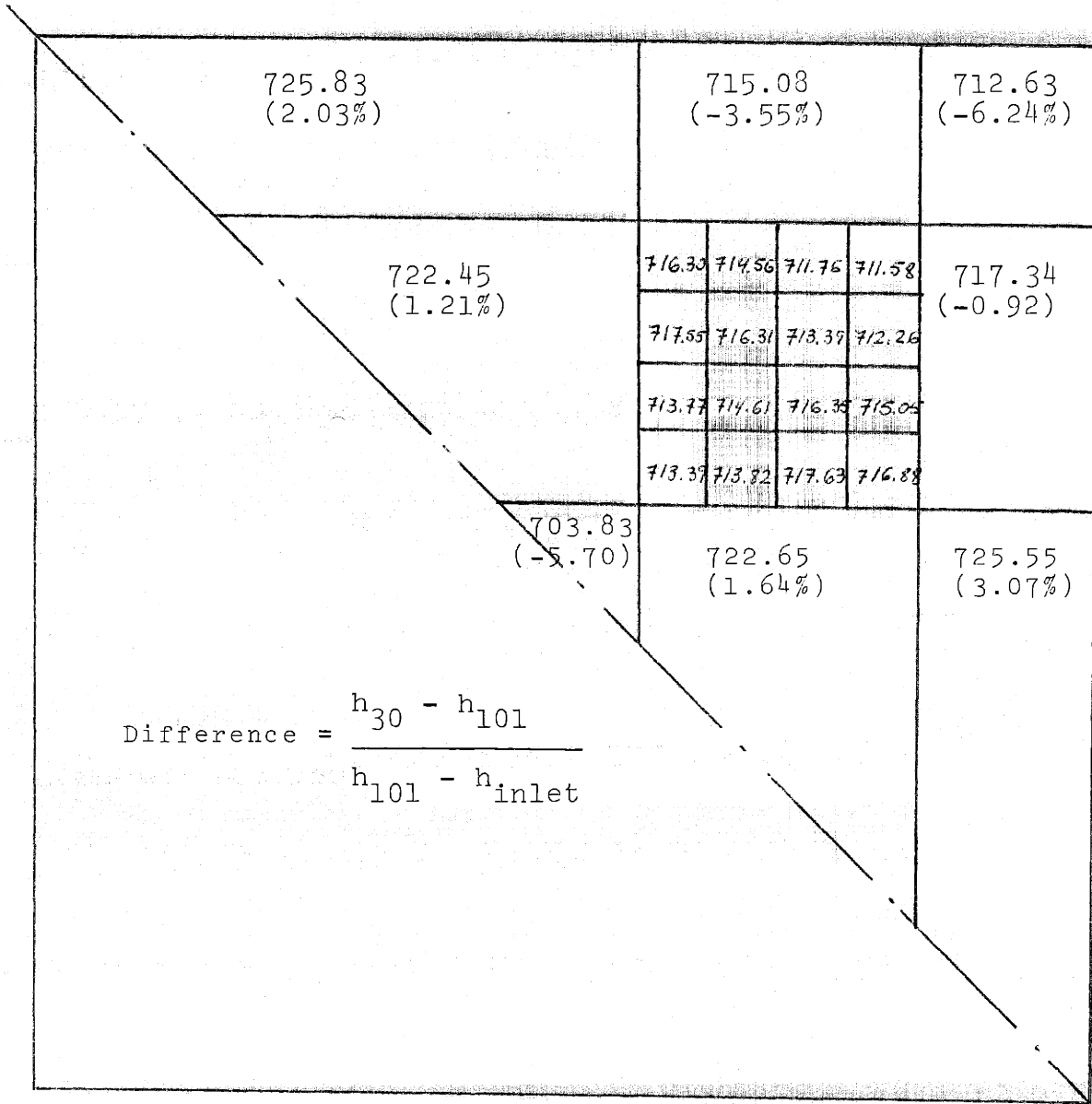


$$\text{Difference} = \frac{h_{30} - h_{101}}{h_{101} - h_{\text{inlet}}} \#100$$

$N_H = N$  and 30 Channel Case

Exit Enthalpies and Differences Outside the Hot Assembly

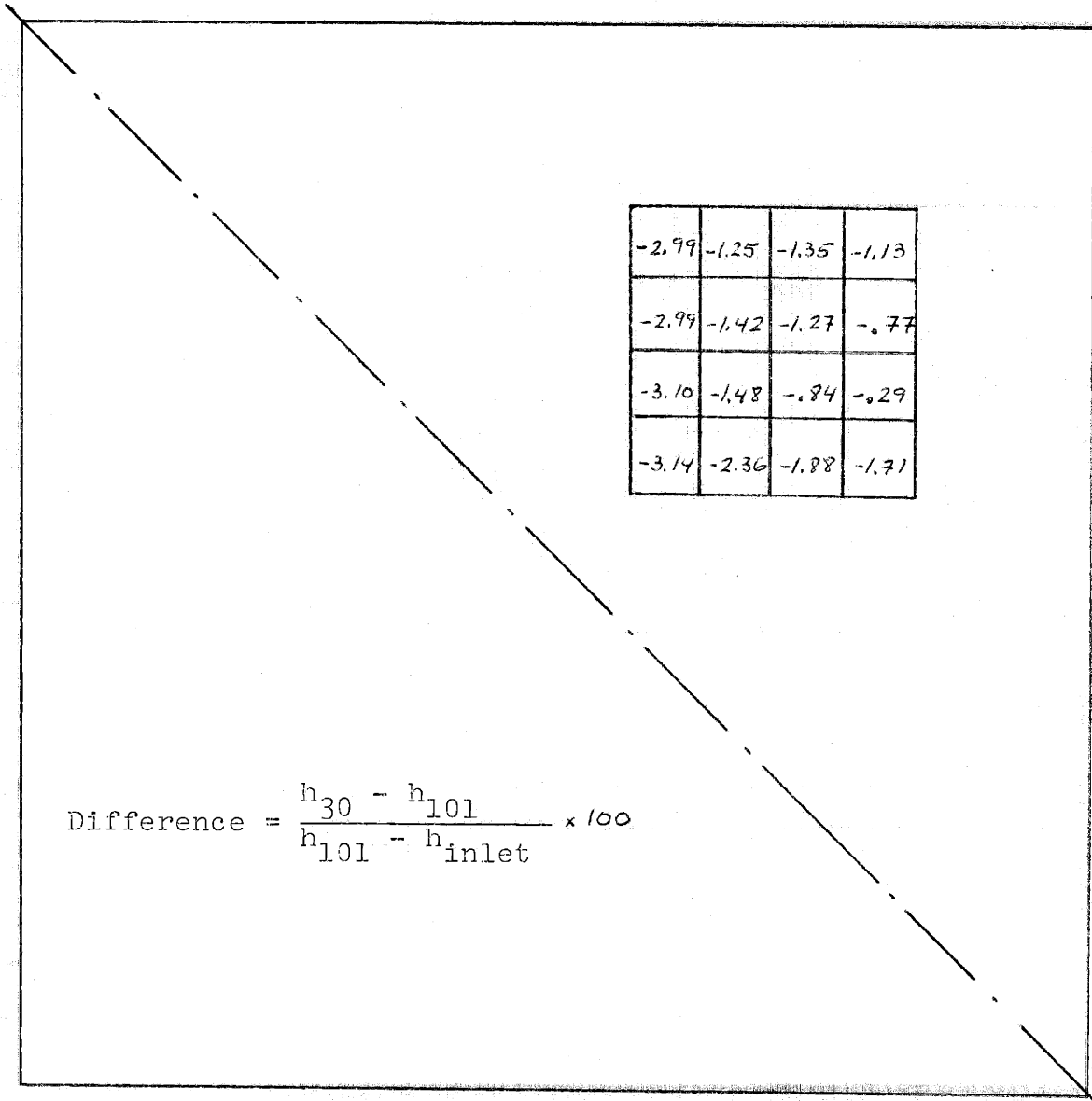
Figure 3.22



$N_H = N$  and 30 Channel Case.

Exit Enthalpies and Differences Inside  
The Hot Assembly

Figure 3.23



$N_H = N$  and 30 Channel Case.

Difference in Enthalpy with Respect to  
the  $N_H = N$  and 101 Channel Case

Figure 3.24

#### 3.2.4 10 channel case

The results are given in Figures 3.25, 3.26 and 3.27.

### 3.3 Analysis of the Results

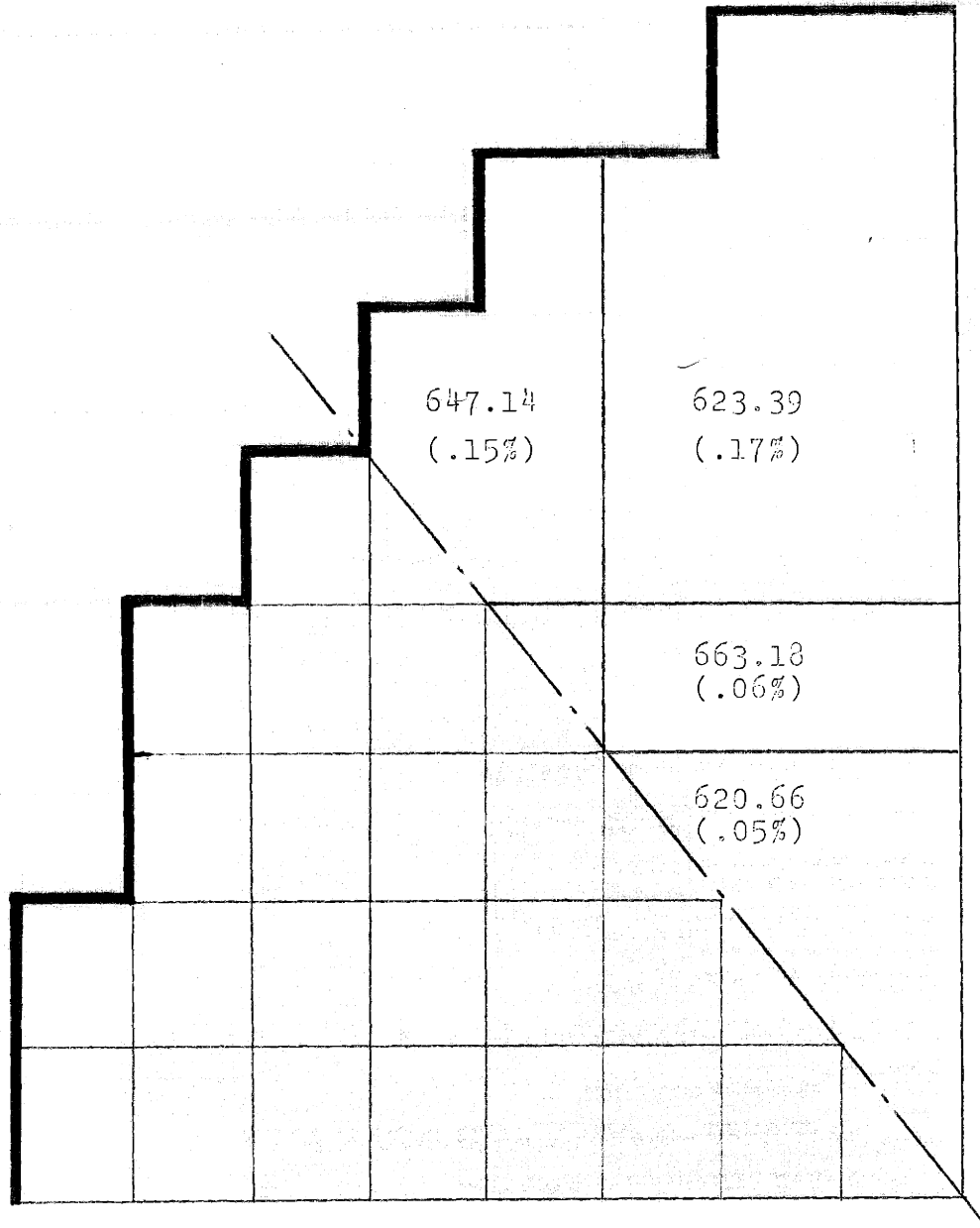
The most limiting variable in the steady state analysis of PWR's is the MDNBR. The values obtained from this variable are compared in Table 3.2. From this table it can be seen that for both cases the MDNBR value is only different when we go to a very low number of channels. Because the  $N_H = 1.0$  case is less precise than the case of considering  $N_H = N$ , no evaluation was done of that case and all further conclusions are drawn from the  $N_H = N$  case.

Transport Parameter

Pattern of Channels	$N_H = 1$	$N_H = N$	$\begin{matrix} N_H \\ N_H \\ \vdots \end{matrix}$	
	101 Channels	1.040	1.047	
	61	1.040	1.042	
	30	1.041	1.043	
	10	1.016	1.013	

MDNBR for the different cases analyzed

TABLE 3.2



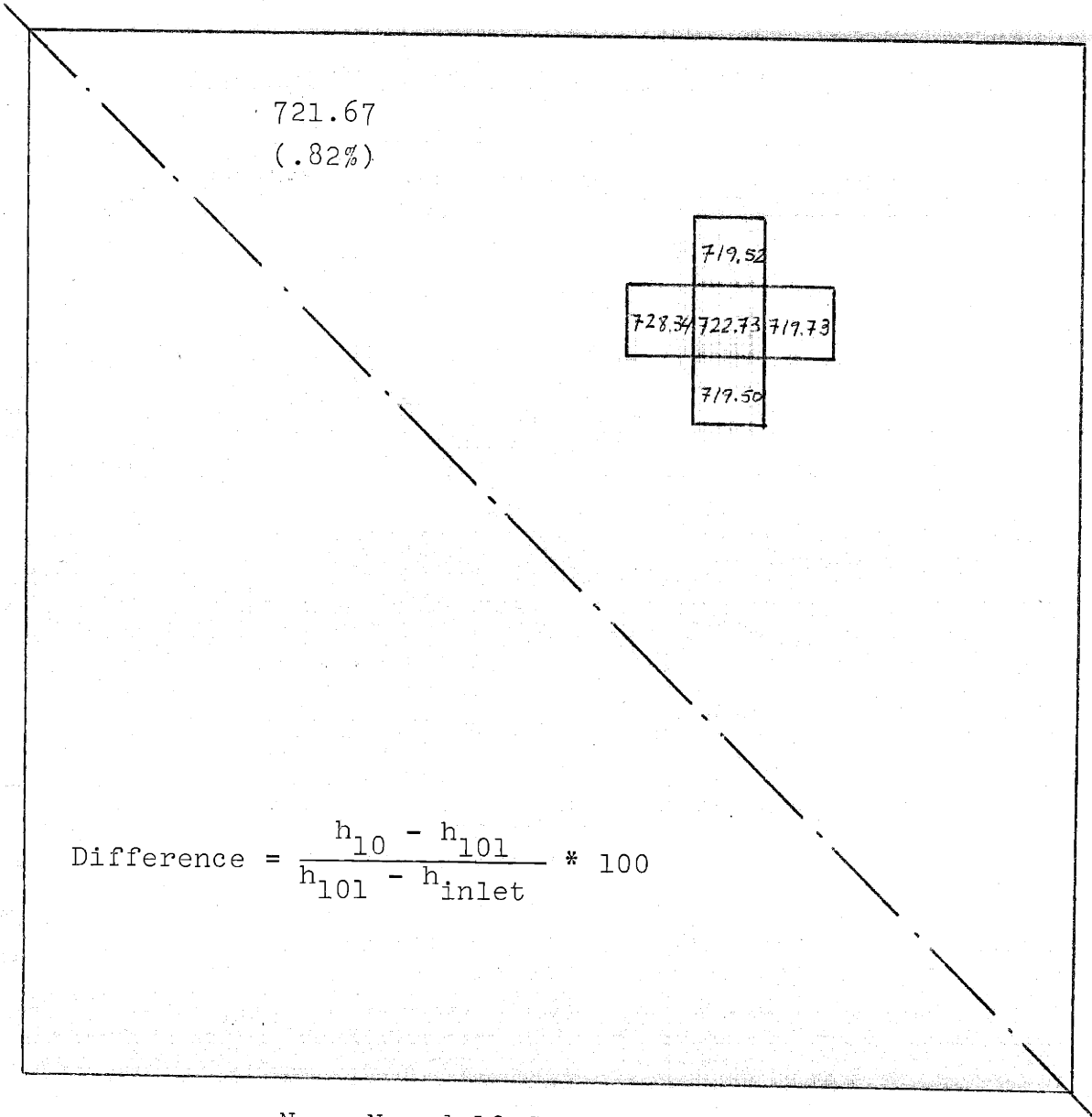
$$\text{Difference} = \frac{h_{10} - h_{101}}{h_{101} - h_{\text{inlet}}} * 100$$

$N_H = N$  and 10 Channel Case.

Exit Enthalpies Outside the Hot Assembly

Figure 3.25

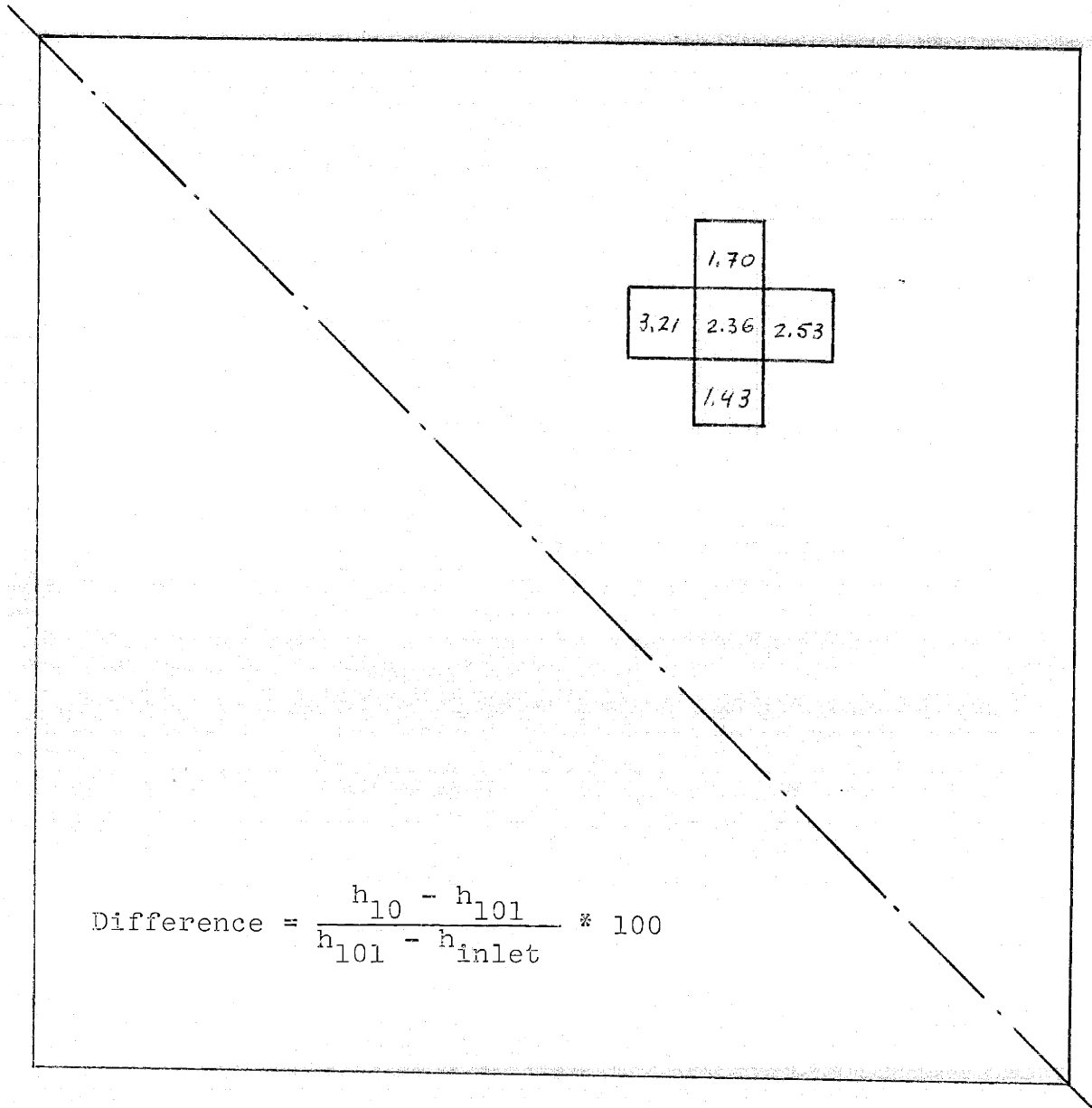




$N_H = N$  and 10 Channel Case.

Exit Enthalpies Inside the Hot Assembly

Figure 3.26



$$\text{Difference} = \frac{h_{10} - h_{101}}{h_{101} - h_{\text{inlet}}} * 100$$

$N_H = N$  and 10 Channel Case.

Difference in Enthalpy with Respect to  
the  $N_H = N$  and 101 Channel Case

Figure 3.37

### 3.3.1 Analysis of the $N_H = N$ Case

#### 3.3.1.1 Analysis of the MDNBR Results

In Table 3.3 the DNBR and MDNBR results are summarized. The MDNBR is a function of the equilibrium quality of the coolant and of the heat flux. The equilibrium quality of the coolant is dependent upon the enthalpy of the coolant.

This implies that the variations observed in the MDNBR are a function of differences in enthalpy because the heat flux in the subchannel where MDNBR occurs is the same for all the cases. This leads us to analyze the variations in enthalpy.

#### 3.3.1.2 Analysis of the Enthalpy Results

An important conclusion can be derived from inspection of the exit enthalpy results given in section 3.2.1. It can be seen that the channel with the largest enthalpy is not that of the largest radial power factor. It is due to the effect of the diversion cross flow and turbulent interchange terms in the calculation of the enthalpy. This may lead to wrong conclusions in some problems where a few

Distance (z)	101 Channels Case		61 Channels Case		30 Channels Case		10 Channels Case	
	Rod 57	Rod 64	Rod 57(31)	Rod 64(38)	Rod 57(14)	Rod 64(19)	Rod 57(7)	-
0.0	0.0	0.0	0.0	0.0	0.0	0.0	0.0	0.0
6.0	0.0	0.0	0.0	0.0	0.0	0.0	0.0	0.0
12.1	8.609	8.609	8.521	8.521	8.796	8.796	4.005	4.005
18.1	5.297	5.297	5.288	5.288	5.315	5.315	4.886	4.886
24.1	3.789	3.789	3.787	3.787	3.792	3.792	3.735	3.735
30.2	2.940	2.940	2.939	2.940	2.941	2.940	2.929	2.929
36.2	2.401	2.402	2.401	2.402	2.402	2.402	2.398	2.398
42.2	2.036	2.037	2.036	2.037	2.035	2.035	2.031	2.031
48.3	1.768	1.770	1.767	1.769	1.768	1.768	1.762	1.762
54.3	1.509	1.512	1.507	1.508	1.503	1.502	1.494	1.494
60.3	1.355	1.362	1.354	1.358	1.362	1.361	1.356	1.356
66.4	1.251	1.259	1.245	1.250	1.253	1.251	1.232	1.232
72.4	1.175	1.189	1.172	1.186	1.165	1.164	1.142	1.142
78.4	1.114	1.121	1.112	1.118	1.108	1.107	1.081	1.081
84.5	1.047	1.058	1.042	1.052	1.044	1.043	1.013	1.013
90.5	1.049	1.061	1.048	1.062	1.054	1.053	1.015	1.015
96.5	1.098	1.106	1.096	1.112	1.098	1.099	1.055	1.055
102.6	1.205	1.205	1.187	1.203	1.193	1.193	1.138	1.138
108.6	1.378	1.376	1.364	1.383	1.375	1.374	1.297	1.297
114.6	1.703	1.712	1.690	1.716	1.713	1.713	1.596	1.596
120.7	2.396	2.431	2.403	2.440	2.456	2.456	2.240	2.240
126.7	3.861	3.932	3.918	3.968	4.048	4.045	3.589	3.589
	MDNBR = 1.047 (57)	MDNBR = 1.047 (57)	MDNBR = 1.048 (57)	MDNBR = 1.042 (57)	MDNBR = 1.048 (64)	MDNBR = 1.043 (64)	MDNBR = 1.013 (57)	MDNBR = 1.013 (57)

DNB Results

TABLE 3.3

number of channels are used to describe the core because the subchannel with the MDNBR may not be represented. It will also be important when the void fraction is a limiting variable because the maximum void fraction corresponds usually with the channel with the largest enthalpy.

For these reasons it was decided to analyze the effects that cause the differences in enthalpy.

The enthalpy increase in steady state problems is calculated using equation (3.1). From this equation it can be seen that four terms affect the enthalpy increase. They are: the energy added to the channel from the rods, the energy added to the channel because of diversion cross-flow, the energy added to the channel because of turbulent interchanges, and the mass flow of the subchannel. All these terms plus the existence of truncation errors and the errors associated with the marching technique used are responsible for the existence of those differences. Notice that since the hot subchannel is surrounded by a set of actual subchannels, the effects of all these terms that are described below are only indirect, in the sense that they are due to lack of good transport coefficients in the lumped channels far outside the hot subchannel. Notice also that since the hot subchannel is in the center of a large mesh of actual subchannels, exact transport parameters are used in the calculations of the properties of

this hot subchannel and then no direct effect of this term exists.

Let us analyze then the influence of each of these five factors on the enthalpy of the subchannel with the MDNBR.

1) Energy added to the channel from the rods.

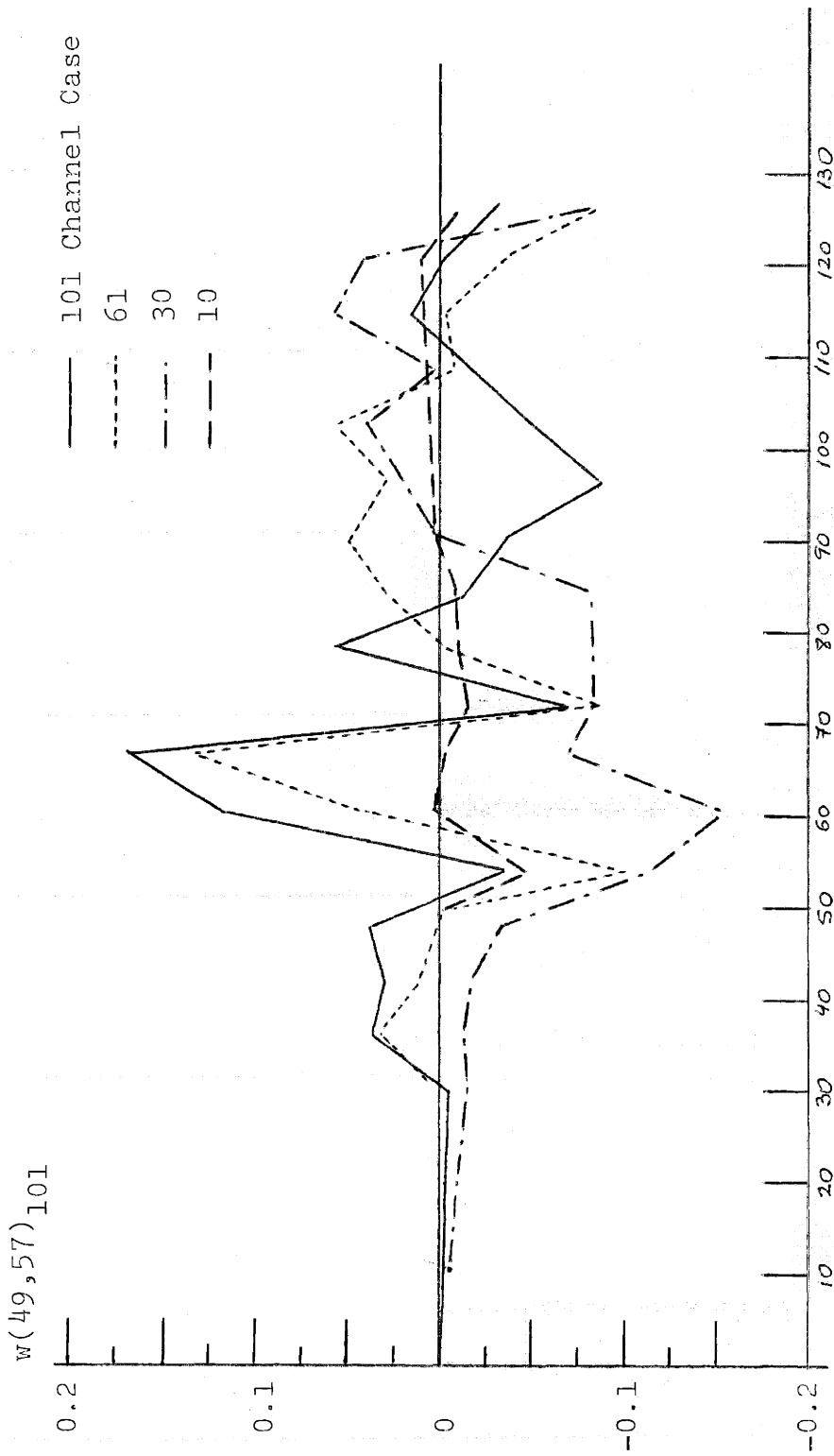
This term does not introduce any difference in the enthalpy results because the heat flux is exactly the same in all the four cases. Thus, no further study of this term is needed.

2) Diversion crossflow term.

As will be described below, this is the term that causes most of the differences. We divided the analysis of the effect of this term in the two following factors:

a) Flows crossing the boundaries of the hot subchannel

In figures 3.28, 3.29, 3.30 and 3.31, the values of the flows crossing each one of the four boundaries of the hot subchannel are given. From these figures it can be noticed that the crossflows are very different. This leads to very different energy interchange between the hot subchannel and its neighbors at every axial step. It is clear then that some transport coefficients have to be developed in order to obtain equivalent crossflows. This is a very difficult task because of the large number of terms involved in the calculation of such crossflows.



$N_H = N$  Case. Comparison Between Flows Crossing the Upper Boundary of the Hot Subchannel in the Four cases.

Figure 3.28

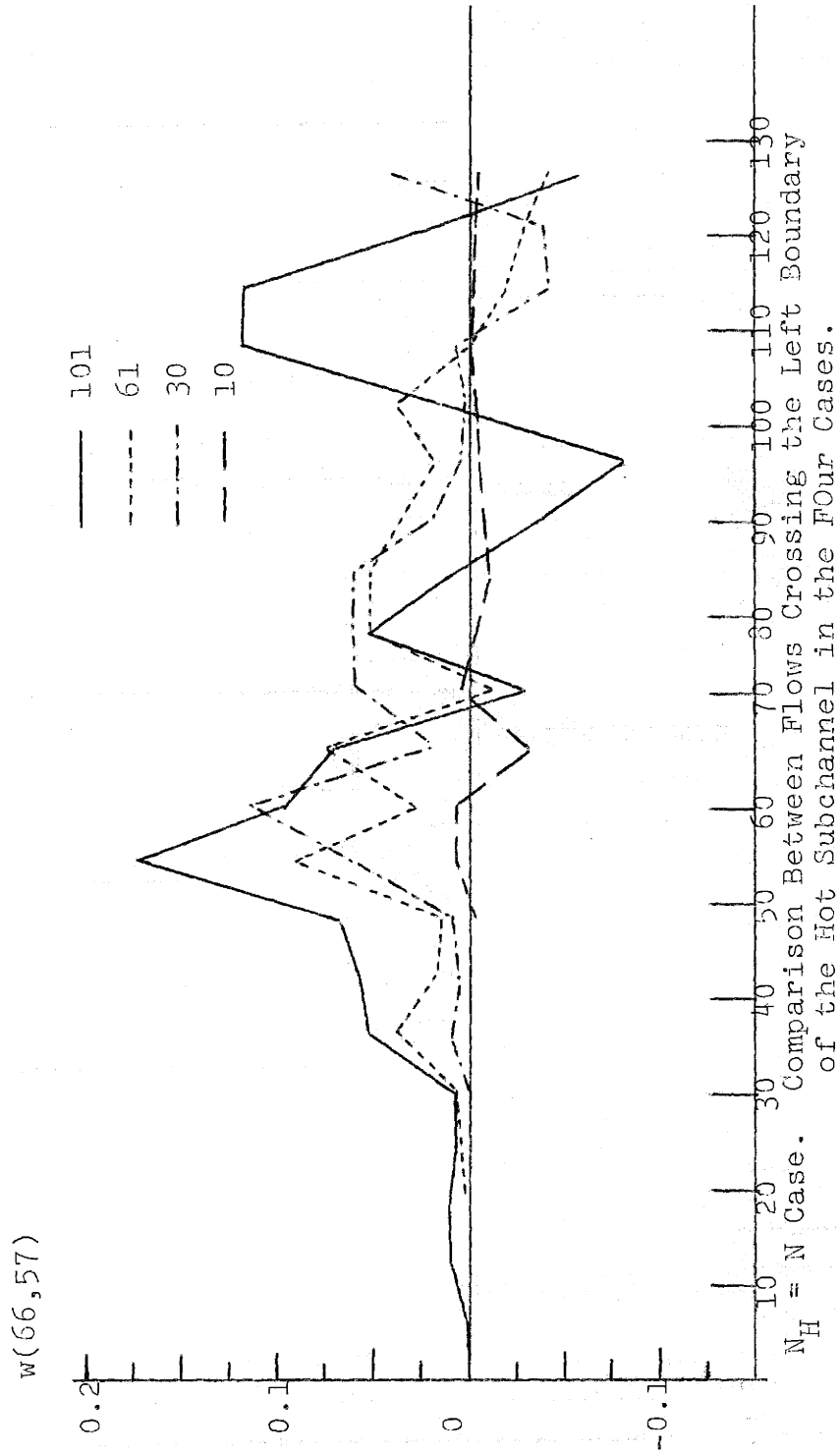
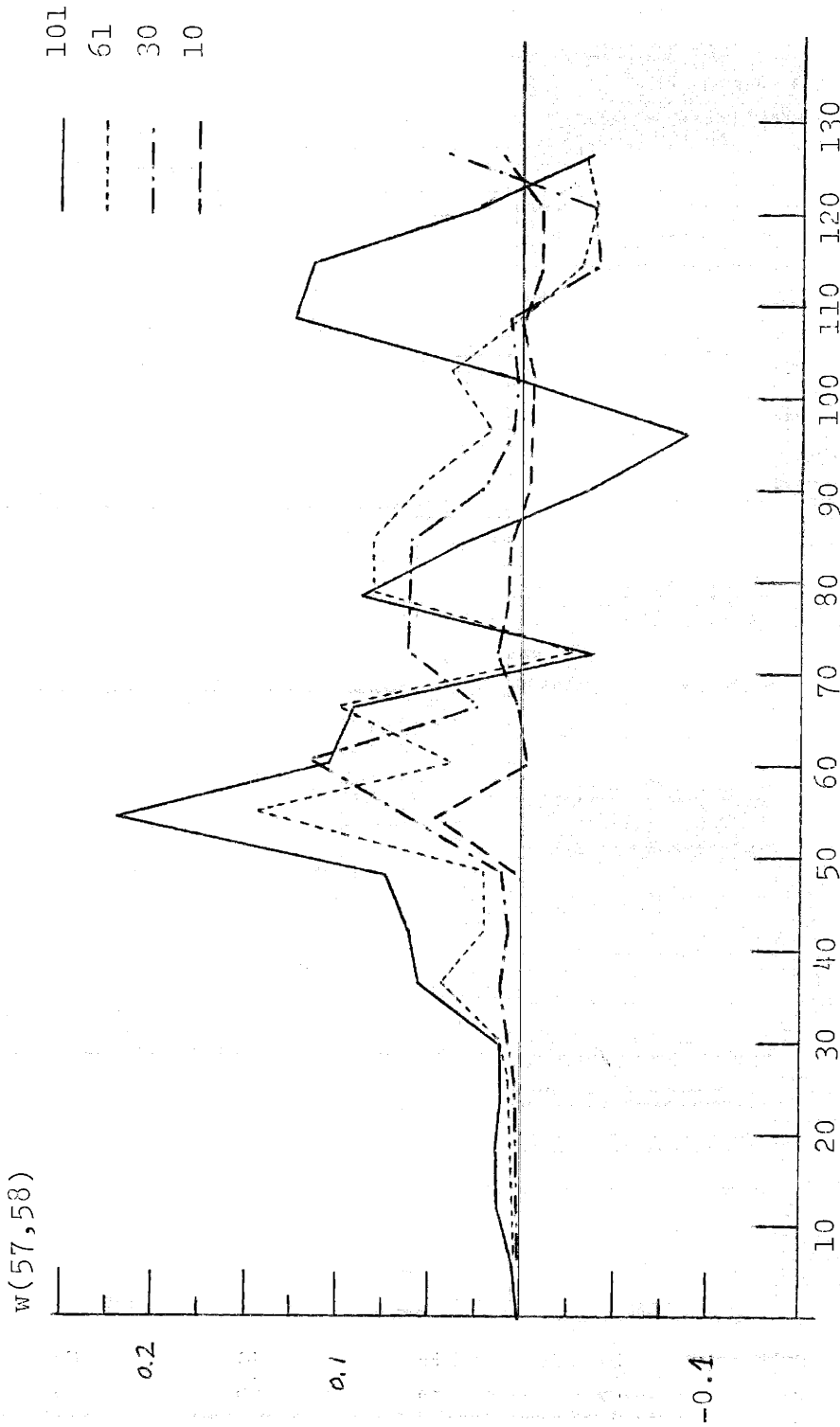


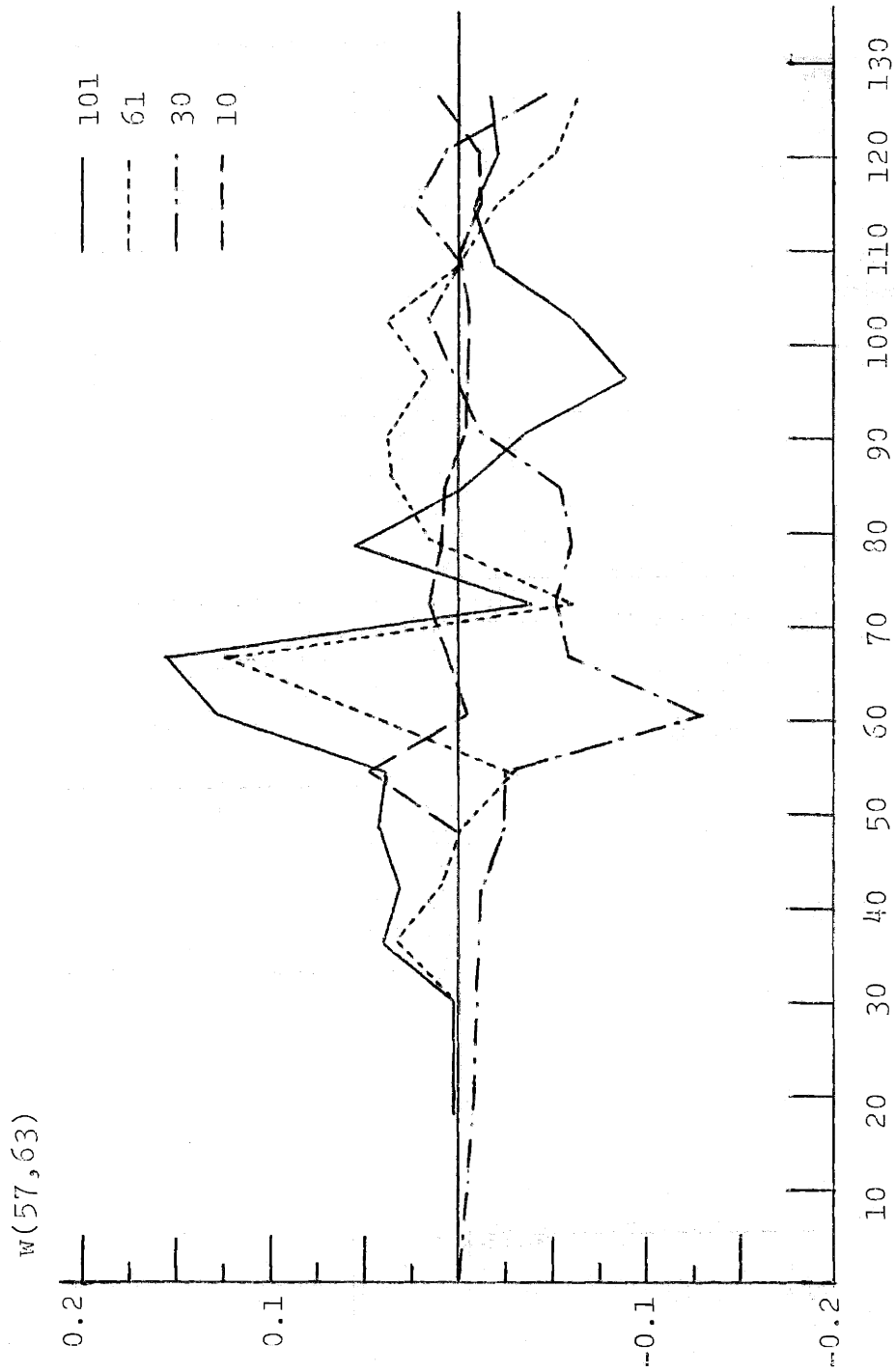
Figure 3.29





$N_H = N$  Case. Comparison Between Flows Crossing the Right Boundary of the Hot Subchannel in the Four Cases.

Figure 3.30



$N_H = N$  Case. Comparison Between Flows Crossing the Lower Boundary of the Hot Subchannel in the Four Cases.

Figure 3.31

b) Energy carried out by the diversion crossflow

In COBRA IIIC/MIT, this energy is taken as the diversion crossflow times the enthalpy of the donor channel. We have seen that the donor channels for the diversion crossflow are the outer channels of the hot assembly and its neighbors. Therefore the enthalpy of the donor channel only has an indirect and small effect on the properties of the hot subchannel. This indirect effect is due to the fact that in the lumped channels no transport coefficient was used. This causes differences in the properties of the lumped channels. These differences propagate and will affect the properties of the hot subchannels. But as indicated above, the effect is quite small unless a coarse mesh of channels is around the hot subchannel.

In Chong Chiu's thesis<sup>(5)</sup>, the transport coefficient ( $N'_H$ ) that should be used in this term, is analyzed for a two dimensional problem.

3) Turbulent interchange term.

This term, when the hot subchannel is surrounded by a set of actual subchannels, has only an indirect and small effect on the properties of the hot subchannel. This indirect effect is again due to the lumped channels and the

lack of good transport coefficients for those channels. In the present work  $N_H = N$  (being  $N$  the number of rods between the centerline of the channels) is taken, as suggested in reference 4. This is, of course, not exact but is a lot better than doing nothing ( $N_H = 1.0$ ). Chiu, in his thesis, developed these transport coefficients for two-dimensional problems.

4) Mass flow of the hot subchannel

This is a very important factor in the calculation of the enthalpy increase because it affects all the terms of the energy conservation equation. Changes in the mass flow affect in the same proportion the enthalpy of the channel. However, as can be seen in figure 3.32, where the total crossflow leaving the hot subchannel is given, differences among mass flows are small and only noticeable in a few axial stations. This causes small perturbations in the enthalpy. In order to eliminate them, transport coefficients in the axial and transverse momentum equation are required. Notice that these transport coefficients will produce identical diversion crossflows which will lead to identical mass flow rates.

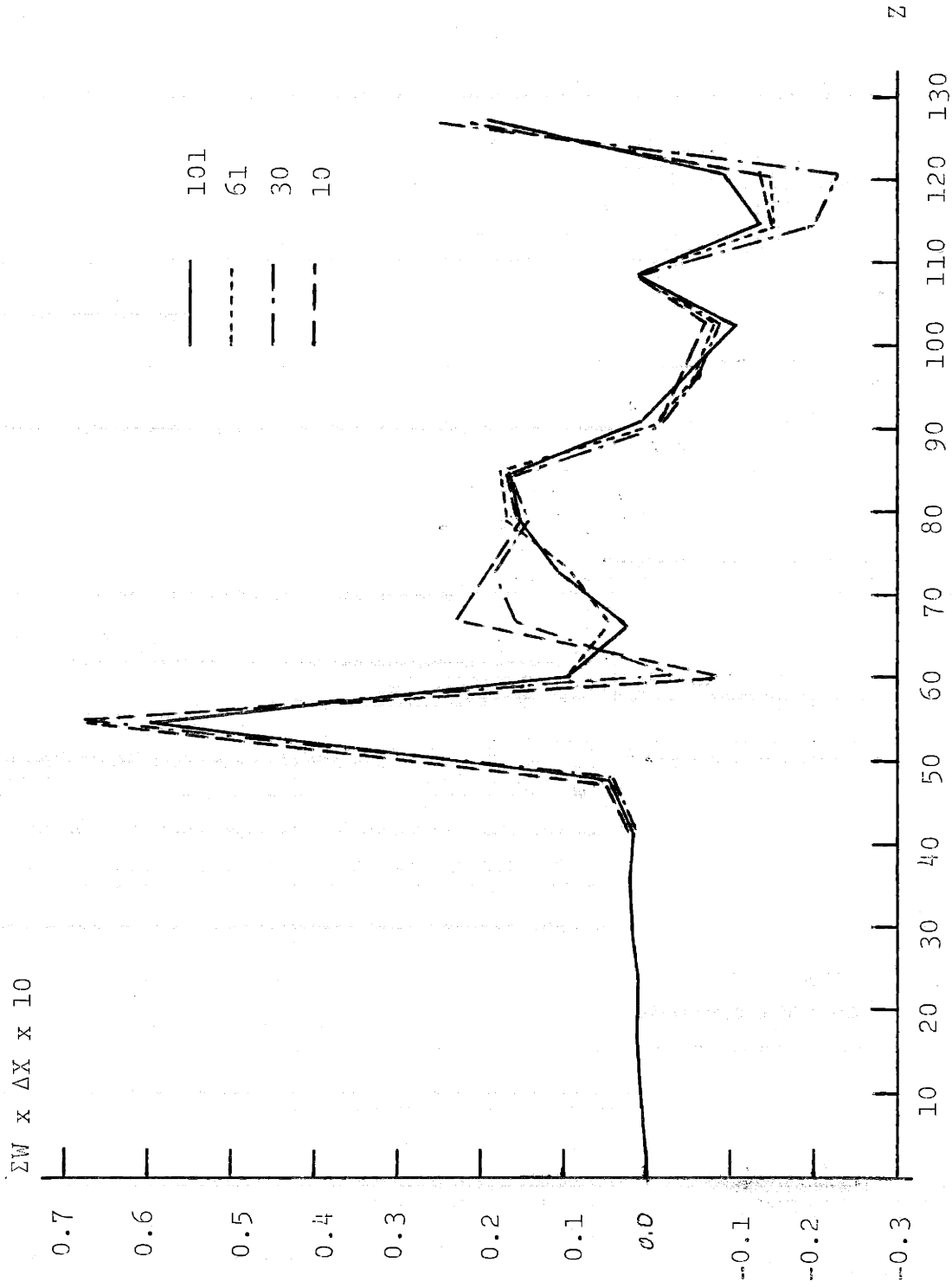


Figure 3.32

Comparison Between the Total Crossflow Leaving  
the Hot Subchannel in the Four Cases

- 5) Truncation and marching technique associated errors.

From the energy values obtained it is clear that different truncation errors exist for every individual case. The errors for the whole core were calculated and the results are given in Table 3.4. It is found that these errors are comparable in all cases and always lower than .1% of the energy added.

Truncation errors for the hot subchannel in all four cases also are important and were evaluated. In Appendix 5 an expression is deduced in order to calculate them and they are calculated for the four cases. From the results given in Table 3.5, it can be seen that there is a large difference in errors between cases and that the error itself is quite large and needs to be reduced in order to obtain good results.

The addition of all these individual problems leads to very important differences in the energy added to the hot channel. The energy added to the hot subchannel was calculated for all cases and from the results presented in Table 3.6, we can notice the large differences existing among the cases.

101 CHANNEL CASE

FLOW ENERGY IN =  $548.8 \times 3220.0012 = 1,767,136.659$   
ENERGY ADDED =  $2.786814 \times 10^5$   
FLOW ENERGY OUT =  $635.29 \times 3219.9661 = 2,045,652.244$   
ENERGY ERROR (% OF ENERGY ADDED) =  $165.816 (.059 \%)$

61 CHANNEL CASE

FLOW ENERGY IN =  $648.8 \times 3220.2197 = 1,767,256.571$   
ENERGY ADDED =  $2.786814 \times 10^5$   
FLOW ENERGY OUT =  $635.33 \times 3220.1785 = 2,045,876.006$   
ENERGY ERROR (% OF ENERGY ADDED) =  $61.96 (0.022 \%)$

30 CHANNEL CASE

FLOW ENERGY IN =  $548.8 \times 3220.3469 = 1,767,326.379$   
ENERGY ADDED =  $278,681.4$   
FLOW ENERGY OUT =  $635.41 \times 3220.3154 = 2,046,220.608$   
ENERGY ERROR =  $-212.829 (-.076 \%)$

10 CHANNEL CASE

FLOW ENERGY IN =  $548.8 \times 3220.3245 = 1,767,314.086$   
ENERGY ADDED =  $278,681.4$   
FLOW ENERGY OUT =  $635.42 \times 3220.2864 = 2,046,234.382$   
ENERGY ERROR =  $0238.9 (-0.085 \%)$

Energy errors of the whole core

TABLE 3.4

	CASE 101	61	30	10
ERROR	-10.56	-12.87	-17.37	-9.96
	(-19.7%)*	(-22.68%)	(-28.11%)	(-18.076%)

\*percent of energy added to the channel

Errors due to truncation and marching technique used  
(By Appendix 5)

TABLE 3.5



	# CHANNEL CASE			
	101	61	30	10
Inlet Energy (Btu/sec)	400.18	400.18	400.18	400.18
Outlet Energy	443.30	444.05	444.61	435.51
Outlet Energy - Inlet Energy	43.12	43.87	44.43	35.33
Energy Errors (from Table 3.5)	-10.56	-12.87	-17.37	-9.96
*Actual Energy added to the subchannel	53.68	56.74	61.79	45.29

$$*ACTUAL ENERGY ADDED \equiv \sum_{J=1}^J [\bar{q}' - \sum_{I=1}^I w'(\Delta h) - \sum_{I=1}^I wh*] \Delta x$$

evaluated as Energy out - Energy In - Error = Row 3 - Row 4

Comparison of energy added to the  
hot subchannel

TABLE 3.6

### 3.4 Simplified Analysis Using Exact Transport Coefficients

This case was not solved because no exact transport parameters were available and no time was left in order to carry the method that far.

Most of these coefficients are very hard to find from analytical analysis because of the large amount of terms involved. It is suggested then that the parameters developed by Chong Chiu be tested to validate them for a three dimensional case. If they do not lead to good results, some other coefficients should be obtained in a similar fashion.

Also, from what was said above, it is clear that the truncation and marching technique associated errors are important and should be eliminated.

The errors can be reduced by decreasing the length of the axial step but in order to obtain errors smaller than one percent of the energy added, the length of the axial step has to be reduced significantly. This will lead to very expensive runs. It is concluded then that a better solution may be the reduction of that error by introducing a few statements into the code. It is suggested that the technique described in Appendix 6 be adopted.

One final point should be noted. If we simply look to Table 3.2 it can be incorrectly concluded that since all the MDNBR results are so close, there is no need for further improvements. In order to obtain that final conclusion we need another column in the table that gives us the measured value of the MDNBR. This value is not available and the only possible way to justify our results is by doing our analysis as correctly as possible. That is why it is considered necessary to develop such parameters and to carry the method as far as possible.

## Chapter 4

### MODIFICATIONS TO THE FIRST VERSION OF COBRA IIIC/MIT

Cobra IIIC/MIT<sup>(2)</sup> was developed in two phases. The first phase was carried out by Dr. Robert Bowring and in this phase the bulk of the modifications incorporated to the code were introduced. But the code at that stage was not able to execute the simplified analysis because it was developed to handle assembly to assembly calculations. Therefore, some new improvements were required in order to analyze cases where no square channels and more than four channels surrounding any single one are needed. Also during the course of these analyses, some small problems with the code were found and remedied.

All these modifications have been incorporated in the COBRA IIIC/MIT Manual<sup>(2)</sup> but because these changes were not made also in MEKIN<sup>(6)</sup> and they were considered of interest for future improvements of this code, it was suggested by Professor Lothar Wolf that the specifics of how these modifications were executed by included in this thesis. Therefore, modifications are listed below and described in detail in Appendix 9.

- 1 - Modifications to allow for more than four channels surrounding any single one.
- 2 - Modifications to allow for no square channels.
- 3 - Modifications to allow for having actual subchannels together with lumped channels.
- 4 - Modifications required to obtain the MDNBR.
- 5 - Modifications required in order to obtain fuel temperatures.
- 6 - Modifications required when wire wraps are used.
- 7 - Modifications required in order to analyze more than one case in the same run.
- 8 - Modifications required to print out more than 14 channels, rods or nodes.
- 9 - Modifications required to use a transport parameter in the turbulent interchange term of the energy equation.

## Chapter 5

### Transport Coefficients

#### 5.0 Introduction

#### 5.1 Two Dimensional Transport Coefficients for the Energy Conservation Equation.

## 5.0 Introduction

In previous chapters the necessity of developing good transport coefficients in order to deal with lumped channels was emphasized. Very little work has been published in this area. In parallel with the present thesis, Chong Chiu<sup>(5)</sup> has been developing such coefficients for two dimensional problems as a preliminary step to development of three dimensional coefficients required by the simplified method. The two dimensional coefficients were developed with COBRA IIIC/MIT and they give a good idea of where the actual values for three dimensions will lay.

This chapter will present, for a two dimensional problem, an analytical deduction of two of such coefficients ( $N_H$ ,  $N_H'$ ) that are required in the energy conservation equation.

## 5.1 Two Dimensional Transport Coefficients for the Energy Conservation Equation

### 5.1.0 Introduction

In this first section of the chapter an analytical deduction of two important transport parameters is given.

The section may be divided into two parts, first an analytical calculation is performed in order to find the enthalpy along the core and across the section chosen.

The two most severe simplifications introduced in this analysis are to assume that there is not diversion cross-flow, and to solve the problem in only two dimensions.

In the second part those transport coefficients are calculated for two particular cases and they are compared against values obtained by Chong Chiu<sup>(5)</sup> using the computer code COBRA IIIC/MIT.

### 5.1.1 Problem Statement

The energy conservation equation used in COBRA IIIC/MIT is (Appendix 6).

$$\begin{aligned}
 h_{J+1}(A) = h_J(A) + \frac{q'_{J+\frac{1}{2}}(A) * \Delta x}{M_J(A)} - \frac{\Delta x}{M_J(A)} \sum_B w'_J(A,B)(h_J(A) - h_J(B)) \\
 - \frac{\Delta x}{M_J(A)} \sum_B w_J(A,B)(h_J^* - h_J(A)) \quad (5.1)
 \end{aligned}$$

where

$h_{J+1}(A)$  is the enthalpy of Channel A at axial station J+1

$h_J(A)$  is the enthalpy of Channel A at axial station J

$q'_{J+\frac{1}{2}}(A)$  is the linear heat generation rate of Channel A at station J+ $\frac{1}{2}$

$\Delta x$  is the length of the axial step

$M_J(A)$  is the massflow rate of Channel A at axial station J

$w'_J(A,B)$  is the interchange of mass between Channel A and one of its adjacent Channels B, due to turbulence at axial station J.



$w_J(A,B)$  is the massflow that leaves Channel A toward Channel B at axial station J

$h_J^*$  is the enthalpy at axial station J of the donor channel (either A or B depending on the sign of  $w_J(A,B)$  )

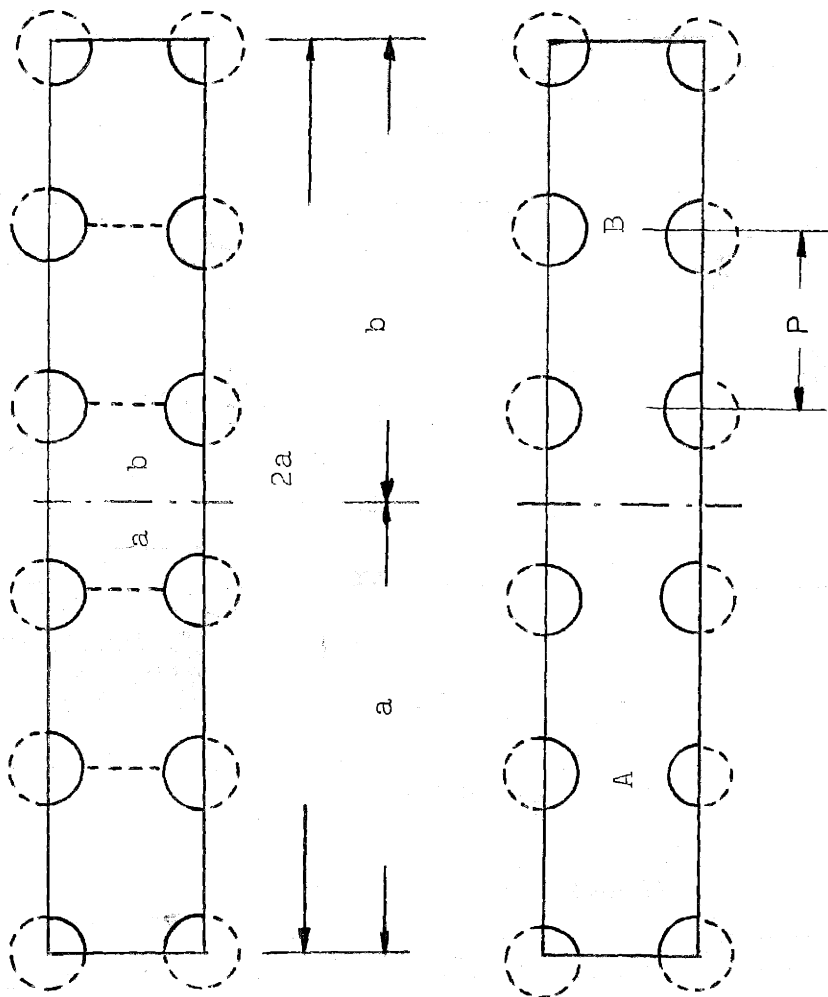
Working with lumped channels, the code will take for  $h_J(A) - h_J(B)$  and  $h_J^*$  the values obtained for the lumped regions (channels A and B) while in fact those enthalpies should be those of the closest subchannel to the lumped region boundaries.

The idea is then to obtain the relationship between these enthalpy values or algebraically to obtain:

$$\frac{1}{N_H(J)} \cong \frac{(h_J(a) - h_J(b))}{(h_J(A) - h_J(B))} \quad (5.2)$$

where a and b will be either the two complete subchannels closest to the boundary when that boundary separates two full subchannels or the two half subchannels closest to the boundary when the boundary splits an actual subchannel into two halves. For the case of Figure 5.1 a and b will be then taken as two half subchannels

$$\frac{1}{N_H(J)} \cong \frac{h_J(a)}{h_J(A)} \text{ or } \frac{h_J(b)}{h_J(B)} \quad (5.3)$$



Two Channel Case and Multichannel Case

Figure 5.1

depending on which is the donor channel.

In order to find these coefficients the enthalpies should be found first.

### 5.1.2 Solution Procedure

The enthalpies will be found for a two dimensional problem utilizing an analytical procedure. Several assumptions will be introduced in the development and they will be pointed out when they appear.

The differential energy conservation equation is:

$$\rho c_p \frac{DT}{Dt} = \text{div} (k \nabla T) + w_i + T \beta \frac{DP}{Dt} + \mu \Phi \quad (5.4)$$

Neglecting viscous and compressibility effects (which in fact are not going to affect the present problem) and for two dimensions (x,z):

$$\rho c_p \left[ \frac{\partial T}{\partial t} + \frac{\partial}{\partial z} (v_z T) + \frac{\partial}{\partial x} (v_x T) \right] = \left[ \frac{\partial}{\partial x} \left( k \frac{\partial T}{\partial x} \right) + \frac{\partial}{\partial z} \left( k \frac{\partial T}{\partial z} \right) \right] + w_i \quad (5.5)$$

For turbulent flows:

$$v = \bar{v} + v' \quad \text{and} \quad T = \bar{T} + T' \quad (5.6)$$

where overbars indicate time average.

Inserting equation 5.6 into 5.5 and time averaging, we obtain the following results:

$$\rho c_p \left[ \frac{\partial \bar{T}}{\partial t} + \bar{v}_z \frac{\partial \bar{T}}{\partial z} + \bar{v}_x \frac{\partial \bar{T}}{\partial x} \right] = \left[ \frac{\partial}{\partial x} \left( k \frac{\partial \bar{T}}{\partial x} - \rho c_p \overline{v_x' T'} \right) + \frac{\partial}{\partial z} \left( k \frac{\partial \bar{T}}{\partial z} - \rho c_p \overline{v_z' T'} \right) \right] + w_1 \quad (5.7)$$

Taking now

$$\overline{v_x' T'} = -\epsilon_H \frac{\partial \bar{T}}{\partial x} \quad (5.8)$$

$$\overline{v_z' T'} = -\epsilon_H \frac{\partial \bar{T}}{\partial z} \quad (5.9)$$

Assuming that the flow is fully developed, which in fact it is not, because it is well known that some diversion crossflow exists:

$$\bar{v}_x = 0 \quad (5.10)$$

Assuming also that  $k$  is independent of the temperature we can transform 5.7 into the following equation:

$$\rho c_p \left[ \frac{\partial \bar{T}}{\partial t} + \bar{v}_z \frac{\partial \bar{T}}{\partial z} \right] = \left[ (k + \rho c_p \epsilon_H) \frac{\partial^2 \bar{T}}{\partial x^2} + (k + \rho c_p \epsilon_H) \frac{\partial^2 \bar{T}}{\partial z^2} \right] + w_1 \quad (5.11)$$

Now we neglect axial conduction relative to radial conduction because in fact the first is much smaller than the second:

$$\frac{\partial^2 \bar{T}}{\partial x^2} \gg \frac{\partial^2 \bar{T}}{\partial z^2} \quad (5.12)$$

If we consider only the steady state problem Equation 5.11 reduces further to

$$\rho c_p \bar{v}_z \frac{\partial \bar{T}}{\partial z} = (k + \rho c_p \epsilon_H) \frac{\partial^2 \bar{T}}{\partial x^2} + w_i \quad (5.13)$$

Now we define the variable  $z^*$ :

$$z^* = \frac{z}{\bar{v}_z} \quad (5.14)$$

where  $\bar{v}_z$  is not a function of  $x$ .

$$\rho c_p \frac{\partial \bar{h}}{\partial z^*} = [k + \rho c_p \epsilon_H] \frac{\partial^2 \bar{h}}{\partial x^2} + c_p w_i \quad (5.15)$$

This equation can be transformed to obtain:

$$\frac{1}{\left(\frac{k + \rho c_p \epsilon_H}{\rho c_p}\right)} \frac{\partial \bar{h}}{\partial z^*} = \frac{\partial^2 \bar{h}}{\partial x^2} + \frac{c_p w_i}{k + \rho c_p \epsilon_H} \quad (5.16)$$

It is also known that the interchange of energy due to molecular interactions is much smaller than that due to turbulence, therefore:

$$a_t^* \equiv \frac{k + \rho c_p \epsilon_H}{\rho c_p} \approx \epsilon_H \quad (5.17)$$

and equation (5.16) yields:

$$\frac{1}{a_t^*} \frac{\partial \bar{h}}{\partial z^*} = \frac{\partial^2 \bar{h}}{\partial x^2} + \frac{w_i}{\rho \epsilon_H} \quad (5.18)$$

The analogous equation for transient one dimensional heat conduction is:

$$\frac{1}{a_t} \frac{\partial T}{\partial t^2} = \frac{\partial^2 T}{\partial x^2} + \frac{w_i}{k} \quad (5.19)$$

Hence analogous parameters are:

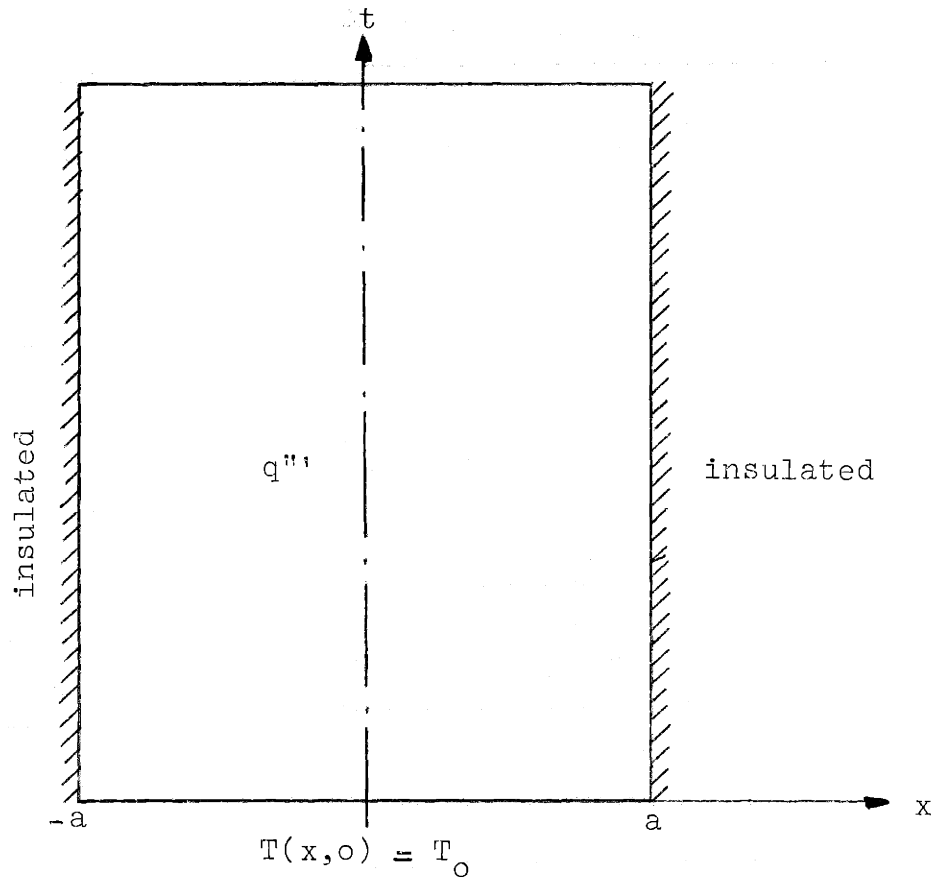
$$T \leftrightarrow \bar{h} \quad (5.20)$$

$$a_t \leftrightarrow a_t^* \quad (5.21)$$

$$t \leftrightarrow z^* \quad (5.22)$$

$$k \leftrightarrow \rho \epsilon_H \quad (5.23)$$

We need to solve this equation (5.19) for the geometry and boundary conditions given in figure 5.2.



Geometrical Description of the Problem

Figure 5.2

5.1.3 Solution to the Problem

5.1.3.1 Equation to be solved:

$$\frac{1}{a_t} \frac{\partial T}{\partial t} = \frac{\partial^2 T}{\partial x^2} + \frac{q'''}{k} \quad (5.24)$$

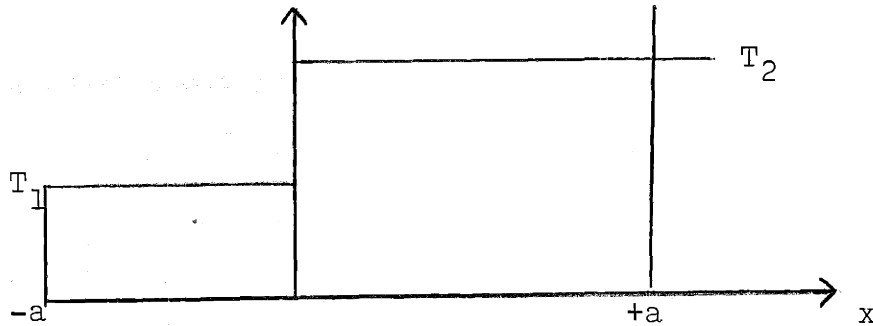
5.1.3.2 Boundary Conditions

For the x-axis:

$$\left. \frac{\partial T(x,t)}{\partial x} \right|_{x = \pm a} = 0 \quad (5.25)$$

The initial condition is:

$T(x,0)$  is given by:



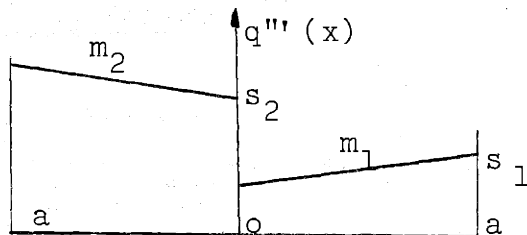
where  $T_1$  and  $T_2$  can be any value.



The heat generation rate will be given by the following equations:

$$q'''(x) = \begin{cases} s_2 - xm_2 & \text{for } -a \leq x < 0 \\ s_1 + (a-x)m_1 & \text{for } 0 < x \leq a \end{cases} \quad (5.26)$$

or graphically:



where  $m_1$ ,  $m_2$ ,  $s_1$  and  $s_2$  can take any finite value.

### 5.1.3.3 Changes of Variables

The following changes of variables will be made:

$$T(x,t) = \psi(x,t) + \phi(x) + \theta(t) \quad (5.27)$$

$$q'''(x) = q_1''' + q_2'''(x) \quad (5.8)$$

where

$q_1'''$  will be the average value of  $q'''(x)$  along the x-axis.

$$q_1''' = \frac{\int_{-a}^a q'''(x) dx}{\int_{-a}^a dx} = \frac{s_1 + s_2}{2} + \frac{a}{4} (m_1 + m_2) = k_1 \quad (5.29)$$

These changes of variables will produce the following equation:

$$\frac{1}{a_t} \frac{d\theta}{dt} + \frac{1}{a_t} \frac{\partial \psi}{\partial t} = \frac{\partial^2 \psi}{\partial x^2} + \frac{d^2 \phi}{dx^2} + \frac{k_1}{k} + \frac{q_2'''(x)}{k} \quad (5.30)$$

From the separation of variables assumed by equation 5.27, we can split this equation into three equalities:

$$\frac{1}{a_t} \frac{d\theta}{dt} = \frac{k_1}{k} \quad (5.31)$$

$$\frac{1}{a_t} \frac{\partial \psi(x,t)}{\partial t} = \frac{\partial^2 \psi(x,t)}{\partial x^2} \quad (5.32)$$

$$\frac{\partial^2 \phi(x)}{\partial x^2} = - \frac{q_2'''(x)}{k} \quad (5.33)$$

The boundary conditions can be also divided as follows:

$$\left. \frac{\partial T(x,t)}{\partial x} \right|_{x=\pm a} = 0 \quad \Rightarrow \quad \left( \frac{\partial \psi(x,t)}{\partial x} + \frac{\phi(x)}{dx} \right) \Big|_{x=\pm a} = 0 \quad (5.34)$$

which implies:

$$\left. \frac{\partial \psi(x,t)}{\partial x} \right|_{x=\underline{+a}} = 0 \quad (5.35)$$

$$\left. \frac{\partial \phi}{\partial x} \right|_{x=\underline{+a}} = 0 \quad (5.36)$$

and the initial boundary condition:

$$T(x,0) = \psi(x,0) + \phi(x) + \theta(0) \quad (5.37)$$

#### 5.1.3.3.1 Solution of Equation 5.31

This equation is:

$$\frac{d\theta}{dt} = a_t \frac{k_1}{k}$$

which has the solution:

$$\theta(t) = a_t \frac{k_1}{k} t + c_1 \quad (5.38)$$

and  $c_1$  will be found from the initial temperature condition, equation 5.37.

5.1.3.3.2 Solution of Equation (5.32)

Assuming it is possible to make the following separation of variables:

$$\psi(x,t) = X(x) F(t) \quad (5.39)$$

Equation 5.32 becomes:

$$\frac{1}{a_t F(t)} \frac{dF(t)}{dt} = -\alpha^2 \quad (5.40)$$

$$\frac{d^2 X(x)}{dx^2} + \alpha^2 X(x) = 0 \quad (5.41)$$

Solving now equation (5.40)

$$F(t) = c_2 e^{-\alpha^2 a_t T} \quad (5.42)$$

Solving Equation (4.51)

$$X_n(x) = c_3 \sin \alpha_n x + c_4 \cos \alpha_n x \quad (5.43)$$

Using boundary condition Equation 5.35:

$$\left. \frac{\partial \psi(x,t)}{\partial x} \right|_{x=\pm a} = F(t) \left. \frac{\partial X(x)}{\partial x} \right|_{x=\pm a} = 0 \quad (5.44)$$

From the previous equation we can conclude:

$$\left. \frac{\partial X(x)}{\partial x} \right|_{x=\pm a} = 0 \quad (5.45)$$

This implies:

$$c_3 \alpha_n \cos \alpha_n a - c_4 \alpha_n \sin \alpha_n a = 0 \quad (5.46)$$

$$c_3 \alpha_n \cos \alpha_n a + c_4 \alpha_n \sin \alpha_n a = 0 \quad (5.47)$$

In order to have a solution other than trivial case of

$c_3 = c_4 = 0$ , we must have

$$0 = \begin{vmatrix} \cos \alpha_n a & -\sin \alpha_n a \\ \cos \alpha_n a & \sin \alpha_n a \end{vmatrix} = \sin 2 \alpha_n a \quad (5.48)$$

From Equation 5.48 we can conclude:

$$\alpha_n = \frac{n\pi}{2a} \quad \text{with } n = 0, 1, 2, 3, \dots \quad (5.49)$$

From Equation 5.46 we can relate  $c_3$  and  $c_4$ :

$$c_3 = c_4 \tan \alpha_n a \quad (5.50)$$

Plugging this equation into Equation 5.43 we can obtain:

$$X_n(x) = c_4 \cos \alpha_n (x-a) \quad (5.51)$$

$$\begin{aligned} c_3 \sin \alpha_n x + c_4 \cos \alpha_n x &= \\ = c_4 \left[ \frac{\sin \alpha_n a \sin \alpha_n x + \cos \alpha_n a \cos \alpha_n x}{\cos \alpha_n a} \right] \\ = \frac{c_4}{\cos \alpha_n a} \left[ \cos \alpha_n (x-a) \right] \end{aligned}$$

These results lead finally to:

$$\psi(x,t) = \sum_{n=1}^{\infty} c_n \cos \alpha_n (x-a) e^{-\alpha_n^2 a t} \quad (5.52)$$

so far we have obtained  $\theta(t)$  and  $\psi(x,t)$  and we still have to find  $\phi(x)$ .

### 5.1.3.3.3 Solution of Equation 5.3.3

This equation is:

$$\frac{d^2 \phi(x)}{dx^2} = - \frac{q_2'''(x)}{k}$$

It is possible to express  $q_1'''(x)$  plus  $q_2'''(x)$  as a Fourier series:

$$q'''(x) = b_0 + \sum_{n=1}^{\infty} b_n \cos \alpha_n(x-a) \quad (5.53)$$

where

$$b_0 = \frac{\int_{-a}^a q'''(x) dx}{\int_{-a}^a dx} = q_1''' = k_1 \quad (5.54)$$

and

$$b_n = \frac{\int_{-a}^a q'''(x) \cos \alpha_n(x-a) dx}{\int_{-a}^a \cos^2 \alpha_n(x-a) dx} \quad (5.55)$$

It is clear from equations 5.53 and 5.54 and 5.28 that:

$$q_2'''(x) = \sum_{n=1}^{\infty} b_n \cos \alpha_n(z-a) \quad (5.56)$$

where  $b_n$  is calculated from 5.55, its value being:

$$b_n = \frac{1}{2\alpha_n} [ [ (s_1 - s_1) + m_1 a ] \sin \alpha_n a - \frac{m_1}{\alpha_n} (1 - \cos \alpha_n a) - \frac{m_2}{\alpha_n} (\cos \alpha_n a - \cos 2\alpha_n a) ] \quad (5.57)$$

Now integrating equation 5.33:

$$\frac{d\phi(x)}{dx} = \frac{1}{k} \sum_{n=1}^{\infty} \frac{b_n}{\alpha_n} \sin \alpha_n(x-a) + c_5 \quad (5.58)$$

applying the boundary condition of equation 5.36

$$\left. \frac{d\phi(x)}{dx} \right|_{x=\underline{+}a} = 0 \implies c_5 = 0 \quad (5.59)$$

and integrating again we finally have

$$\phi(x) = \frac{1}{k} \sum_{n=1}^{\infty} \frac{b_n}{\alpha_n^2} \cos \alpha_n(x-a) + c_6 \quad (5.60)$$

#### 5.1.3.4 Final Result

Combining equations (5.60), (5.52), and (5.38):

$$T(x,t) = c_1 + \frac{a_t k_1 t}{k} + \sum_{n=0}^{\infty} c_n \cos \alpha_n(x-a) e^{-\alpha_n^2 a_t t} + \frac{1}{k} \sum_{n=1}^{\infty} \frac{b_n}{\alpha_n^2} \cos(\alpha_n a) \quad (5.61)$$

where we have combined the old  $c_1$  and  $c_6$  in only one constant,  $c_1$ .



In this expression,  $c_1$  and  $c_n$  are still unknown and they have to be found from the initial boundary condition.

Expressing  $T(x,0)$  as the following Fourier series:

$$T(x,0) = b'_0 + \sum_{n=1}^{\infty} b'_n \cos \alpha_n (x-a) \quad (5.62)$$

where:

$$b'_0 = \frac{\int_{-a}^a T(x,0) dx}{a} = \frac{T_1 + T_2}{2} \quad (5.63)$$

and  $b'_n$  can be found by setting  $m_1 = m_2 = 0$ ,

$s_1 = T_2$  and  $s_2 = T_1$  in equation 5.57:

$$b'_n = \frac{1}{a\alpha_n} (T_2 - T_1) \sin \alpha_n a \quad (5.64)$$

Plugging equations (5.63) and (5.64) into (5.62):

$$T(x,0) = \frac{T_1 + T_2}{2} + \sum_{n=1}^{\infty} \frac{T_2 - T_1}{a\alpha_n} \sin \alpha_n a \cos \alpha_n (x-a) \quad (5.65)$$

Comparing this equation with equation (5.61) when

$t = 0$  we obtain:

$$\begin{aligned}
 c_1 + \sum_{n=0}^{\infty} c_n \cos \alpha_n (x-a) + \frac{1}{k} \sum_{n=1}^{\infty} \frac{b_n}{\alpha_n^2} \cos \alpha_n (x-a) &= \\
 &= \frac{T_1 + T_2}{2} + \sum_{n=1}^{\infty} \frac{T_2 - T_1}{a\alpha_n} \sin \alpha_n a \cos \alpha_n (x-a)
 \end{aligned}
 \tag{5.66}$$

or:

$$\begin{aligned}
 c_1 + c_0 + \sum_{n=1}^{\infty} \left( c_n + \frac{b_n}{k\alpha_n^2} - \frac{T_2 - T_1}{a\alpha_n} \sin \alpha_n a \right) \cos \alpha_n (x-a) &= \\
 &= \frac{T_1 + T_2}{2}
 \end{aligned}
 \tag{5.67}$$

Equation 5.67 leads to the following conclusions:

$$\begin{aligned}
 c_1 + c_0 &= \frac{T_1 + T_2}{2} \\
 c_n &= \frac{T_2 - T_1}{a\alpha_n} \sin \alpha_n a - \frac{b_n}{k\alpha_n^2}
 \end{aligned}
 \tag{5.68}$$

By substituting these two values into equation (5.61) we obtain finally:

$$T(x,t) = \frac{T_1 + T_2}{2} + \frac{a_t k_1 t}{k} + \sum_{n=1}^{\infty} \left[ \frac{T_2 - T_1}{a\alpha_n} \sin \alpha_n a - \frac{b_n}{k\alpha_n^2} \right]$$

$$e^{-\alpha n^2 a t} + \frac{b_n}{k \alpha n^2} \left\} \cos \alpha_n (x-a) \quad (5.69)$$

which expressed in terms of  $h$ ,  $\epsilon_H$ ,  $\frac{z}{v_z}$  and  $\rho \epsilon_H$  leads to the final expression:

$$h(x,z) = \frac{h_1 + h_2}{2} + \frac{\epsilon_H k_1 z}{\rho \epsilon_H v_z} + \sum_{n=1}^{\infty} \left\{ \left[ \frac{h_2 - h_1}{a \alpha_n} \sin \alpha_n a - \frac{b_n}{\rho \epsilon_H \alpha_n^2} \right] e^{-\alpha_n^2 \epsilon_H z / v_z} + \frac{b_n}{\rho \epsilon_H \alpha_n^2} \right\} \cos \alpha_n (x-a) \quad (5.70)$$

All the parameters in this expression are known except  $\epsilon_H$ .

In order to calculate the average value of  $\epsilon_H$  at the gap we use equation A.13 of reference 8 which yields

$$\epsilon_H \Big|_{x=0} = \frac{w_{ij} (h_j(a) - h_j(b))}{\rho s_{ij} \frac{\partial h}{\partial x} \Big|_{x=0}} \quad (5.71)$$

under translation of nomenclature and the following applicable conditions

a)  $Pr = 1$

b) Turbulent flow i.e.  $\frac{\epsilon_H \phi}{\nu} \Big|_{\phi=0} > \frac{1}{Pr}$

Taking now  $w'_{ij}$  as COBRA does:

$$w'_{ij} \equiv \beta s_{ij} \bar{G} \quad (5.72)$$

This value of  $\bar{\epsilon}_H \Big|_{x=0}$  is the average value at the gap

but we are interested in the average value along the x-axis. Let us relate both values by using the following equation:

$$\bar{\epsilon}_H = \bar{\epsilon}_H \Big|_{x=0} f_\epsilon \quad (5.73)$$

Then finally, by plugging into equation 5.73, equations 5.71 and 5.72 and using the following definition of effective mixing distance  $z_{ij}$ , we obtain:

$$\frac{h_J(a) - h_J(b)}{\frac{\partial h}{\partial x} \Big|_{x=0}} \equiv z_{ij} \quad (5.74)$$

$$\bar{\epsilon}_H = \beta v_z [ z_{ij} * f_\epsilon ] \quad (5.75)$$

Two unknowns appear in this equation, they are  $z_{ij}$  and  $f_\epsilon$ . The product of these values which should be used is that product which will yield  $N_H$  values matching the numerically generated values by Chong for each standard case, i.e. for given geometry,  $N$ , over a range of  $\beta$ 's. This is in accordance with the objective of Chapter 5 of producing an analytic approach consistent with the Chong numerical method, both of which match standard cases i.e. multisubchannel COBRA runs utilizing assumed  $\beta$ 's. Note that we are presently unsure which  $\beta$  corresponds to reality. Therefore we have not utilized available literature (8,9,11,12) to estimate the best values for  $z_{ij}$  and  $f_\epsilon$  since the analysis and experimental literature is in disagreement. The product  $z_{ij} \times f_\epsilon$  was therefore fit in such a way that the value taken will produce identical enthalpy profiles for a variety of cases to those obtained with multisubchannel COBRA IIIC runs.

From this fitting technique a value of:

$$z_{ij} * f_\epsilon = 0.200 \quad (5.76)$$

The value was determined by checking cases  $q'''$  upset for  $\beta = 0.02$ ,  $N = 3$  and  $4$  (cases of 3 and 15 channels, 4 and 2 channels on either side of the gap were examined)

for the full range of  $z$  were examined. Considerably improved fits utilizing  $z_{ij} \times f_{\epsilon} = 0.200$  versus  $0.250$  were found as illustrated in figures 5.3 through 5.8 for several typical cases. However as shown in the same figures, since this variation in product  $z_{ij} \times f_{\epsilon}$  has a measurable effect on the predicted  $N_H$ . It is anticipated that because the solutions exhibit a developing length which decreases with small  $N$  and large  $P$ , the product will be a function of  $N$ ,  $\beta$  and  $z$ . The significance of these factors on the numerical value of the product and consequently  $N_H$  need further exploration.

Substituting equation 5.76 into 5.75:

$$\bar{\epsilon}_H = 0.2 \beta v_z \quad (5.77)$$

and the final expression for  $h(x,z)$  will be:

$$h(x,z) = \frac{h_1 + h_2}{2} + \frac{k_1 z}{G} + \sum_{n = \text{odd}}^{\infty} \left\{ \left[ \frac{h_2 - h_1}{a \alpha_n} \sin \alpha_n a - \frac{b_n}{0.2 \beta \bar{G} \alpha_n^2} \right] e^{-\alpha_n^2 z \beta 0.2} + \frac{b_n}{0.2 \beta \bar{G} \alpha_n^2} \right\} \cos \alpha_n (x-a) \quad (5.78)$$

with:

$$k_1 = \frac{s_1 + s_2}{2} + \frac{a}{4} (m_1 + m_2) \quad (5.29)$$

$$b_n = \frac{1}{a\alpha_n} [ [(s_1 - s_2) + m_1 a] \sin \alpha_n a - \frac{m_1}{\alpha_n} (1 - \cos \alpha_n a) - \frac{m_2}{\alpha_n} (\cos \alpha_n a - \cos 2\alpha_n a) ] \quad (5.57)$$

$$\alpha_n = \frac{nr}{2a} \quad (5.49)$$

#### 5.1.4 Calculation of $N_H$ and $N_H'$

Once the spatial distribution of  $h$  is known the calculation of the  $N_H$  and  $N_H'$  is very simple:

$$\frac{1}{N_H(z)} = \frac{(h(a,z) - h(b,z))}{(h(A,Z) - h(B,Z))} \quad (5.2)$$

where if the subchannels are defined as in figure 5.1:

$$\frac{1}{N_H(z)} = \frac{\frac{1}{P/2} [ \int_{-P/2}^0 h(x,z) dx - \int_0^{P/2} h(x,z) dx ]}{\frac{1}{a} [ \int_{-a}^0 h(x,z) dx - \int_0^a h(x,z) dx ]} \quad (5.79)$$

For a different definition of subchannels  $a$  and  $b$ , the formula will be identical except for the limits of the integrals.

The process for finding  $N_H'(z)$  will be analogous.

5.1.5 Comparison of  $N_H(z)$  obtained as previously indicated with the values obtained by using COBRA IIIC/MIT.

#### 5.1.5.0 Introduction

As noted in section 5.0, parallel to the development of this method to find  $N_H$ , Chong Chiu<sup>(5)</sup> determined the same parameters using the computer code COBRA IIIC/MIT. Notice that while the parameter developed by Chiu only covers a limited range of cases, the use of the expressions developed here will cover a much larger number of problems.

In order to establish how the assumptions introduced in the present method effect the results and then how good they are,  $N_H(z)$  was compared with that obtained by Chiu.

The comparison was made for two of the cases analyzed by Chiu; enthalpy upset at the inlet without heat generation and heat generation upset with constant inlet enthalpy.



5.1.5.1 Enthalpy Upset with Heat Generation Rate  
Equal to Zero.

For this case  $b_n = k_1 = 0$  (5.8.0)

Equation (5.78) becomes:

$$h(x,z) = \frac{h_1 + h_2}{2} + \sum_{n = \text{odd}}^{\infty} \frac{h_2 - h_1}{a\alpha_n} \sin \alpha_n a e^{-\alpha_n^2 z \beta 0.2} \cos \alpha_n (x-a) \quad (5.8.1)$$

where:

$$\sin \alpha_n (x-a) \equiv \sin \alpha_n a (\cos \alpha_n x \cos \alpha_n a + \sin \alpha_n a * \sin \alpha_n x) \quad (5.8.2)$$

but:

$$\sin \alpha_n a \cos \alpha_n a = 0 \quad \text{for } n = 1, 2, 3 \dots \quad (5.8.3)$$

$$\sin^2 \alpha_n a = \begin{cases} 0 & \text{for } n = 2, 4, 6 \dots \\ 1 & \text{for } n = 1, 3, 5 \dots \end{cases}$$

Applying these conclusions to equation (5.8.2)

$$\sin \alpha_n a \cos \alpha_n (x-a) = \sin \alpha_n x \quad \text{with } n = 1, 3, 5 \quad (5.8.5)$$

It gives us finally for  $h(x,z)$

$$h(x,z) = \frac{h_1 + h_2}{2} + \sum_{n \text{ odd}} \frac{h_2 - h_1}{a\alpha_n} e^{-\alpha_n^2 z\beta 0.2} \quad (5.86)$$

Using now the same definition for  $N_H$  that the Chiu method does, equation 5.79 becomes :

$$\frac{1}{N_H(z)} = \frac{\frac{1}{2P} \left| \int_{-\frac{3P}{2}}^{-\frac{P}{2}} h(x,z) dx - \int_{\frac{P}{2}}^{\frac{3P}{2}} h(x,z) dx \right|}{\frac{1}{a} \left| \int_{-a}^0 h(x,z) dz - \int_0^a h(c,z) dz \right|} \quad (5.87)$$

$$N_H(z) = \frac{2}{\left(\frac{a}{P}\right)} * \frac{\sum_{n \text{ odd}} \frac{1}{n^2} e^{-\alpha_n^2 z\beta * 0.2} \cos \frac{\alpha_n P}{2}}{\sum_{n = \text{odd}} \frac{1}{n^2} e^{-\alpha_n^2 z\beta 0.2} \left( \cos \frac{\alpha_n P}{2} - \cos \frac{3\alpha_n P}{2} \right)} \quad (5.88)$$

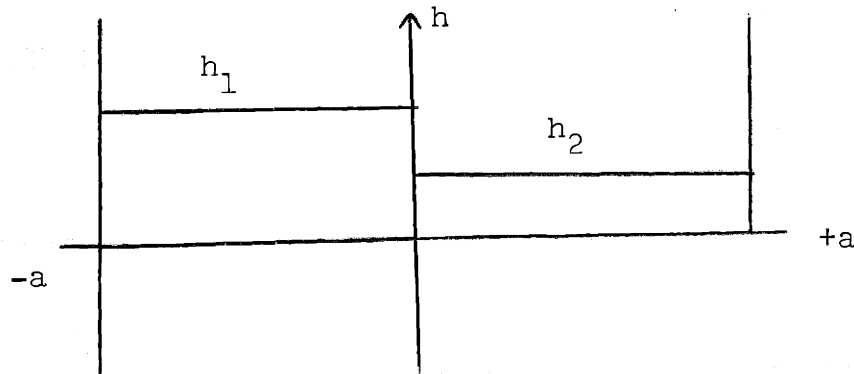
where  $P$  is the centroid to centroid distance between subchannels.

Using this expression a small computer program was developed in order to obtain  $N_H$  as a function of  $z$ .

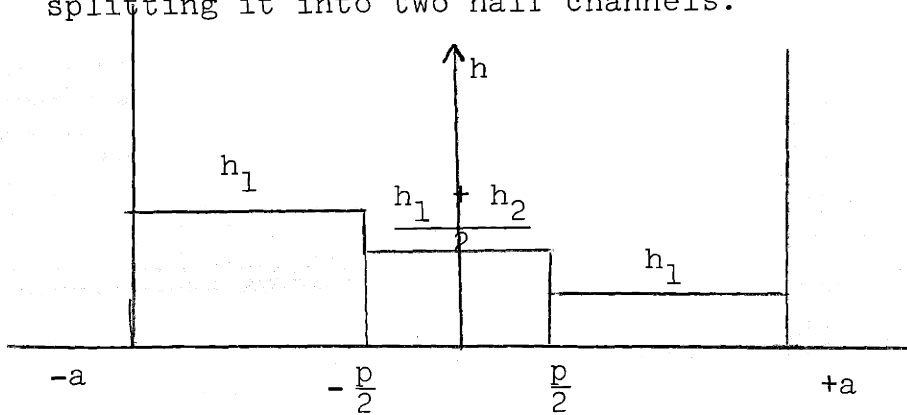
This computer program is given in Appendix 7. In figures

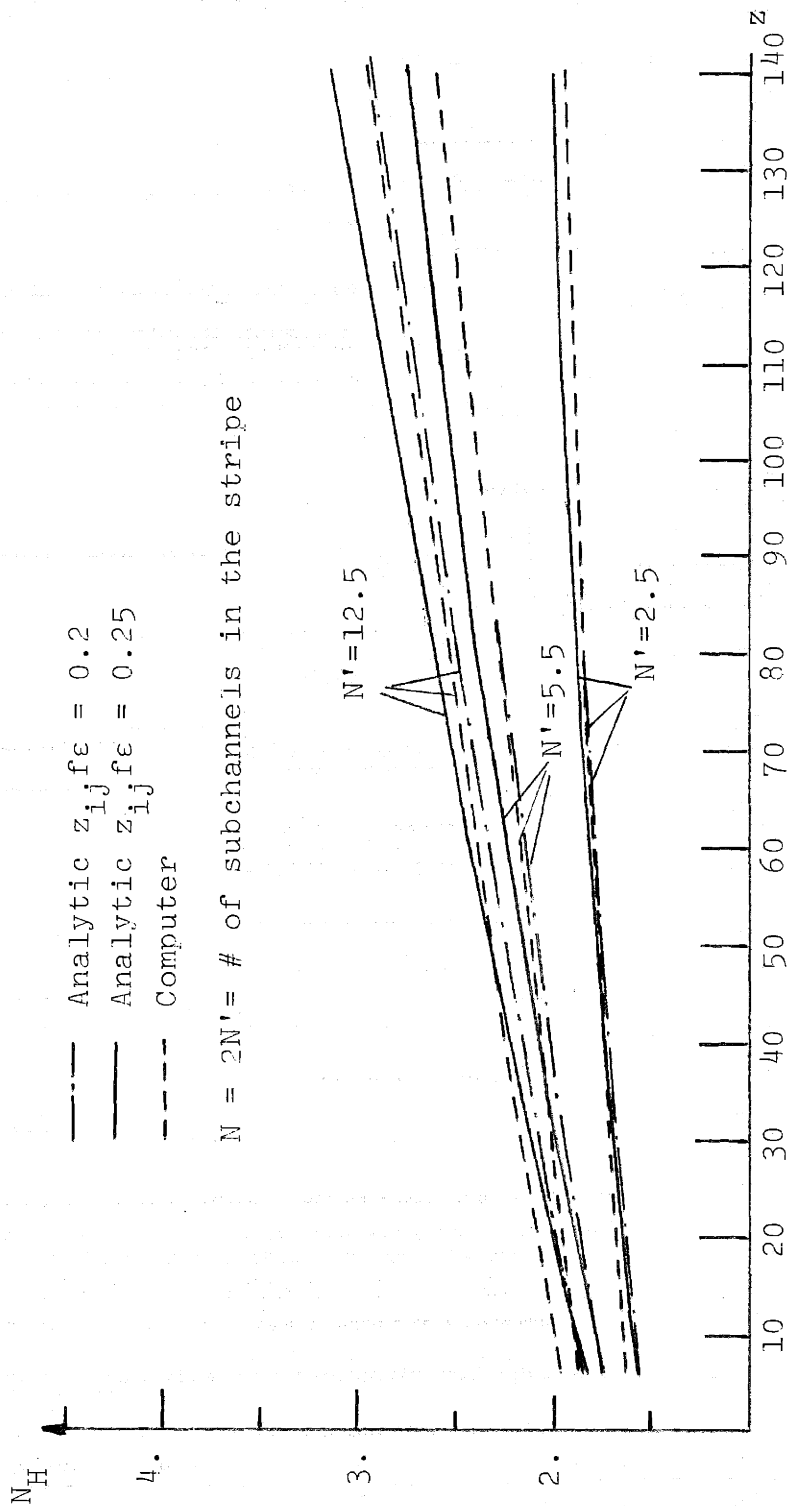
5.3, 5.4 and 5.5 the values of  $N_H$  obtained with both method are compared.

Slight differences can be noticed between results. They come from both uncertainties in the product  $z_{ij} \cdot f_e$  and the different profiles specified for the inlet enthalpy. With the analytical method the following profile was taken:



for Chiu's method early in his work the subchannel spanning the gap was utilized in full rather than splitting it into two half channels.

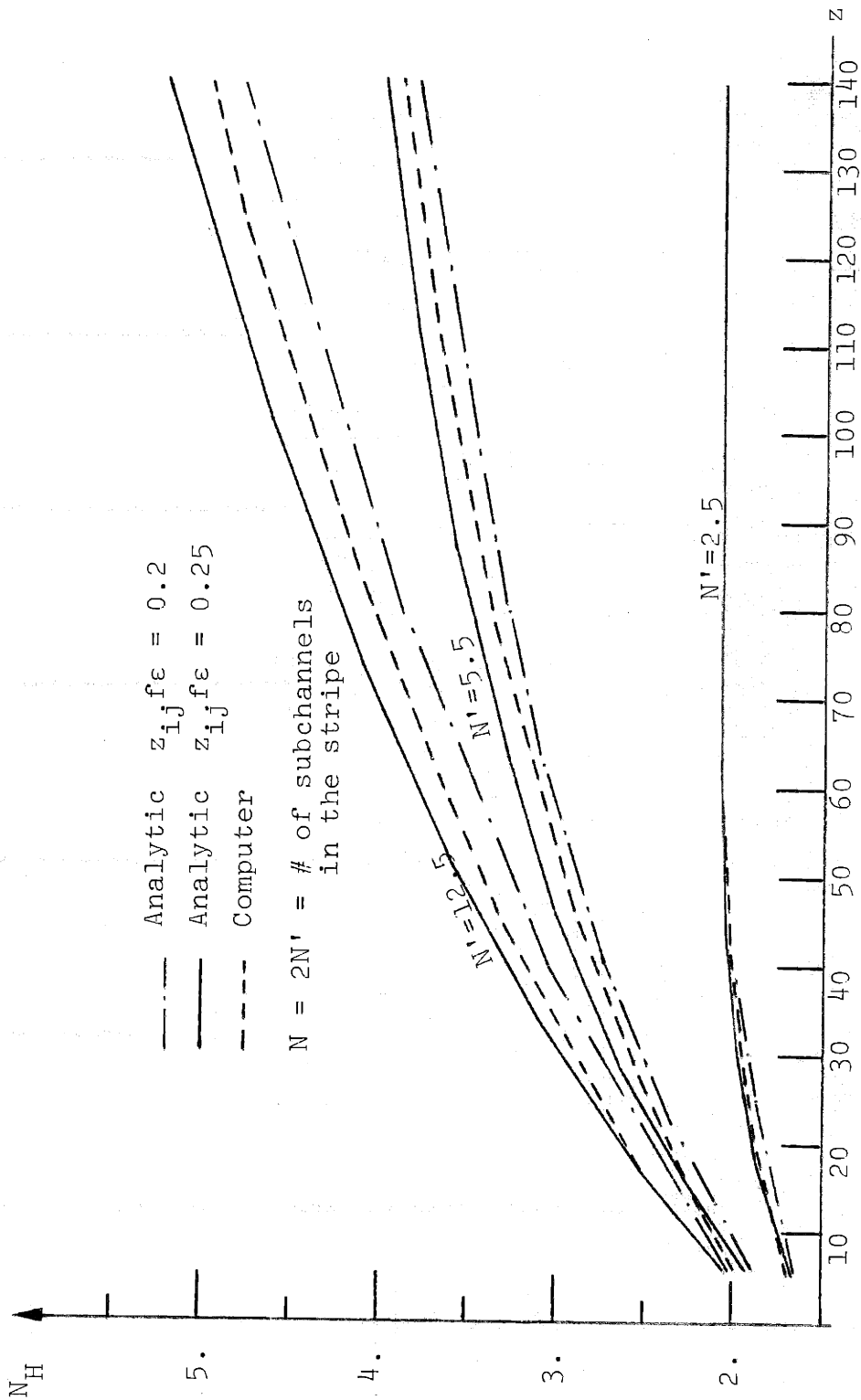




$N = 2N'$  = # of subchannels in the stripe

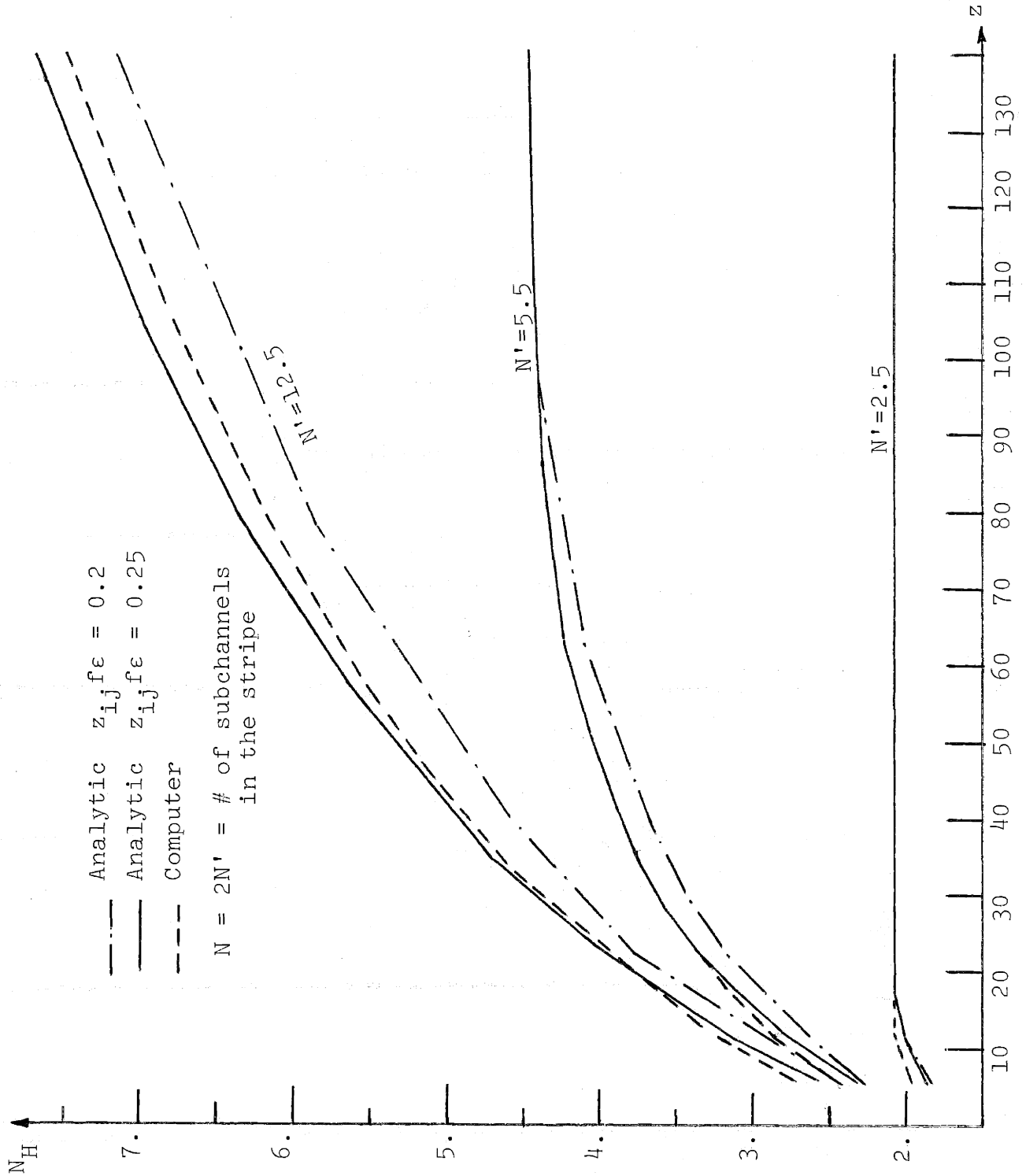
Comparison of the analytical results: Enthalpy upset:  $\beta = 0.005$

Figure 5.3



Comparison of the analytical results: Enthalpy upset:  $\beta = 0.02$

Figure 5.4



Comparison of the analytical results: Enthalpy upset:  $\beta = 0.06$

Figure 5.5

Notice that the effect of the difference of profiles will be important at the inlet of the core, but after a few steps the mixing will make this effect decrease. Notice also that when the number of subchannels is small the effect will be transmitted quite soon to all the subchannels and again the mixing will decrease the effect. These differences can be observed on figures 5.3, 5.4 and 5.5.

#### 5.1.5.2 Heat Generation Upset with Constant Inlet Enthalpy.

In this case:

$$h_1 = h_2 \quad (5.89)$$

$$m_1 = m_2 = 0 \quad (5.90)$$

Then

$$k_1 = \frac{s_1 + s_2}{2} \quad (5.91)$$

$$b_n = \frac{1}{a\alpha_n} (s_1 - s_2) \sin \alpha_n a \quad (5.92)$$

Introducing these values into equation (5.78) we obtain:

$$h(x,z) = \frac{h_1 + h_2}{2} + \frac{s_1 + s_2}{2\rho v_z} z + \sum_{n \text{ odd}}^{\infty} \frac{(s_1 - s_2)}{a\bar{G}\beta\alpha_n^2 0.2} (1 - e^{-\alpha_n^2 \beta z 0.2}) \sin \alpha_n x \quad (5.93)$$

which yields the following value of  $N_H(z)$ :

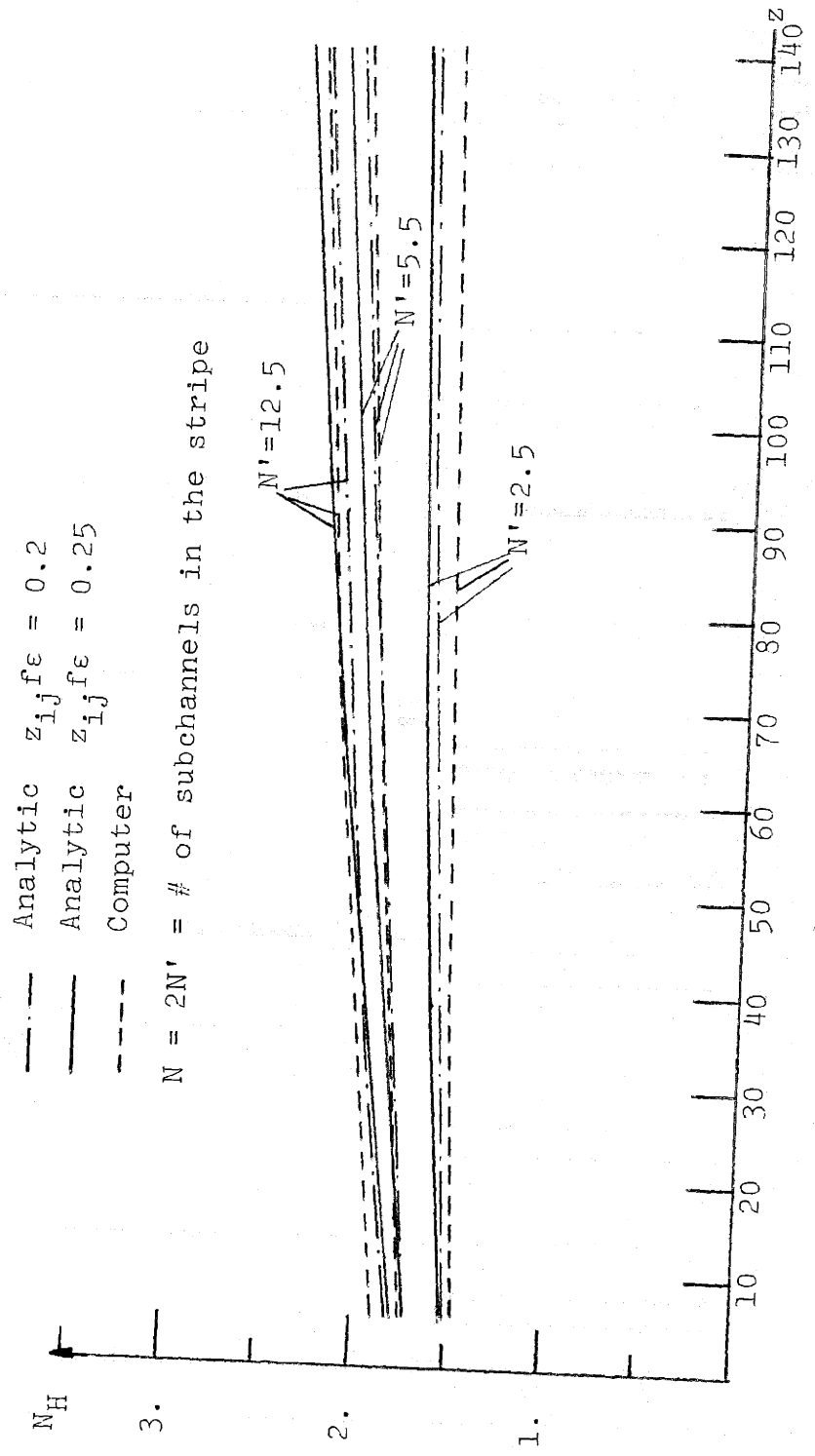
$$N_H(z) = \frac{2}{\left(\frac{a}{P}\right)} \frac{\sum_{n \text{ odd}} \frac{1}{n^4} (1 - e^{-\alpha_n^2 \beta z 0.2}) \cos \frac{\alpha_n P}{2}}{\sum_{n = \text{odd}}^{\infty} \frac{1}{n^4} (1 - e^{-\alpha_n^2 \beta z * 0.2}) \left( \cos \frac{\alpha_n P}{2} - \cos \frac{3\alpha_n P}{2} \right)} \quad (5.94)$$

The computer program used to find the numerical values of  $N_H(z)$  is given in Appendix 8.

In figures 5.6, 5.7 and 5.8, the results obtained are compared against those obtained by Chong Chiu.

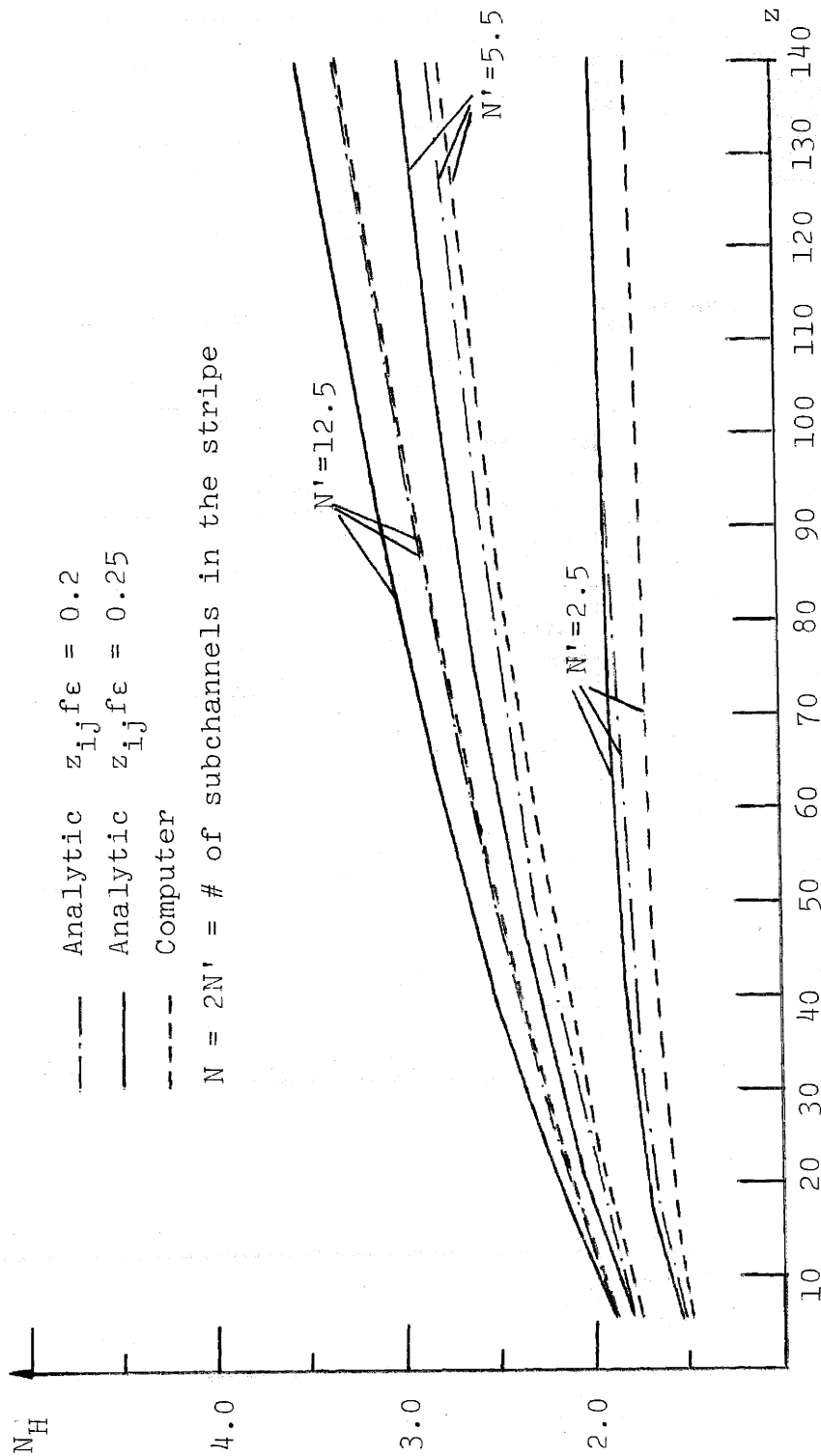
An analogous problem to that of the previous case occurs here. The following volumetric energy generation rate profile is taken for the analytical calculation:





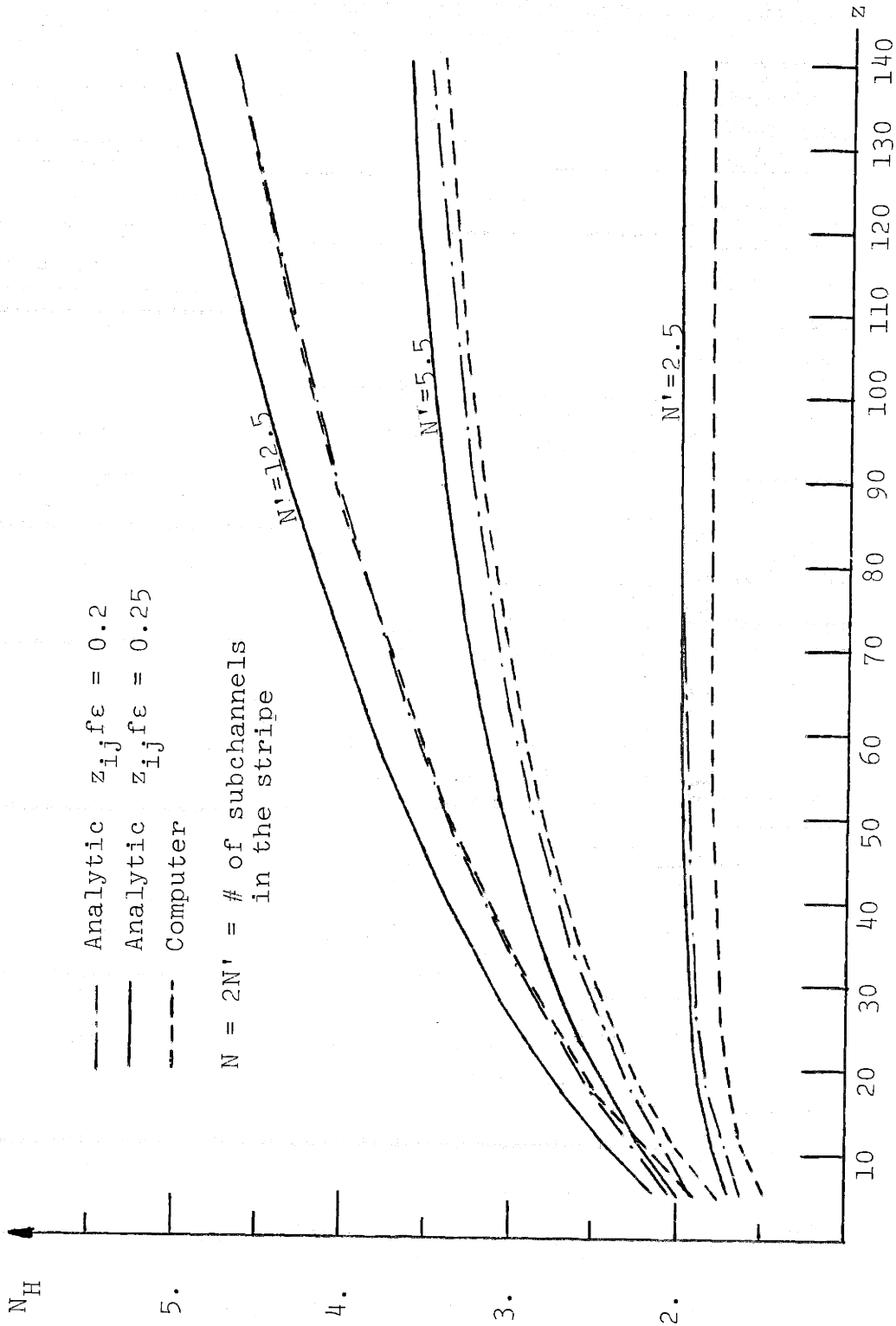
Comparison of the analytical results: Power upset:  $\beta = 0.005$

Figure 5.6



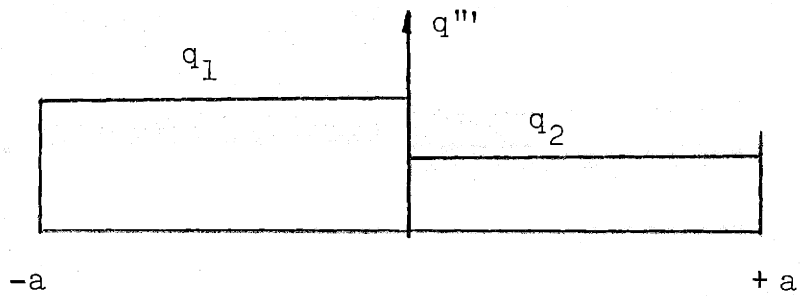
Comparison of the analytical results: Power upset:  $\beta = 0.02$

Figure 5.7

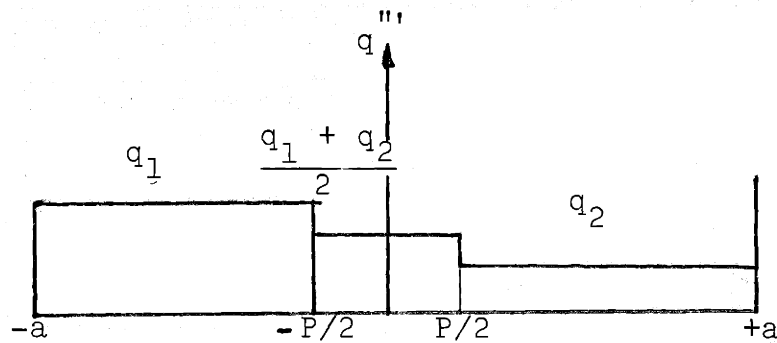


Comparison of the analytical results: Power upset:  $\beta = 0.06$

Figure 5.8



Chiu's results are obtained for:



Notice then, that the effect of this difference will be more important for small number of channels where the continuously added perturbation to the central subchannel will be more important.

## Chapter 6

### CONCLUSIONS AND RECOMMENDATIONS FOR FUTURE WORK

#### 6.1 Conclusions.

From the comparison between the cascade and the simplified method, when a similar division of the hot assembly in channels is taken for both methods, it can be concluded that the simplified method yields better results than the cascade. Additionally it costs less and requires considerable less effort in order to execute the analysis.

From the analysis of the simplified method two conclusions can be achieved. First that the reduction in the number of channels in which the core is divided do not have a large effect on the properties of the hot subchannel when the hot assembly and its neighbors are divided in a fine mesh of channels. But when this mesh get coarser (10 channel case) the effect on the properties of hot subchannels of this reduction (because of the lack of good transport coefficients) becomes larger and the results, worse.

The second conclusion is that from the analysis of the effect of  $N_H$  in the results, it can be concluded that its influence is significant and that the development of

good transport coefficients is required. This effect however, may be manifest through crossflows versus turbulent energy transport.

## 6.2 Recommendations for Future Work

Three main recommendations for future work can be derived from the present thesis: First, the development of appropriate transport coefficients for three dimensional problems either for the energy equation and for the axial and momentum equations. Second, the reduction of the truncation and marching technique associated errors in COBRA IIIC/MIT and third, the study of the cross flows calculated by COBRA IIIC/MIT because from the analysis of the results presented in Chapter 3 and the conclusions being obtained by R. Masterson <sup>(10)</sup> in his thesis, serious doubts exist about the exactness of the cross flows.

Appendix 1

DESCRIPTION OF THE DATA USED IN THE ANALYSIS

- A.1.0 Introduction
- A.1.1 Operating Conditions
- A.1.2 Dimensions of the assemblies
- A.1.3 Dimensions of the subchannels
- A.1.4 Dimensions of the rods
- A.1.5 Axial heat flux distribution
- A.1.6 Radial power factors
  - A.1.6.1 Assemblies
  - A.1.6.2 Subchannels
- A.1.7 Spacer Data
- A.1.8 Thermal-Hydraulic Model
  - A.1.8.1 Mixing
  - A.1.8.2 Single-phase friction
  - A.1.8.3 Two-phase friction
  - A.1.8.4 Void fraction
  - A.1.8.5 Flow division at inlet
  - A.1.8.6 Constants
  - A.1.8.7 Iteration
  - A.1.8.8 Coupling parameters

A.1.0 Introduction

In this appendix the data used in the present thesis will be given. The reactor analyzed is CONNECTICUT YANKEE.

A.1.1 Operating Conditions

System Pressure 2150

Uniform Inlet Enthalpy 548.8 BTU/lb

Uniform Inlet Mass Velocity  $2.217 \times 10^6$  lb/hr ft<sup>2</sup>

Average Heat Flux  $0.2034 \times 10^6$  BTU/hr ft<sup>2</sup>

A.1.2 Dimensions of the Assemblies

The geometrical characteristics of the assemblies are:

Area 38.37 in<sup>2</sup>

Wetter Perimeter 322.8 in

Heated Perimeter 270.5 in

Boundary Gap 2.0 in

Hydraulic Diameter 0.4755 in

Channel Length 126.7 in

Channel Orientation 0.0 degrees



A.1.3 Dimension of the Subchannels.

The geometrical characteristics of the subchannels are:

Area 0.1705 in<sup>2</sup>

Wetted Perimeter 1.435 in

Boundary gap 0.133 in

Hydraulic diameter 0.4755 in

A.1.4 Discussions of the Rods

All the rods are taken as having the same diameter of 0.422 inches.

A.1.5 Axial Heat Flux Distribution

The following heat flux distribution was used:

<u>Position</u> (X/L)	<u>Relative Flux</u>
0.0	0.039
0.05	0.289
0.1	0.531
0.15	0.759
0.2	0.968
0.25	1.151
0.3	1.303
0.35	1.421
0.4	1.502

<u>Position</u>	<u>Relative Flux</u>
0.45	1.544
0.465	1.548
0.475	1.55
0.5	1.545
0.55	1.505
0.6	1.426
0.65	1.391
0.7	1.58
0.75	0.977
0.8	0.770
0.85	0.542
0.9	0.30
0.95	0.051
1.0	0.0

#### A.1.6 Radial Power Factors

##### A.1.6.1 Assemblies.

The radial power factors of each assembly are given in Figure 2.1. These values were taken from Figures 4.2-16 of the report GTS-75-A-136 sent to Dr. E. Khan by J. Chunis of Northeast Utilities.

##### A.1.6.2 Hot Assembly

In Figure A.1.1 the radial power factors for the subchannels of the hot assembly are given. These values were assumed by Dr. E. Khan.

### A.1.7 Spacer Data

In the following table the relative location and the type of spacer situated at that location are given.

Location (X/L)	0.005	0.159	0.324	0.492	0.658	0.824	0.995
Spacer Type No.	1	2	3	3	3	3	3

The drag coefficients assumed for each spacer type are:

Spacer Type No.	1	2	3
Drag Coefficient	4.011	0.978	1.565

### A.1.8 Thermal-Hydraulic Model.

#### A.1.8.1 Mixing

In calculations of Chapter 2, the mixing coefficient  $\beta$  was taken as equal to zero, while in chapter 3 it was assumed to be 0.02.

The two-phase mixing coefficient is taken as equal to that of single phase in both cases.

Thermal conduction is neglected.

#### A.1.8.2 Single-Phase Friction

It is calculated by:

$$f = \frac{0.184}{R_e^{0.2}}$$

where  $R_e$  = n Reynolds Number

#### A.1.8.3 Two-Phase Friction

The homogeneous model friction multiplies was selected to describe the two-phase pressure drop due to friction.

#### A.1.8.4 Void Fraction

It was calculated using the Levy model and a slip ratio equal to one.

#### A.1.8.5 Flow Division at Inlet

The inlet mass velocity was taken as uniform, equal to  $2.217 \times 10^6$  lb/hr ft<sup>2</sup> for all channels.

#### A.1.8.6 Constants

The constants used are:

Cross-flow resistance (KIJ) = 0.5

Momentum Turbulent Factor (FTM) = 0.0

Transverse Momentum Factor (S/L) = 0.5

The CHF correlation used in all the calculations was W-3.

#### A.1.8.7 Iteration

The flow convergence factor used was 0.01.

The number of axial steps in which the core was divided was 21. Then the length of each axial step was 6.003 inches.

All the calculations were done for steady state.

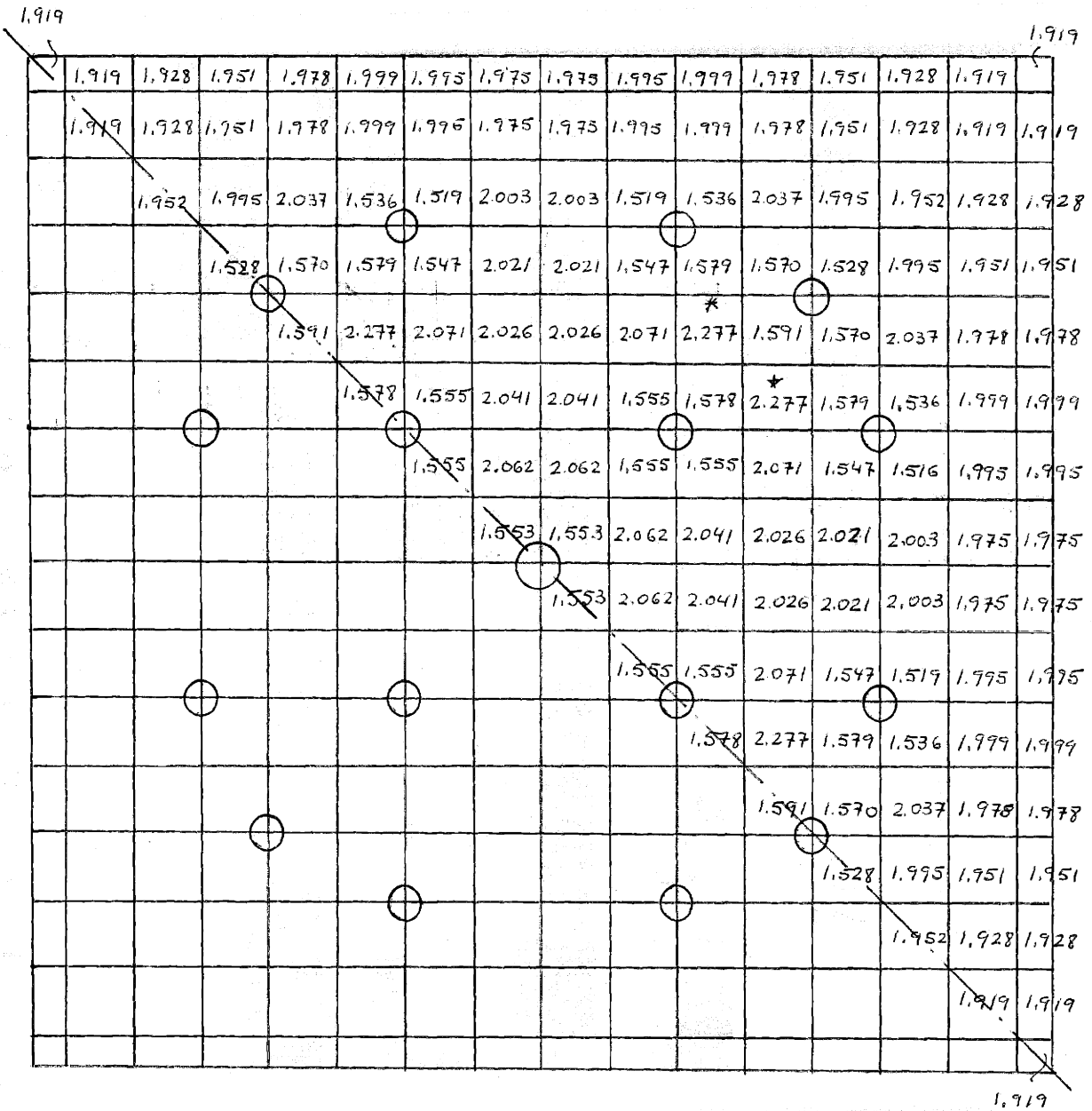
#### A.1.8.8 Coupling Parameter

In Chapter 2 no coupling parameter was used. In Chapter 3, Section 3.1, no coupling parameter was used either. While in Section 3.2 the following coupling parameter was used:

$$N_H = N$$

where

N = number of rods between the center lines of the channels making up the boundary conditions.



\* Hot Subchannel

○ Control Rods

Radial Peaking Factors Inside the Hot Assembly

Figure A.1.1

Appendix 2

ACTUAL CALCULATION OF THE AVERAGE ENTHALPY OF THE  
HOT ASSEMBLY IN THE HOT ASSEMBLY ANALYSIS

The average enthalpy of the assembly ( $h'_3$ ) is calculated as the average of the enthalpies of each individual channel weighted with the mass flow of each sub-channel:

$$h'_3 = \frac{\sum_{i=1}^N h_3(i) m_3(i)}{\sum_{i=1}^N m_3(i)} \quad \text{where } N = \# \text{ of channels} \quad (\text{A.2.1})$$

If there was not truncation errors in the equations used in COBRA III-C/MIT), equation A.2.1 will yield exactly:

$$h'_3 = h'_1 + \left[ \frac{\bar{q}'_1}{m_1} \right] \Delta X' \quad (\text{A.2.2})$$

but because of the truncation errors the equation is different:

$$h'_3 = h'_1 + \left[ \frac{\bar{q}'_1}{m_1} \right] \Delta X' + f(w_1 w'_1 \left( 1 - \frac{m_J}{m_{J-1}} \right)) \quad (\text{A.3.3})$$

where the function  $f$  depends upon diversion crossflows, turbulent interchange terms and mass flows, but all these terms are very small when the axial step has a short length, and they are negligible for cases like this. For some cases,

however, it may be necessary to keep track of this factor  
in order to understand what is happening.



Appendix 3

MASS FLOW RATES OF EACH CHANNEL AT THE INLET OF A  
SLICE AS A FUNCTION OF THE VALUES AT THE  
OUTLET OF THE PREVIOUS SLICE

3.0 General Expressions

Let us take the case represented in Figure A.3.1. If  $i$  is one of the channels facing assembly I:

$$m'_J(i) = m'_{J-1}(i) - \left[ w_{2J}(21,I) + w_{2J-1}(21,I) \right] \Delta X \frac{GAP(i,I)}{GAP(21,I)} \quad (A.3.1)$$

where:

$m'_J(i)$  = mass flow rate of channel  $i$  at the inlet of slice  $J$

$m'_{J-1}(i)$  = mass flow rate of channel  $i$  at the outlet of slice  $J-1$

$w_{2J}(21,I)$  = diversion crossflow between assemblies 21 and I at axial station  $2J$  of the assembly to assembly analysis.

$w_{2J-1}(21,I)$  = diversion crossflow between assemblies 21 and I at axial station  $2J-1$  of the assembly to assembly analysis.

Analogously the mass flow rate can be found for the rest of the outer channels. Recall that the corner channels have two boundaries from which is assumed that flow is leaving or entering. For this channel we have:

$$m'_J(X) = m'_{J-1}(X) - \left[ w_{2J}(21,I) + w_{2J-1}(21,I) \right] \Delta X \frac{GAP(X,I)}{GAP(21,I)} -$$

$$- \left[ w_{2J}(21,Y) + w_{2J-1}(21,Y) \right] \Delta X \frac{GAP(X,Y)}{GAP(21,Y)} \quad (A.3.2)$$

The mass flow rate per unit area (G) will be:

$$G'_J(X) = \frac{m'_J(X)}{A(X)} = G'_{J-1}(X) - \left[ w_{2J}(21,I) + w_{2J-1}(21,I) \right]$$

$$\frac{\Delta X}{A(X)} \frac{GAP(X,I)}{GAP(21,I)} - \left[ w_{2J}(21,Y) + w_{2J-1}(21,Y) \right]$$

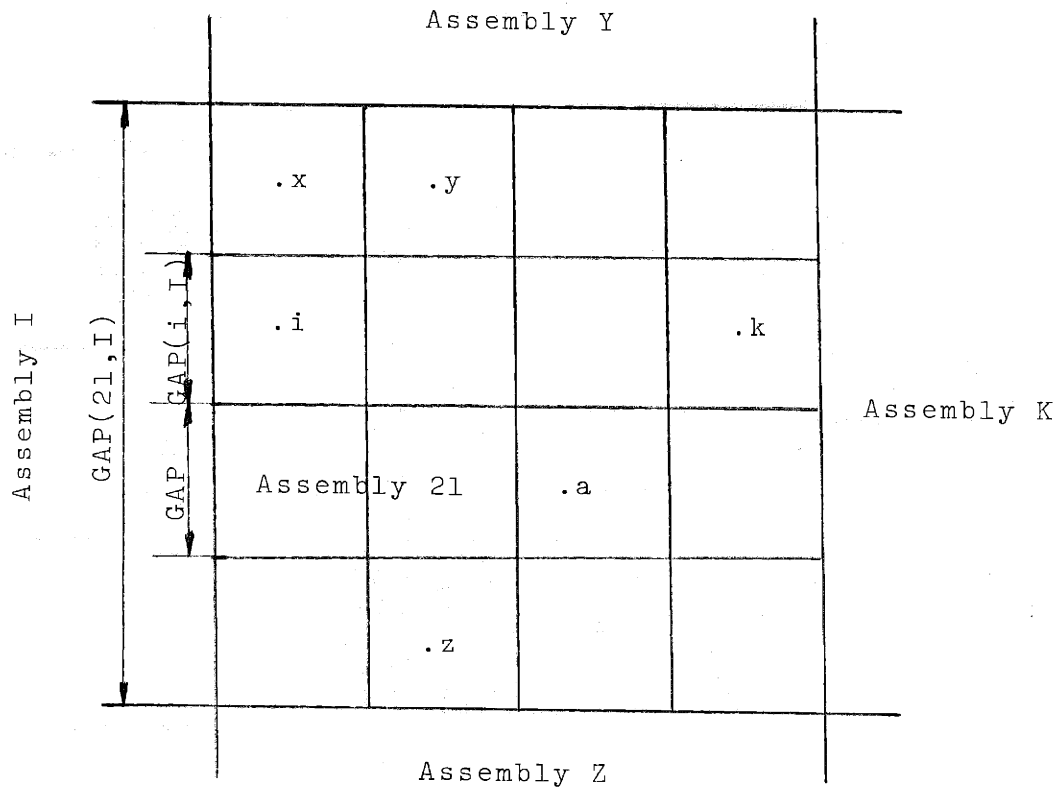
$$\frac{\Delta X}{A(X)} \frac{GAP(X,Y)}{GAP(21,Y)} \quad (A.3.3)$$

where  $A(X)$  = area of the channel X

For channels in the interior of the assembly there is no modification:

$$G'_J(a) = G'_{J-1}(a) \quad (A.3.4)$$

or putting it in words the mass flow rate for channel a at the inlet of slice J, should be equal to the mass flow rate of channel a at the outlet of slice J-1.



Example Case

Figure A.3.1

Appendix 4

SUBROUTINE TABLES

SUBROUTINE TABLES(CARD)

IMPLICIT INTEGER (\*)

```

COMMON /CORRA1/ ABETA , AFLUX , ATOTAL , BBETA , DIA , DT , DX ,
1 FLEV , FERROR , FLO , FIM , GC , GK , GRID , HSURF , HF ,
2 HFG , HG , I2 , I3 , IERROR , IQP3 , ITERAT , J1 , J2 ,
3 J3 , J4 , J5 , J6 , J7 , KDEBUG , KF , KIJ ,
4 NAFACT , NARAMP , NAX , NAXL , NBBC , NCHANL , NCHF , NDX , NF ,
5 NGAPS , NGRID , NGRIDT , NGTYPE , NGXL , NK , NODES , NODESF , NPROP ,
6 NRAMP , NROD , NSCBC , NV , NVISCW , PI , PITCH , POWER , PREF ,
7 QAX , RHOF , RHOG , SIGMA , SL , TF , TFLUID , THETA , THICK ,
8 UF , VF , VFG , VG , Z

```

LOGICAL GRID

```

REAL KIJ , KF , KKF , KCLAD , KFUEL

```

```

COMMON /CORRA3/ MA , MC , MG , MN , MR , MS , MX ,
1 $$$ , $A , $AAA , $AC , $ALPHA , $AN , $ANSWF , $B ,
1 $CCHAN , $CD , $CHER , $CON , $COND , $CP , $D , $DC , $DFDX ,
2 $DHDX , $DHYD , $DHYDN , $DIST , $DPDX , $DPK , $DUR , $DR , $F ,
3 $FACTO , $FDIV , $FINLE , $FLUX , $FMULT , $FOLD , $FSP , $FSPLT , $FXFLO ,
4 $GAP , $GAPN , $GAPS , $H , $HFILM , $HINLE , $HOLD , $HPERT , $IDARE ,
5 $IDFUE , $IDGAP , $IK , $JBOIL , $JK , $LC , $LENGT , $LOCA , $LR ,
6 $MCHER , $MCFRC , $MCFRR , $NTYPE , $NWRAP , $NWRPS , $P , $PERIM , $PH ,
7 $PHI , $PRNTC , $PRNTR , $PRVTN , $PW , $PWRF , $QC , $QF , $QPRIM ,
8 $QUAL , $RADIA , $RHO , $RHOOL , $SP , $T , $TDUMY , $TINLE , $TROD ,
9 $U , $UH , $USAVE , $USTAR , $V , $VISC , $VISCW , $VP , $VPA ,
10 $W , $WOLD , $WP , $WSAVE , $X , $XCROS

```

COMMON DATA(1)

LOGICAL LDAT(1)

INTEGER IDAT(1)

EQUIVALENCE (DATA(1), IDAT(1), LDAT(1))

```

COMMON /LINK2/ CROSS(6) , DATE(2) , FG(30) , FH(30) , FP(30) , FQ(30) , IM(9) ,
1 JM(9) , OUTPUT(10) , PRINT(12) , TEXT(17) , TIME(3) , YG(30) , YH(30) , YP(30) ,
2 YQ(30)

```

```

COMMON /LINK3/ DXX , ETIME , GIN , HIN , I8 , IG , IH , ISAVE , JUMP , KASE , KT , MAXT ,
1 NDT , NDXPI , NFUEL , NG , NH , NJUMP , NOUT , NP , NPCHAN , NPNOE , NPROD , NQ , NR ,
2 NSKIPT , NSKIPX , NTRIES , PEXIT , PHTOT , SAVEDT , TIN , TTIME , ZZ

```

DIMENSION CARD(20)

SET PRINTING PARAMETERS

FOR INPRIN

IF (J1.GT.1) GO TO 4

DO 2 I=1,11

2 PRINT(I) = .TRUE.

PRINT(5) = .FALSE.

PRINT(6) = .FALSE.

FOR CALC (CARD GROUP 9)

4 READ (I2,1001) CARD , KDEBUG

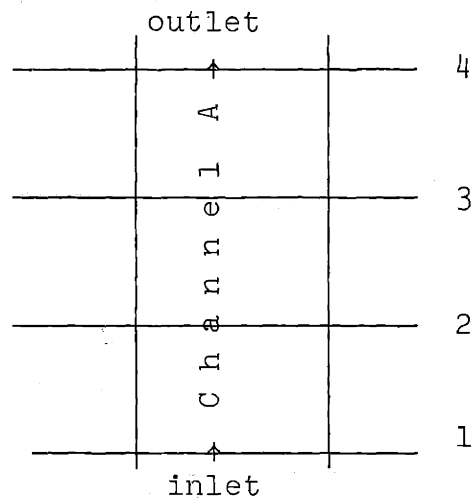
```
WRITE (I3,1002) CARD
C
C FOR EXPRIN (CARD GROUPS 9, 12)
READ (I2,1001) CARD, NSKIPX, NSKIPT, NOUT, NPCHAN, NPROD, NPNODE
WRITE (I3,1003) CARD
C NSKIPX. EVERY NSKIPX AXIAL STEP PRINTED. (0 = 1)
C NSKIPT. EVERY NSKIPT TIME STEP PRINTED. (0 = 1)
C NOUT = 0-3 FOR PRINTING (0) CHANNEL ONLY, (1) CHAN + CROSS FLOWS,
C (2) CHAN + FUEL TEMP, (3) CHAN + C-F + FUEL TEMP
C NPCHAN = 0, ALL CHAN PRINTED. .GT.0 READ CHANS REOD.
C NPROD, NPNODE AS NPCHAN BUT FOR RODS AND NODES.
IF (NSKIPX.LT.1) NSKIPX = 1
IF (NSKIPT.LT.1) NSKIPT = 1
IF (NPCHAN.LT.1) GO TO 6
MROSI=1
7209 MMJAVI=MIN0((MROSI+13),NPCHAN)
READ (I2,1001) CARD, (IDAT($PRNTC+I), I=MROSI, MMJAVI)
WRITE (I3,1004) CARD
MROSI=MMJAVI+1
IF (MROSI.LE.NPCHAN) GO TO 7209
6 IF (NPROD.LT.1) GO TO 8
MROSI=1
8209 MMJAVI=MIN0((MROSI+13),NPROD)
READ (I2,1001) CARD, (IDAT($PRNTR+I), I=MROSI, MMJAVI)
WRITE (I3,1006) CARD
MROSI=MMJAVI+1
IF (MROSI.LE.NPROD) GO TO 8209
8 IF (NPNODE.LT.1) GO TO 10
MROSI=1
6209 MMJAVI=MIN0((MROSI+13),NPNODE)
READ (I2,1001) CARD, (IDAT($PRNTN+I), I=MROSI, MMJAVI)
WRITE (I3,1007) CARD
MROSI=MMJAVI+1
IF (MROSI.LE.NPNODE) GO TO 6209
C
10 IF (NPCHAN.GT.0) GO TO 14
NPCHAN = NCHAN1
DO 12 I=1, NCHAN1
12 IDAT($PRNTC+I) = I
14 IF (NPROD.GT.0) GO TO 18
NPROD = NPROD
DO 16 I=1, NPROD
16 IDAT($PRNTR+I) = I
18 IF (NPNODE.GT.0) GO TO 22
NPNODE = NODESF+1
DO 20 I=1, NPNODE
20 IDAT($PRNTN+I) = I
22 CONTINUE
C
RETURN
C
1001 FORMAT(20A4, T1, 14I5)
1002 FORMAT(' KDEBUG', 22X, '***', 20A4, '*** TABLE')
1003 FORMAT(' PRINTING', 20X, '***', 20A4, '*** TABLE')
1004 FORMAT(' PRINT CHANNELS ', 11X, '***', 20A4, '*** TABLE')
1005 FORMAT(' PLUS REMAINDER')
1006 FORMAT(' PRINT RODS ', 11X, '***', 20A4, '*** TABLE')
```

1007 FORMAT(' PRINT NODES ', 11X, '\*\*\*', 20A4, '\*\*\* TABLES')

END

Appendix 5  
DEVELOPMENT OF AN EXPRESSION TO CALCULATE THE TRUNCATION  
AND MARCHING TECHNIQUE ERRORS ASSOCIATED  
WITH COBRA IIIC/MIT

Let us take a case with three axial steps. It will make the deduction simpler than in a general case and the results are completely general.



For any channel (i.e.A) the energy error introduced by the code can be defined:

$$E.E(A) \equiv M_4(A)h_4(A) - M_1(A)h_1(A) - E.A.(A) \quad (A.5.1)$$



where:

$M_4(A)$  = mass flow at the outlet of Channel A

$h_4(A)$  = enthalpy at the outlet of Channel A

$M_1(A)$  = mass flow at the inlet of Channel A

$h_1(A)$  = enthalpy at the inlet of Channel A

$E.A(A)$  = total energy added to Channel A between points 1 and 4. This energy comes from the fission reaction as well as the diversion crossflows and turbulent interchanges between the channel and its neighbors.

On the other hand:

$$E.A(A) = \sum_{i=1}^3 E.A_i(A) \quad (A.5.2)$$

where

$E.A_i(A)$  = energy added to channel A in axial step i.

The differential form of the combined energy-mass conservation equation (A-7 of BNWL-1695 corrected) written for steady state is:

$$M_i \frac{\partial h_i}{\partial x} = \bar{q}'_i - (h_i - h_j) w'_{ij} + (h_i - h^*) w_{ij} \quad (A.5.3)$$

where

$$h^* = h_i \text{ if } w_{ij} > 0$$

$$h^* = h_j \text{ if } w_{ij} < 0$$

taking channel i as A and j as B equation (A.5.3) becomes:

$$M(A) \frac{\partial h(A)}{\partial x} = \bar{q}'(A) - (h(A) - h(B)) w'(A,B) + (h(A) - h^*) w(A,B) \quad (A.5.4)$$

The COBRA form of the corresponding difference equation

$$M_1(A) \left( \frac{h_2(A) - h_1(A)}{\Delta x} \right) = \bar{q}_{1+\frac{1}{2}} - (h_1(A) - h_1(B)) w_1'(A,B) + (h_1(A) - h_1^*) w_1(A,B) \quad (A.5.5)$$

where the subindices indicate the axial location where that property is measured.

Equation (A.5.5) becomes:

$$h_2(A) = h_1(A) + \frac{[\bar{q}_{1+\frac{1}{2}} - (h_1(A) - h_1(B)) w_1'(A,B) - h_1^* w_1(A,B)]}{M_1(A)} + \frac{w_1(A,B) h_1(A) \Delta x}{M_1(A)} \quad (A.5.6)$$

Introducing the definition of energy added and taken all the channels adjacent to A:

$$h_2(A) = h_1(A) + \frac{E.A_1(A)}{M_1(A)} + \frac{w_1(A) h_1(A)}{M_1(A)} \Delta x \quad (A.5.7)$$

where  $w_1(A)$  is the total diversion crossflow between channel A and its neighbors. In the code  $w_1(A)$ , for the calculation of the enthalpy increase in the first axial step, is always taken as zero. Then equation (2.5.7) becomes:

$$E.A_1(A) = M_1(A) [ h_2(A) - h_1(A) ] \quad (A.5.8)$$

Analogously for the second axial step:

$$h_3(A) = h_2(A) + \frac{E.A_2(A)}{M_2(A)} + \frac{w_2(A) h_2(A)}{M_2(A)} \quad (A.5.9)$$

Then:

$$E.A_2(A) = M_2(A) [ h_3(A) - h_2(A) ] - w_2(A) h_2(A) \Delta x \quad (A.5.10)$$

for the third axial step:

$$E.A_3(A) = M_3(A) [ h_4(A) - h_3(A) ] - w_3(A) h_3(A) \Delta x \quad (A.5.11)$$

Taking equations (A.5.8), (A.5.10), (A.5.11) and (A.5.2) into equation (A.5.1) we obtain:

$$\begin{aligned}
 E.E. (A) = & [ M_4(A) - M_3(A) ] h_4(A) + \\
 & [ M_3(A) - M_2(A) + w_3(A) \Delta x ] h_3(A) + \\
 & [ M_2(A) - M_1(A) + w_2(A) \Delta x ] h_2(A) \quad (A.5.12)
 \end{aligned}$$

and it can be proven that for N axial steps:

$$\begin{aligned}
 E.E(A) = & [ M_{N+1}(A) - M_N(A) ] h_{N+1}(A) + \sum_{N=2}^N [ M_n(A) - \\
 & - M_{n-1}(A) + \Delta x w_n(A) ] h_n(A) \quad (A.5.13)
 \end{aligned}$$

This is the final expression for the energy error. If COBRA IIIC/MIT would use the exact mass conservation equation we could use the following expression:

$$E.E(A) = [ M_{N+1}(A) - M_N(A) ] h_{N+1}(A) \quad (A.5.14)$$

But because the mass conservation equation is:

$$w_N(A) = \frac{ [ M_N(A) - 0.2 * M_N^*(A) ] - 0.8 M_{N-1}(A) }{ 0.8 } \quad (A.5.15)$$

where  $M_N^*(A)$  = massflow of Channel A at axial station N  
in the previous iteration.

Equation (A.5.13) should be used to express the energy error.

Equation (A.5.13) was tested using the code output values for Channel # 10 of the 10 channel case against values obtained by using the following equation:

$$E.E_N(A) = M_{N+1}(A)h_{N+1}(A) - M_N(A)h_N(A) - E.A_N(A) \quad (A.5.16)$$

The results obtained are those of Table A.5.1. The small differences observed are due to round-off errors.

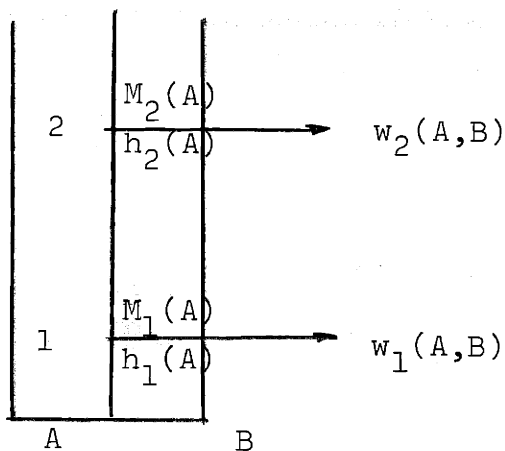
Distance	Equation - (A.5.16)		Equation - (A.5.13)	
	Total	Partial	Total	Partial
6.0	24.98	24.98	26.97	26.97
12.1	56.07	31.08	58.58	31.61
18.1	87.57	31.50	86.99	28.41
24.1	119.22	31.65	116.60	29.61
30.2	133.41	14.19	129.84	13.24
36.2	146.31	12.90	143.89	14.05
42.2	182.31	36.00	177.90	34.01
48.3	252.61	70.30	247.41	69.51
54.3	255.38	2.77	251.04	3.63
60.3	324.95	69.57	319.47	68.43
66.4	360.74	35.79	354.84	35.37
72.4	298.34	-62.40	296.15	-58.69
78.4	288.07	-10.27	281.55	-14.60
84.5	299.93	+11.86	296.65	15.10
90.5	181.13	-118.80	174.40	-122.25
96.5	64.51	-116.82	61.69	-112.71
102.6	- 9.03	- 73.54	- 14.39	- 76.08
108.6	64.95	+ 73.98	60.16	74.55
114.6	-98.90	-163.85	- 98.33	-158.49
120.7	-119.63	- 20.73	-118.50	- 20.17
126.7	133.11	252.74	133.14	251.64
TOTAL	133.11		133.14	

Testing of equation (A.5.13)  
Table A.5.1

Appendix 6

IMPROVEMENTS SUGGESTED IN ORDER TO ELIMINATE TRUNCATION  
 ERRORS AND ERRORS ASSOCIATED WITH THE MARCHING TECHNIQUE  
 USED IN COBRA IIIC/MIT

Let us take an example:



$$\text{where } w_2(A,B) \approx M_2(A) - M_1(A) \quad (\text{A.6.1})$$

$$w_1(A,B) \approx M_1(A) - M_0(A) \quad (\text{A.6.2})$$

as indicated in previous chapters, the energy conservation equation used in the code is:

$$M_1(A)h_2(A) + w_1(A,B)h_1(A)\Delta x - M_1(A)h_1(A) = E.A_1(A) =$$

$$\bar{q}'_{1+\frac{1}{2}} * \Delta x - w'_1(A,B) [h_1(A) - h_1(B)] \Delta x + w_1(A,B)h_1^* \Delta x$$

(A.6.3)

The correct energy equation should be:

$$M_2(A)h_2(A) - M_1(A) = E.A'(A) \quad (A.6.4)$$

where:

$$M_2(A)h_2(A) = M_1(A)h_1(A) + M_1(A) [h_2(A) - h_1(A)] + \Delta x w_2(A,B)h_1(A) + \Delta x w_2(A,B) [h_2(A) - h_1(A)] \quad (A.6.5)$$

$E.A'(A)$  should be the energy added to the channel in the axial step considered. A better approximation for this value will be:

$$E.A'(A) = \bar{q}'_{1+\frac{1}{2}} \Delta x - w'_{1+\frac{1}{2}}(A,B) [h_{1+\frac{1}{2}}(A) - h_{1+\frac{1}{2}}(B)] \Delta x + w_{1+\frac{1}{2}}(A,B) h_{1+\frac{1}{2}}^* \Delta x \quad (A.6.6)$$

where:

$$h_{1+\frac{1}{2}}(A) = \frac{h_1(A) + h_2(A)}{2} \quad (A.6.7)$$

$$w_{1+\frac{1}{2}}(A,B) = \frac{w_1(A,B) + w_2(A,B)}{2} \quad (A.6.8)$$

$$w'_{1+\frac{1}{2}}(A,B) = \frac{w'_1(A,B) + w'_2(A,B)}{2} \quad (A.8.9)$$



To be able to execute these changes we will need to follow a scheme similar to that presented below:

- a) Having  $h_1$ ,  $w_1$ ,  $w_1'$  and  $M_1$  (from the previous step),
- b) Calculate  $h_2$  with the actual energy equation,
- c) With the value of  $h_2$ , calculate  $w_2$  exactly like it is done in COBRA IIIC/MIT,
- d) Instead of stopping the calculations for the step here, do the following:
  - d.1) calculate  $w_{1+\frac{1}{2}}'$ ,  $h_{1+\frac{1}{2}}$ ,  $w_{1+\frac{1}{2}}$ , and  $M_2$
  - d.2) Using equations (A.6.4) and (A.6.6) we can calculate  $h_2(A)$  in a more correct fashion.

Appendix 7

COMPUTER PROGRAM TO CALCULATE  $N_H$   
FOR THE ENTHALPY UPSET CASE

```

REAL*8 LOW(26)
DIMENSION BETA(3),XX(5),C(200),D(200)
DATA BETA/0.005,0.02,0.05/
DATA XX/12.5,5.5,2.5/
DO 2J=1,3
DO 3K=1,3
PRINT 102,BETA(J),XX(K)
102 FORMAT (5X,'BETA=',F10.5,10X,'N=',F10.2)
ZIJ=0.496
Z=5.76
20 BX=.20*BETA(J)
303 C1=0.
DO 8L2=1,200,2
Y2=L2
109 C(L2)=(1./(Y2**2))/EXP(BX*Z*((1.5708*Y2/XX(K)/ZIJ)**2))*
1(COS(Y2*0.7854/XX(K))-COS(2.3562*Y2/XX(K)))
111 C1=C1+C(L2)
IF (C(L2)-0.0000001)9,9,8
8 CONTINUE
9 D1=0.
DO 10L3=1,200,2
Y3=L3
D(L3)=(1./(Y3**2))/EXP(BX*Z*((1.5708*Y3/XX(K)/ZIJ)**2))*
1(COS(Y3*0.7854/XX(K)))
D1=D1+D(L3)
IF (D(L3)-0.0000001)11,11,10
10 CONTINUE
11 PR=XX(K)*C1/D1/2.
1001 RP=1./PR
PRINT 101,7,RP
101 FORMAT (5X,'Z=',F10.3,10X,'NH=',F10.3)
Z=Z+(144./25.)
IF (Z-144.) 20,20,21
21 CONTINUE
3 CONTINUE
2 CONTINUE
STOP
END

```

Appendix 8  
COMPUTER PROGRAM TO CALCULATE  $N_H$   
FOR THE POWER UPSET CASE

```

REAL*8 LOW(26)
DIMENSION BETA(3),XX(5),C(200),D(200),E(200),F(200)
DATA BETA/0.005,0.02,0.05/
DATA XX/12.5,5.5,2.5/
DO 2J=1,3
DO 3K=1,3
PRINT 102,BETA(J),XX(K)
102 FORMAT (5X,'BETA=',F10.5,10X,'N=',F10.2)
ZIJ=0.496
Z=5.76
20 BX=.20*BETA(J)
303 C1=0.
DO 8L2=1,200,2
Y2=L2
109 C(L2)=(1./(Y2**4))/EXP(BX*Z*((1.5708*Y2/XX(K)/ZIJ)**2))*
1(COS(Y2*0.7854/XX(K))-COS(2.3562*Y2/XX(K)))
111 C1=C1+C(L2)
IF (C(L2)-0.0000001)9,9,8
8 CONTINUE
9 D1=0.
DO 10L3=1,200,2
Y3=L3
D(L3)=(1./(Y3**4))/EXP(BX*Z*((1.5708*Y3/XX(K)/ZIJ)**2))*
1(COS(0.7854*Y3/XX(K)))
D1=D1+D(L3)
IF (D(L3)-0.0000001)11,11,10
10 CONTINUE
11 E1=0.
DO 14L4=1,200,2
Y4=L4
E(L4)=(1./(Y4**4))* (COS(Y4*0.7854/XX(K))-COS(2.3562*Y4/XX(K)))
E1=E1+E(L4)
IF (E(L4)-0.0000001)17,17,14
14 CONTINUE
17 F1=0.
DO 23L5=1,200,2
Y5=L5
F(L5)=(1./(Y5**4))*COS(0.7854*Y5/XX(K))
F1=F1+F(L5)
IF (F(L5)-0.0000001)24,24,23
23 CONTINUE
24 RP=(2./XX(K))*(F1-D1)/(F1-C1)
PRINT 101,Z,RP
101 FORMAT (5X,'Z=',F10.3,10X,'NH=',F10.3)
Z=Z+(144./25.)
IF (Z-144.) 20,20,21
21 CONTINUE
3 CONTINUE
2 CONTINUE
STOP
END

```

Appendix 9

DESCRIPTION OF THE MODIFICATIONS INTRODUCED IN COBRA IIIC/MIT

A.9.1 Modifications to Allow for More Than Four Channels Surrounding Any Single One.

A.9.1.1 LOCA Array

When more than four channels are surrounding any single one, we may have one boundary influenced by more than six boundaries. Then the dimension of the array LOCA, which was (NK,8), is not enough. It was concluded to increase it to (NK,14) where the simplified analysis is made. It is clear this value of 14 does not cover all possible cases but it is large enough to cover an important spectrum of cases. If a problem is selected where the array LOCA needs to be larger than LOCA (NK,14) an error statement will be printed out and then the pattern of channels should be modified in order to bring it into the 14 prescribed spaces.

The modifications introduced include:

- a) Define in which cases the array LOCA has to be (NK,14).

It is done by setting the variable IPILE (Cards C3 and T1) equal to zero. This implies that the simplified analysis is being executed and it triggers some of the other changes described below.

b) Increase the dimension of the LOCA array to (NK,14) instead of (NK,8)

It is done by changing statement \$LX(51) = MG\*8 of subroutine CORE by \$LX(51) = MG\*14.

c) Find all the 14 values of the LOCA array.

It is done by introducing in subroutine ACOL the following statements:

```
DO 8K = 1,NK
IF(IPILE .GT.0) GO TO 107
DO 103 L = 2,13
103 LOCA(K,L) = 0
GO TO 110
107 DO 3L = 2,7
3 LOCA(K,L) = 0
110 N = 1
.
.
.
```

The transmission of the IPILE value from subroutines CARDS4, INDAT and CHAN to ACOL is done via the argument list. Then it is necessary to change the statement call ACOL in all those subroutines by:

```
CALL ACOL (1,IDAT($IK+1), IDAT($JK+1), KMAX, IDAT($LOCA+1), MA, MS, NK,
1 MG, IPILE)
```

The subroutine ACOL initial statement is now:

Subroutine ACOL (IFROM,IK,JK,KMAX,LOCA,MA,MS,NK,MG,IPILE)

d) Find the stripe width for AAA matrix.

This segment of subroutine ACOL also required some modifications. The new statements are:

```
      .  
      .  
      .  
      DO 10 K=1,NK  
      N = LOCA(K,8)  
      IF (IPILE.GT.0) GO TO 111  
      N = LOCA(K,14)  
111 DO 10 L = 2,N  
      .  
      .  
      .
```

e) Calculation of NBOUND in subroutine DIVERT

In order to find NBOUND (number of boundaries that interact with boundary K) some small modifications were required:



```
IF(IPILE,GT.0) GO TO 7213
NBOUND = IDAT ($LOCA + K + MG * 13)
GO TO 7214
7213 NBOUND = IDAT ($LOCA + K + MG * 7)
7214 DO 300 LL = 1, NBOUND
      .
      .
      .
```

It was also needed to introduce the following statement to define IPILE: IPILE = J7

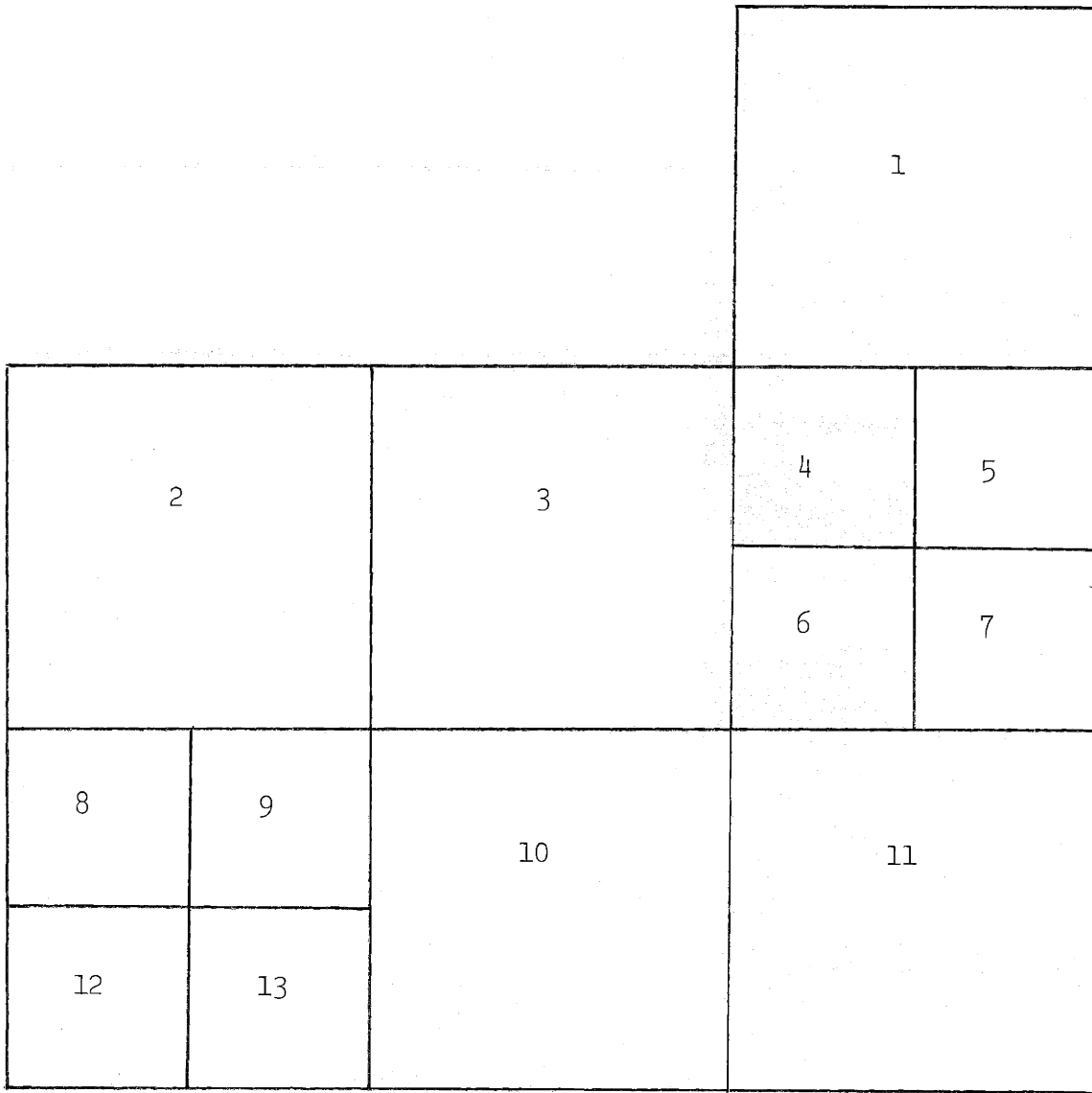
#### A.9.1.2 Find the IK and JK arrays

In the simplified analysis we may have cases like the one of Figure A.9.1. It is clear that this case could not be represented with the New Input Data Presentation of the first version of COBRA IIIC/MIT because in that version it is assumed that each channel is surrounded by a maximum of four channels.

Some modifications are then required in order to allow such cases:

##### a) New arrangements of the New Input Data Presentation

As will be explained below, in order to generate the IK and JK arrays the pattern of channels should be input in a different way than in the first version. This way is shown by considering the example of Figure A.9.1.



Sample problem

Figure A.9.1

To input the mapping of channels we should first redivide the core as indicated in Figure A.9.2 and second to input this array, using the IMAP = 3 option.

The cards required would be:

First Card	1	0	0	1	1
Second Card	2	2	3	4	5
Third Card	2	2	3	6	7
Fourth Card	8	9	10	11	11
Fifth Card	12	13	10	11	11

b) Calculation of the IK and JK arrays.

The system used is that of the first version of the code but suppressing any boundary created by only one channel and avoiding the double account of some boundaries that appear more than once.

Then the following statements were added:

·  
·  
·

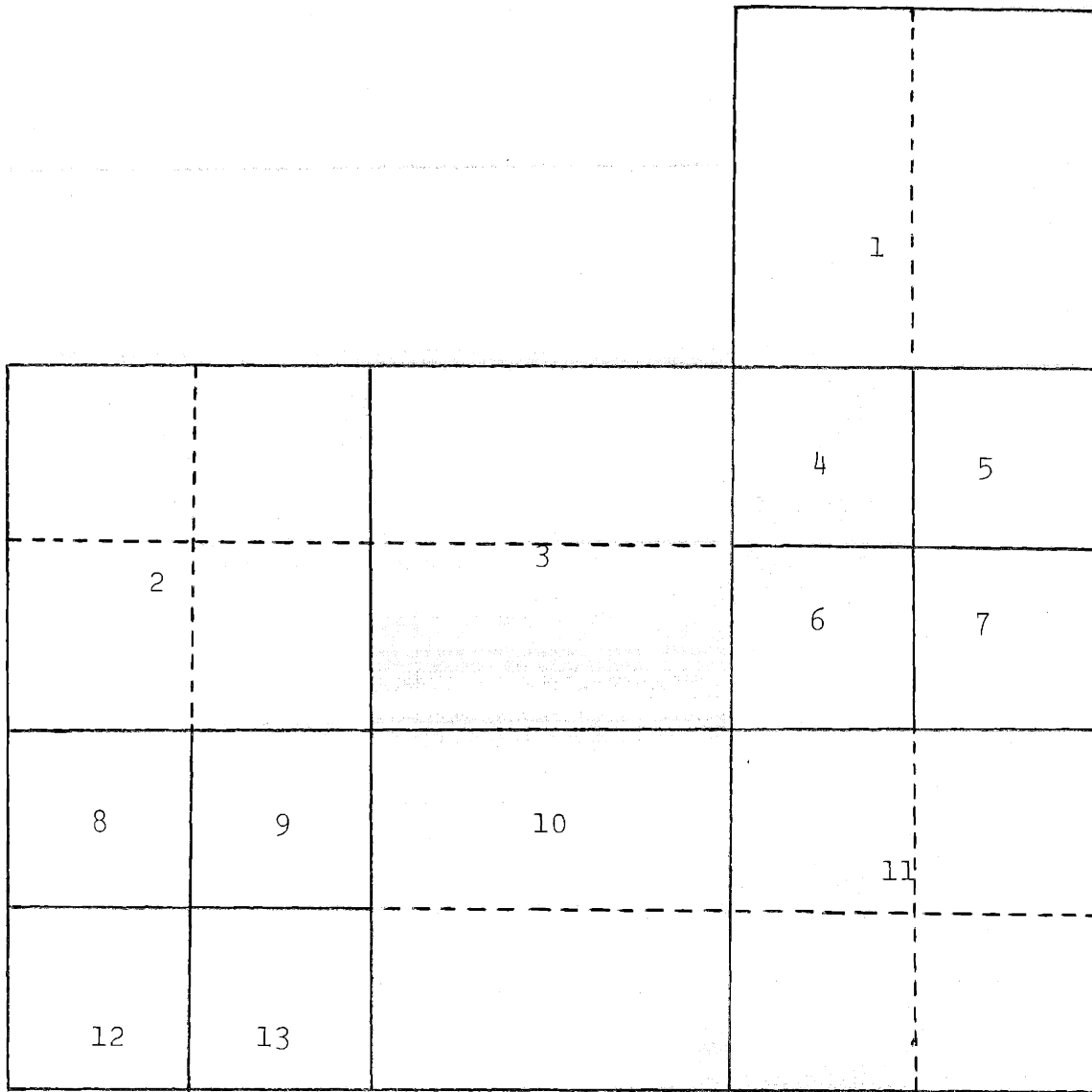
C SET GAP BOUNDARY NUMBERING SYSTEM

IF (IPILE.GT.0) GO TO 3010

DO 242 ND2 = 1, ND2X

DO 238 ND1 = 2, ND1X

I = NTHBOX (ND1 -1, ND2)



Redivision of the sample problem

Figure A.9.2

```
J = NTHBOX (ND1,ND2)
IF = ( (I.LE.O).OR.(J.LE.O) ) GO TO 238
IF ( (I-J).EQ.O) GO TO 238
DO 5216 K = 1,NK
IF ( (I.EQ.IDAT($IK+K) ) .OR. (I.EQ.IDAT($JK+K) ) )
1   GO TO 5215
    GO TO 5216
5215 IF ( ( J.EQ.IDAT ($JK + K)) .OR.(J.EQ.IDAT($IK+K)))
1   GO TO 238
5216 CONTINUE
    NK = NK + 1
    IDAT ($IK + NK) = I
    IDAT ($JK + NK) = J
238 CONTINUE
    IF(ND2.EQ.ND2X) GO TO 242
    DO 240 ND1 = 1, ND1X
    J = NTHBOX (ND1,ND2)
    I = NTHBOX (ND1,ND2 +1)
    IF = ((I.LE.O).OR.(J.LE.O)) GO TO 240
    IF((I-J).EQ.O) GO TO 240
    DO 6216 K = 1,NK
    IF((I.EQ.IDAT($IK+K)).OR.(I.EQ.IDAT($JK+K)))
1   GO TO 6215
    GO TO 6216
```

```
6215 IF((J.EQ.IDAT($JK+K)).OR.(J.EQ.IDAT($IK+K)))
      1 GO TO 240
6216 CONTINUE
      NK = NK + 1
      IDAT ($IK + NK) = I
      IDAT ($JK + NK) = J
240 CONTINUE
242 CONTINUE
      GO TO 3020
3010 DO 42 ND2 = 1,ND2X
```

With this system the boundaries, and the channels that make up each boundary for the case of figure A.9.1 are those of Table A.9.1.

## A.9.2 Modifications to Allow for No Square Channels

### A.9.2.0 Introduction

One of the problems in the first version of COBRA IIIC/MIT was that all the channels are assumed to be square. As a consequence, only the description of one of the four gaps of each channel is required, But in the simplified analysis some channels may not be squares. They will have different gap dimensions for each boundary. This implies that information related with all the boundaries is needed.

Boundary	Pair of channels that make up boundary
1	1-4
2	1-5
3	2-3
4	3-4
5	4-5
6	4-6
7	5-7
8	3-6
9	6-7
10	2-8
11	2-9
12	3-10
13	6-11
14	7-11
15	8-9
16	9-10
17	10-11
18	8-12
19	9-13
20	12-13
21	13-10

Boundaries for the example problem

TABLE A.9.1

A.9.2.1 Coding

It was solved by adding the following statements in  
subroutine CHAN:

```
      .  
      .  
      .  
      DIMENSION GAPREC (400)  
      .  
      .  
3020  IF(IPILE.GT.0) GO TO 9006  
      M = 1  
9014  MM = MINO((M+13),NK)  
      READ (I2,9007) CARD,(GAPREC(I), I=M,MM)  
9007  FORMAT(20A4,T1,14E5.0)  
      WRITE (I3,9107)CARD  
9107  FORMAT('  GAP INTERCONNECTIONS', 8X,'***',  
            20A4, '***CHAN')  
      M = MM + 1  
      IF (M.LE.NK) GO TO 9014  
      DO 9008 K = 1,NK  
9078  I = IDAT($IK+K)  
      IF(I-IDAT($JK+K)) 9084, 9080, 9082  
9080  WRITE(I3,2003) K,I,IDAT($JK+K)  
      IERROR = 1  
      RETURN  
9082  IDAT($IK+K) = IDAT($JK+K)  
      IDAT($JK+K) = J  
      GO TO 9078
```



```
9084 M = IDAT($JK+K)
      DATA($GAPN+K) = GAPREC(K)/12.
      DATA($GAP+K) = DATA($GAPN+K)
      DATA($LENGT+K) = 0.0
      DATA($FACTO+K) = 1.0
9080 CONTINUE
      GO TO 9009
9006 DO 90 K = 1,NK
      .
      .
      .
      IF(IPILE.EQ.0) GO TO 132
      DO 131 K+1,NK
131  GAPREC(K) = DATA($GAPN+K)*12.0
C    PRINT ARRAYS IK,JK AND LOCA
      .
      .
      WRITE (I3,1066) M,(IDAT($IK+K),IDAT($JK+K)
1      , GAPREC(K), K = M,MM)
      .
      .
      .
      IF(IPILE .GT.0) GO TO 4207
      DO 8138 L = 1,14
8138 WRITE(I3,1068) L,(IDAT($LOCA+K+MG*(L-1),
1      K=M,MM)
      GO TO 4208
4207 DO 138 L=1,8
      .
      .
      .
```

### A.9.3 Modifications to Allow for Having Actual Subchannels Together with Lumped Channels.

#### A.9.3.0 Introduction

When the simplified analysis is used, it is possible to have actual subchannels and lumped channels. In this case we will have rods which share their power with several subchannels while in the lumped channels it is assumed that one rod corresponds to one channel.

To solve this problem the Input Data Presentation of COBRA IIIC could be used, but it requires so many cards to describe the case that it was decided to modify again the new Input Data Presentation in order to allow for this possibility.

#### A.9.3.1 Coding

The following statements were incorporated to the code in subroutine CHAN:

```
.  
. .  
. .  
DATA ($DR+J) = DATA ($D+M) * 12.  
. .  
. .  
IDAT ($IDFUE+J) = 1  
IF(DATA($RADIA+J).EQ.0.0) GO TO 17  
DATA ($PHI+J) = DATA ($PHI+M)  
DATA ($PHI+J+MR*(1-1)) = DATA ($PHI+M)
```

```
      IDAT ($LR+J) = J
      IDAT ($LR+J+MR*(I-1) ) = J
17  CONTINUE
      .
      .
      .
C    READ ROD LAYOUT
      30  IF (IPILE) 2031, 2031, 2032
2031  READ (I2,2033) CARD,NN11, NN22, NN33, NN44
2033  FORMAT (20A4, T1, 4I5)
      WRITE (3,2034) CARD
2045  FORMAT ('  ROD INDICATORS', 14x, '***', 20A4,
1     '*** CHAN')
      NROD = NN22

      DO 2181 J = 1, NN11
      READ (I2,2035) CARD,N,I,DATA($DR+I),DATA($RADIA+I),
1 ( IDAT($LR+I+MR*(L-1) ), DATA ($PHI+I+MR*(L-1)),
      L = 1,6)
2035  FORMAT (20A4, T1, I1, I4, 2E5.0,6(I3,37.0) )
      WRITE (I3, 2047) CARD
2047  FORMAT ('ROD DATA', 20X, '***', 20A4, '*** CHAN')
      IDAT ($IDFUE+I) = N
      IF (N.LT.1) IDAT ($IDFUE+I) = 1
```

```
2181 CONTINUE
      DO 2185 I = 1, NROD
      DO 2184 L = 1,6
      IF (IDAT ($LR+I+MR*(L-1))) 2184, 2184, 2183
2183 K = IDAT ($LR+I+MR*(L-1))
      DATA ($PWRP+K+MC+(I-1)) = DATA ($PHI+I+MR*(L-1))
2184 CONTINUE
2185 DATA ($D+I) = DATA ($DR+I) / 12.
      IF (J1.LE.1) PRINT (8) = .TRUE.
      NODESF = NN33
      NFUELT = NN44
2032 IF (N0 DESF.EQ.0) GO TO 34
      .
      .
124 IF (IPILE.GT.0) GO TO 125
      WRITE (I3,2008) (I,IDAT($IDFUE+I),DATA($DR+I),
1 DATA ($RADIA+I), (DATA($PHI+I+MR*(L-1))),
3 IDAT ($LR+I+MR*
2 (L-1), L = 1,6), I = 1, NROD)
      .
      .
```

With this system the data for the lumped rods is given as part of the channel data (like in the first version of the code), while the data for the actual rods will be given as described in this section. This system yields a large reduction in Input Data Cards.

#### A.9.4 Modifications Required to Obtain the MDNBR.

##### Introduction

When it was desired to obtain the MDNBR with the first versions of COBRA IIIC/MIT, two problems were found. First, a variable in subroutine CHF was determined and second, an overflow problem in subroutine CHF2 took place. The errors were tracked and the following statements were changed:

##### A.9.4.1 Coding

###### A.9.4.1.1 Subroutine CHF

Statement CHF00770 should be:

```
IDAT($MCFRR + J) = CHFROD
```

###### A.9.4.1.2 Function CHF2

Statements CHF20330, CHF20340, CHF20341, CHF20350, and CHF20360 were taken out and in their place the following statements were added:

```
CE = C/2.
```

```
DO 5 JJ = JS,J
```

```
5  SUM+SUM+DATA($FLUX+N+MR*(JJ-1))*(EXP(CE*DATA($X+JJ)) +  
1  EXP(CE*DATA($X+JJ-1)))*(EXP(CE*DATA($X+JJ))-EXP(CE*DATA(  
2  $X+JJ-1)))  
   FAXIAL+SUM*EXP(-CE*DATA($X+JJ))/DATA($FLUX+N+MR*(J-1))/  
1  (1.-EXP(-C*(DATA($X+J) - DATA($X+JS-1))))
```

A.9.5 Modifications Required in Order to Obtain the Fuel Temperatures When the Original COBRA IIIC Input Data Presentation is Used.

A.9.5.0 Introduction

When this Input Data Presentation was used, and it was desired to obtain the temperature of the fuel rod, an overflow message in subroutine TEMP appeared. The cause of the error was investigated and it was found that because one small error in subroutine INDAT, one of the variables, was undefined.

A.9.5.1 Coding

In subroutine INDAT, the statement after MAIN 7670 was taken out and in its place the following was introduced:

185 DATA (\$D + I) = DATA (\$ DR + I) / 12.

A.9.6 Modifications Required When Wire Wraps are Used.

A.9.6.0 Introduction

One case with wire wrape was analyzed using the first version of COBRA IIIC/MIT. Some problems appeared and an error, because of overflow in subroutine DECOMP, was obtained. The problem was due to errors in subroutine DIVERT when the modifications of the simultaneous equations to account for specified values of crossflow given in sub-

routine FORCE are done.

A.9.6.1 Coding

In order to correct the error, statements from DVRT 0740 to DVRT 0870 were removed and in their place the following statements were introduced:

```
DO 90 K = 1,NK
IF(LDAT($FDIV+K)) GO TO 90
DO 85 L=1,NK
LL = MID-K+L
IF(LL.EQ.MID) GO TO 85
IF(LL.GT.LMAX.OR.LL.LT.1) GO TO 85
IF(LDAT($FDIV+L))
1 DATA($B+K) = DATA($B+K) - DATA($AAA+K+NK(LL-1) *
2 DATA($W+L+MG*(J-1))
85 CONTINUE
90 CONTINUE
DO 100K = 1,NK
IF(.NOT.LDAT($FDIV+K)) GO TO 100
DO 95 L=1,LMAX
DATA($AAA+K+NK*(L-1)) = 0.0
LL = MAXO(1,(L+K-MID))
LL = MINO(LL,NK)
MPICU = MID+K-LL
99 DATA($AAA+LL+NK*(MPICU-1)) = 0.0
```

A.9.7 Modifications Required in Order to Analyze More Than One Case in the Same Run.

A.9.7.0 Introduction

When two identical cases were analyzed in the same run it was observed that they yield slightly different answers.

This behavior was due to reinitialization problem. The variable SP was not initialized to zero in all its terms. The problem was found also in COBRA IIIC. In the first version of the COBRA IIIC/MIT code that problem was solved but one of the cards was misplaced and then SP was only initialized partially.

A.9.7.1 Coding

The coding is rather easy. It is only needed to place card:

```
DATA($SP+K+MG*(J-1)) = 0.
```

after card:

```
DATA($W+K+MG*(J-1)) = 0.
```

A.9.8 Modifications Required to Print Out More than 14 Channels, Rods or Nodes.

A.9.8.0 Introduction

When trying to printout results of more than 14 channels and less than the total number of channels in the



case, the following problem was observed. The results for the first fourteen channels were right while for the remainder, only zeros were obtained.

The same problem appeared when instead of channels, we obtained rods or nodes.

The problem was investigated and it was found to be due to undefinition of what channels (rods or nodes) should be printed out. The error was located in subroutine TABLES, which was rewritten.

#### A.9.8.1 Coding

The new subroutine TABLES is given in Appendix 4. It was needed to take out cards from:

```
READ(I2,1001) CARD,(IDAT($PRNTC+I), I=1,NPCHAN)
```

to

```
IF(NPNODE.GT.20) WRITE (I3,1005)
```

and to put in their place those given in Appendix 4.

#### A.9.9 Modifications Required to Use a Transport Parameter in Turbulent Interchange Term of the Energy Equation.

#### A.9.9.0 Introduction

As indicated in previous chapters, in order to improve the simplified method, transport coefficients should be calculated and incorporated into the general equations. In this first stage the only transport parameter used ( $N_H$ ) was that indicated by Weisman and Bowring<sup>(3)</sup>. Some new statements were required to allow for this coefficient.

#### A.9.9.1 Coding

##### A.9.9.1.1 Initialization of the New Variable (ENEH(L))

The variable ENEH(K), has to be initiated to one at the start of each new case. So in cases where ENEH(K) is not needed the value is kept as in COBRA IIIC (equal to one).

Because this variable was considered as part of the Mixing Parameters it was initiated in the segment of the Input that read in that Mixing Parameter.

When the old Input Data Presentation is used, the variable is initiated in INDAT after statement MAIN 8060.

```
DO 206 I = 1, MG
```

```
206 ENEH(I) = 1.0
```

When the Input Data Presentation is selected, the variable is initiated in subroutine MODEL. The statements added are:

```
      C   (N9) COUPLING PARAMETER
      DO   3201 K = 1,NK
3201    ENEH(K) = 1.0
```

#### A.9.9.1.2 Definition of the Values of ENEH(K)

The new variable ENEH(K) is read in by subroutine MODEL. The following statements were introduced in that subroutine:

```
      .
      .
      READ(I2,1001) CARD,N1,N2,N3,N4,N5,N6,N7,NPROP,N9
      WRITE(I3,1009) CARD
      IF(N1+N2+N3+N4+N5+N6+N7+NPROP+N9 .EQ.0)RETURN
      IF(N9.EQ.0) TO GO 3206
      M=1
3204    MM = MINO((M+13),NK)
      READ(I2,3202)CARD,(ENEH(K),K = M,MM)
3202    FORMAT(20A4,T1,14E5.0)
      WRITE(I3,3203) CARD
3203    FORMAT('COUPLING FACTOR NH',10X,'***',20A4,'***MODEL')
      M=MM+1
      IF(M.LE.NK) GO TO 3204
```



```
DATA($DHDX+I) = DATA($DHDX+I)+HWI-WV*DATA($WP+K)
2   /ENEH(K) - (
1  DATA($T+I) - DATA($T+L))*DATA($COND+K)
DATA($DHDX+L) = DATA($DHDX+L)+HWL+WV*DATA
2   ($WP+K) / ENEH(K) + (
1  DATA($T+I) - DATA($T+L))*DATA($COND+K)
.
.
.
```

REFERENCES

1. COBRA IIIC. Donald Rowe. BNWL-1695, Pacific Northwest Laboratories (1973).
2. COBRA IIIC/MIT Computer Code Manual. Robert Bowring, Pablo Moreno.
3. Methods for Detailed Thermal and Hydraulic Analysis of Water-Cooled Reactors. Joel Weisman; Robert Bowring. Nuclear Science and Engineering 57, 255-276 (1975).
4. H. Chelemer, J. Weisman, and L.S. Tong. Nuclear Engineering and Design 21, 3 (1972).
5. Chong Chiu, SM Thesis, 1976.
6. MEKIN: MIT-EPRI Nuclear Reactor Core Kinetics Code. Robert Bowring, John Stewart, Robert Shober, Randal Sims. September 1975.
7. Heat Transfer in Rod Bundles J.T. Rogers and N.E. Todreas, presented at Winter Annual Meeting of American Society of Mechanical Engineers, New York, N.Y., December 5, 1968.
8. "Single Phase Transport within Bare Rod Arrays, at Laminar, Transition and Turbulent Flow Conditions" H. Ramm, K. Johannsen, and N. Todreas, Nuclear Engineering and Design 30(1974) 186-204.
9. "Turbulent Interchange Mixing Rod Bundles and the Role Secondary Flows" J.T. Rogers and A.E.E. Tahir, Department of Mechanical and Aeronautical Engineering, Carleton University Ottawa, Ontario, Canada, January, 1975.
10. Personal communication with Robert Masterson, Spring 1976.
11. "Prediction of Local and Integral Turbulent Transport Properties for Liquid-Metal Heat Transfer in Equilateral Triangular Rod Arrays", H. Ramm, K. Johannsen. Paper No. 75-HT-NN. Journal of Heat Transfer.
12. "Evaluation of Intersubchannel Heat Transport in Bare Liquid - Metal Cooled Rod Arrays of Equilateral Triangular Arrangement: H. Ramm, K. Johannsen. 75-HT-32. The American Society of Mechanical Engineers.